



**HAL**  
open science

# In situ and Operando Spectroscopies in Photocatalysis: Powerful Techniques for a Better Understanding of the Performance and the Reaction Mechanism

Houeida Issa Hamoud, Lukasz Wolski, Ilia Pankin, Miguel Bañares, Marco Daturi, Mohamad El-Roz

► **To cite this version:**

Houeida Issa Hamoud, Lukasz Wolski, Ilia Pankin, Miguel Bañares, Marco Daturi, et al.. In situ and Operando Spectroscopies in Photocatalysis: Powerful Techniques for a Better Understanding of the Performance and the Reaction Mechanism. Topics in current chemistry, 2022, 380 (5), pp.37. 10.1007/s41061-022-00387-5 . hal-04254230

**HAL Id: hal-04254230**

**<https://hal.science/hal-04254230>**

Submitted on 23 Oct 2023

**HAL** is a multi-disciplinary open access archive for the deposit and dissemination of scientific research documents, whether they are published or not. The documents may come from teaching and research institutions in France or abroad, or from public or private research centers.

L'archive ouverte pluridisciplinaire **HAL**, est destinée au dépôt et à la diffusion de documents scientifiques de niveau recherche, publiés ou non, émanant des établissements d'enseignement et de recherche français ou étrangers, des laboratoires publics ou privés.

# *In-situ* and *Operando* spectroscopies in photocatalysis: powerful techniques for a better understanding of the performance and the reaction mechanism

Houeida Issa Hamoud<sup>a</sup>, Lukasz Wolski<sup>b</sup>, Ilia Pankin<sup>c</sup>, Miguel A. Bañares<sup>d</sup>, Marco Daturi<sup>a</sup>, Mohamad El-Roz<sup>\*a</sup>

<sup>a</sup>Normandie Université, ENSICAEN, UNICAEN, CNRS, Laboratoire Catalyse et Spectrochimie, 14050 Caen, France.

<sup>b</sup>Adam Mickiewicz University, Poznań, Faculty of Chemistry, Uniwersytetu Poznańskiego 8, 61-614 Poznań, Poland.

<sup>c</sup>Smart Materials, Research Institute, Southern Federal University, Sladkova Street 174/28, 344090, Rostov-on-Don, Russia.

<sup>d</sup>Catalytic Spectroscopy Laboratory, Instituto de Catalisis, ICP-CSIC, E-28049 Madrid, Spain.

\* Corresponding author: E-mail address: mohamad.elroz@ensicaen

## Table of Contents

<b>Abstract</b> .....	1
<b>2. <i>In-situ</i> techniques in photocatalysis</b> .....	3
2.1. <i>In-situ</i> FTIR spectroscopy .....	3
2.1.1. <i>In-situ</i> FTIR spectroscopy in the photocatalysts characterization .....	4
2.1.2. <i>In-situ</i> IR studies for investigating photocatalysis in gas phase.....	5
2.1.3. <i>In-situ</i> IR for investigating photocatalysis in liquid phase .....	7
2.2. <i>In-situ</i> Raman spectroscopy.....	9
2.2.1. <i>In-situ</i> Raman spectroscopy in the photocatalysts characterization .....	9
2.2.2. <i>In-situ</i> Raman spectroscopy for investigating photocatalysis in liquid phase .....	11
2.3. <i>In-situ</i> electron paramagnetic resonance (EPR) spectroscopy .....	12
2.4. <i>In-situ</i> XAS spectroscopy .....	13
<b>3. <i>Operando</i> techniques in photocatalysis</b> .....	15
3.1. <i>Operando</i> FTIR spectroscopy in photocatalysis.....	15
3.1.1. <i>Operando</i> FTIR for investigating photocatalytic reactions in gas-phase.....	15
3.1.2. <i>Operando</i> FTIR for investigating photocatalytic reactions in liquid-phase .....	20
3.2. <i>Operando</i> Raman spectroscopy .....	21
3.2.1. <i>Operando</i> Raman for investigating photocatalysis in liquid-phase .....	21
3.3. <i>Operando</i> XAS spectroscopy .....	24
3.3.1. <i>Operando</i> XAS for investigating photocatalysis in gas-phase.....	24
3.3.2. <i>Operando</i> XAS for investigating photocatalysis in liquid-phase .....	26
<b>4. Time-resolved techniques in photocatalysis</b> .....	28
4.1. Time-resolved FTIR .....	28
4.2. Time Resolved Microwave Conductivity (TRMC) .....	30
4.3. Photoluminescence spectroscopy (PL) .....	31
4.4. Transient absorption spectroscopy (TA).....	32
5. Summary, limitations and outlooks.....	33
<b>6. Concluding remarks</b> .....	35
<b>References</b> .....	37

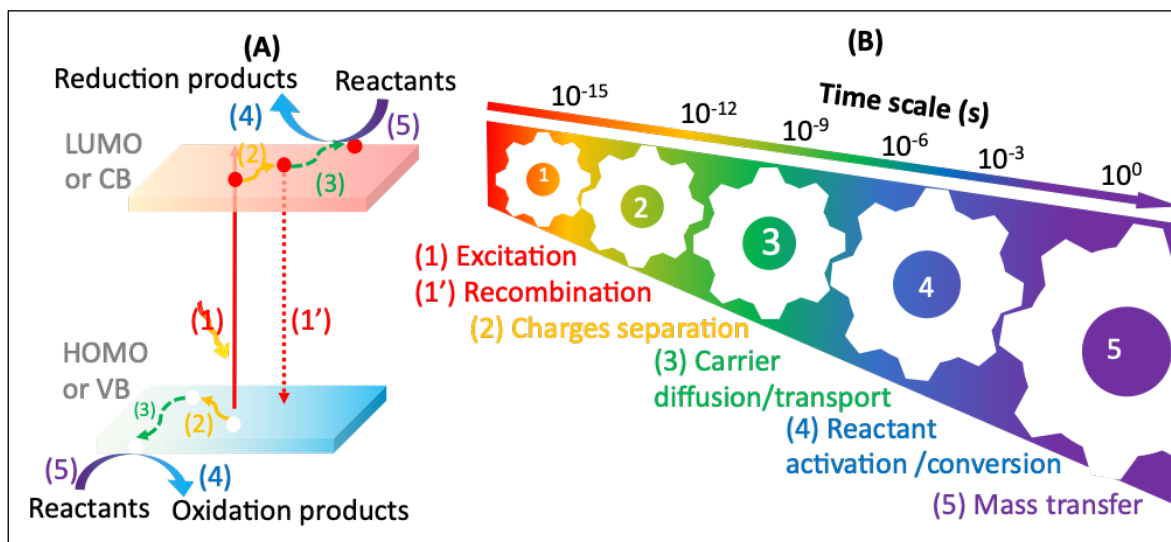
## Abstract

In photocatalysis, a set of elemental steps are involved together at different time scales to govern the overall efficiency of the process. These steps are divided as follow: 1) photon absorption and excitation (in femtoseconds), 2) charge separation (femto-to picoseconds), 3) charge carrier diffusion/transport (nano-to microseconds), 4 & 5) reactant activation/conversion and mass transfer (micro-to milliseconds). The identification and quantification of these steps, using the appropriate tool/technique, can provide the guidelines to emphasize the most influential key parameter that improve the overall efficiency and to develop the “photocatalyst by design” concept. In this review, the identification/quantification of reactant activation/conversion and mass transfer (steps 4&5) is discussed in details using the *in-situ/operando* techniques, especially the infrared (IR), Raman and XAS spectroscopy. The use of these techniques in photocatalysis was highlighted by the most recent and conclusive case studies which allow a better characterization of the active site and revealing the reaction pathways in order to establish a structure-performance relationship. In each case study, the reaction conditions and the reactor design for photocatalysis (pressure, temperature, concentration, etc.) were thoroughly discussed. In the last part, some examples in the use of time-resolved techniques (time-resolved FTIR, photoluminescence and transient absorption) are also presented as an author’s guideline to study the elemental steps in photocatalysis at shorter time scale (ps, ns and  $\mu$ s).

**Keywords:** *In-situ*, *Operando*, photocatalysis, FTIR, Raman, XAS.

## 1. Introduction

Photocatalysis is a process in which light energy drives the chemical reactions. This process is initiated by photon absorption and involves at least five separate reaction steps that occurred at different time scales, including: i) excitation of electron upon photon absorption from the valence band (VB) of the photocatalyst to the conduction band (CB), yielding electron and hole pairs charge carriers in femtosecond time-scale (step 1, Fig. 1), ii) separation (or recombination) of the charge carriers, in femto- to picoseconds [1,2,3] (steps 1’ and 2, Fig. 1), iii) diffusion/transport of the charge carriers from the bulk of the photocatalyst to the surface redox sites, generally in nano- to microseconds [1] (step 3, Fig. 1), iv) activation/conversion of the reactants by their interaction with the charge carriers (oxidation or reduction) in microseconds to milliseconds [4,5] (step 4, Fig. 1) and finally v) mass transfer/diffusion of the reactants and products that occurred in milliseconds to seconds [4] (step 5, Fig. 1). Therefore, all these steps, involved together at different time scales, govern the overall efficiency of the photocatalytic process. Thus, each elementary step in photocatalysis must be identified and quantitatively described by performing the appropriate experiments using adequate tools/techniques in order to provide the guidelines for the “photocatalyst by design” concept and improve the overall efficiency. Consequently, it is crucial to describe the different steps which occurred from the first interaction of the light with the photocatalyst to the formation of the final products. Thus, it is crucial to identify the electronic structure as well as the optical properties (band gap, band positions, absorption coefficient, etc.) of the chosen photocatalyst. These measurements can be achieved using X-ray absorption and UV-Visible absorbance spectroscopy. The femto-picosecond time-resolved absorbance/emission spectroscopies can be also used to investigate the lifetime and the quantum yield of the excited states upon interaction of the photocatalyst with the light. After photon absorption and generation of excitons, the latter should be separated to form free charge carriers. This step can be investigated by measuring the exciton binding energy, i.e. the energy required to ionize an exciton from its lowest energy state, using photoemission, optical absorption, photoconductivity screening potential and magneto-optical spectroscopies [6]. Moreover, DFT calculations are currently used to estimate the exciton binding energy with high accuracy [7]. The absorption transient and photoluminescence spectroscopies are also useful techniques, in which the quantum yield of the triplet excited state and the quenching rate constants can be determined. Once the exciton is separated, free charge carriers are transferred from the bulk to the surfaces for successful photocatalysis. The conductivity and the redox potential of the photocatalyst in this step can be measured by cyclic voltammetry and conductivity/impedance. Finally, the reaction mechanism/formation of the intermediates can be studied by time-resolved IR spectroscopy from ns- $\mu$ s (step scan measurement) to  $\mu$ s-ms (rapid scan measurement); Raman is a molecular spectroscopy, that can give complementary information to infrared insight; however, experimental challenges result in the overlap of excitation photons with Raman photons, rendering *operando* Raman spectroscopy more challenging; this review show approaches to circumvent such hurdle. *In-situ* and *operando* spectroscopies (e.g.: infrared (IR), Raman, UV-Vis, X-ray absorption spectroscopy (XAS) among others) may combine to shed light on the different stages of the photocatalytic act. The diverse techniques used for the characterization and investigation of the various elemental steps in photocatalysis are summarized in Table 1.



**Scheme 1.** Illustration of the elemental steps of photocatalysis process (A) occur at different time scale (B).

**Table 1.** List of the elemental steps, their properties and some useful characterization techniques for photocatalysis process [2].

Elemental step	properties	characterization techniques
1) photon absorption and excitation	-band gap -band positions -absorption coefficient -optical penetration depth -life-time/quantum yield of singlet excited state	X-ray diffraction UV-visible spectroscopy (for liquid and solid) femto-picosecond time-resolved absorbance/emission spectroscopy
2) charge separation	-Exciton binding energy -life-time/quantum yield of triplet excited-state	optical absorption spectroscopy photoemission spectroscopy photoconductivity screening potential spectroscopy magneto-optical spectroscopy photoluminescence spectroscopy transient absorption spectroscopy photoluminescence spectroscopy
3) charge carrier diffusion/transport	-deactivation/quenching of the triplet state -diffusion length -conductivity/resistivity - surface state	transient absorption spectroscopy time-resolved FTIR conductivity/impedance cyclic voltammetry
4 & 5) reactant activation/conversion and mass transfer	-activation energy -rate constant/catalytic activity -intermediate formation -molecular structures of the catalyst and reactants - electronic and geometric structures of transient species	time-resolved FTIR transient absorption spectroscopy <i>In-situ</i> and <i>operando</i> spectroscopies (infrared, Raman, UV-Vis, X-ray absorption spectroscopy (EXAFS and XANES)

In this review, we will mainly focus on the *in-situ* and *operando* techniques used in photocatalysis. By definition, the “*in-situ*” spectroscopy, widely used in the catalysis literature, refers to the real-time investigation of catalyst pretreated under vacuum during exposure to the reactants or probe molecules. *In-situ* studies may actually mimic reaction conditions, but the design of *in-situ* cells is typically not that of a catalytic reactor, thus activity data (when measured) are compromised by non-appropriate mixing between reactant and catalyst, or temperature gradients, or flow anomalies. Such reaction *in-situ* studies can provide valuable information of the photocatalyst’s state in reaction environment but cannot deliver reliable activity data. However, “*Knowing the before-reaction part or after-reaction part is like studying a life with access only to the prenatal and postmortem states*” as mentioned by Gabor Somorjai [8]. That’s why birth (catalyst preparation and

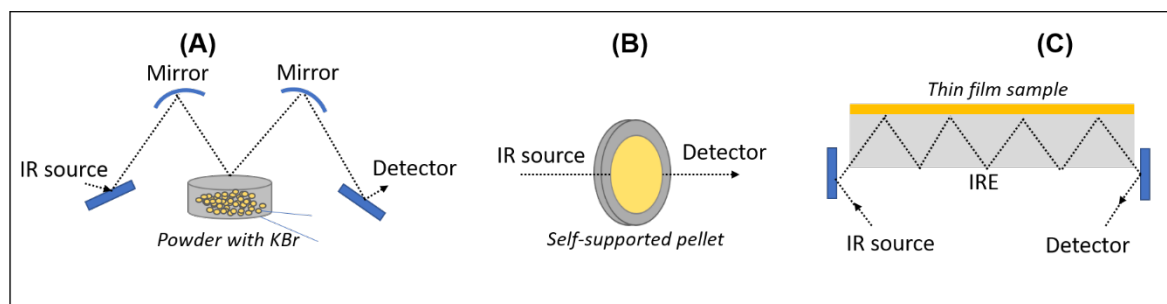
characterization), life (catalyst in action) and death of catalyst (deactivation) need to be studied [9]. Such consideration has inspired the *operando* methodology, where catalysts are actually working (i.e., *operando*) and their performance is simultaneously determined along with their characterization. *Operando* is a Latin word originally proposed by Prof. M. A. Bañares during a discussion with E. Gaigneaux, G. Mestl and B. Weckhusen at the 220<sup>th</sup> ACS National meeting in Washington in 2002) (cf. ref 11 in [10]). Monitoring the catalyst in action, including the observation of reaction intermediates, quantification of metal ions and determination of their oxidation state, discrimination between spectator species and active sites, is crucial for understanding the reaction mechanism and would allow to design high-performant solid catalysts [11,12]. For these reasons, many scientific researches are directed in the last years towards development of *operando* techniques for studying the photocatalytic reaction. Herein, we discuss recent findings related with the most used *in-situ* and *operando* techniques in photocatalysis such as the infrared (IR), Raman and X-ray absorption (XAS) spectroscopy. Detailed case studies are presented along with consideration of the methodology and the proper homemade/commercial reaction cells that are designed and adapted to the requirements of the photocatalytic reaction. Special attention is directed toward the identification of active sites and reaction intermediates as well as the investigation of the reaction mechanism.

## 2. *In-situ* techniques in photocatalysis

In this section, we will focus on the most popular *in-situ* techniques (FTIR, Raman, EPR and XAS) used as a characterization tool or even to study the reaction mechanism during photocatalysis.

### 2.1. *In-situ* FTIR spectroscopy

This technique can operate in three various modes for the present purpose: *Diffuse reflectance infrared Fourier transform* (DRIFTS), *transmission* and *attenuated total reflection* (ATR) (scheme. 2).



**Scheme 2.** IR spectroscopy in (A) diffuse reflectance, (B) transmission and (C) attenuated total reflection modes (IRE: internal reflection element).

Diffuse reflectance originates from multiple reflection, refraction and diffraction (scattering) at surfaces of small particles within the sample (scheme 2A) [13]. One of the most important advantages of this technique is possibility to analyze nontransparent materials at elevated temperatures, which cannot be analyzed by transmission infrared spectroscopy, and easy protocol for the sample preparation. However, this mode presents some limitations for *in-situ* studies such as: i) comparison of samples is challenging due to the different granularity of the sample and ii) quantification of adsorbed species is less straightforward compared to transmission mode. In transmission mode, there are some criteria to be considered such as i) particles of catalysts should have size smaller than 2-25  $\mu\text{m}$  in order avoid scattering of the IR radiation, ii) sample pellets (few mg) should be prepared without KBr or any diluent which could react with some gas molecules (e.g. NO to form  $\text{KNO}_3$ ), or it might change the sorption behavior of the sample and iii) samples should be prepared using a moderate pressure during making pellets to avoid changes in porous structure of the material and thus of its catalytic performance [14]. However, both transmission and DRIFTS modes are not suitable for liquid analysis, where strong absorption of IR radiation resulting from the presence of the liquid may hinder identification of the signals typical of the solid and of the adsorbates. In the last case, the most appropriate spectroscopic technique is based on the *attenuated total reflection* (ATR) mode which is suitable for both solid and liquid analysis. ATR-IR spectroscopy exploits an IR transparent material (internal reflection element (IRE) presenting a refractive index  $\geq 2.4$ , e.g. ZnSe, Ge, Si, diamond) as a waveguide for the total internal reflection at the IRE–medium interface (scheme 2C) [15]. In ATR-IR configuration, the solid sample is “immobilized” as thin layer which can be prepared by physical vapor deposition, by drying of a powder suspension or by chemical growth of the photocatalyst on the IRE, and analyzed via the evanescent wave which penetrates into the sample through  $\sim 1 \mu\text{m}$ . In this section, we give some example on the use of the *in-situ* FTIR technique in photocatalysis.

### 2.1.1. *In-situ FTIR spectroscopy in the photocatalysts characterization*

It is possible to thoroughly characterize the active sites using *in-situ* IR spectroscopy which is highly sensitive to the molecular vibrations and able to distinguish the different geometrical distortion of an adsorbed molecule. In general, two methodologies are used to obtain information on the acidic/redox properties of active sites as well as on their strength and concentration [16]: i) the direct observation of active sites and/or ii) indirect characterization using probe molecules. In the first case, the active sites can be directly identified through their IR fingerprints. For example, the presence of a  $\nu_{\text{OH}}$  band at  $3720\text{ cm}^{-1}$  in the FTIR spectrum of  $\text{TiO}_2$  confirms the presence of TiOH sites in a defective environment [4]. If the direct investigation of the active site is not possible, the appropriate solution is by the use of an IR probe molecule which can selectively interact with a single active site. However, the choice of a probe molecule must respond to certain criteria such as [17]: i) the molecule size depending on the accessibility of active sites; ii) the spectral response with a significant intensity and spectral sensitivity to the band position depending on the type of interaction; iii) the sufficient interaction with the site under study to obtain valuable information; v) the stability on the surface catalyst to avoid decomposition and vi) sufficient vapor pressure to be easily introduced in the IR cell.

The redox properties of photocatalysts can be investigated using CO, NO and/or methanol as probe molecules [18,19]. This gives information about the oxidation/coordination state of the active sites, their acidity and location on the surface. On the other hand, both Lewis and Brønsted acidity of the photocatalyst can be determined using probe molecules with strong basicity such as pyridine, ammonia, lutidine, trimethylamine, etc. More detailed insight into the nature of the active site can be provided by co-adsorption of probe molecules, while structure of the adsorption sites can be determined on the basis of isotopic exchange. As far as potential application of *in-situ* IR studies is concerned, it is important to underline that results obtained from adsorption tests at different temperature may be used to determine entropy and enthalpy of adsorption process. Finally, *in-situ* IR experiments may also provide information about nature of interaction between the reactant and the active site, similar to that observed during the photocatalytic reaction [20,21]. For example, Liu *et al.* [22] used DRIFTS *in-situ* adsorption of CO to identify changes in redox properties of the copper species in  $\text{Cu/TiO}_2$  catalyst after its pre-treatment at  $200\text{ }^\circ\text{C}$  under hydrogen or air before and after its application in photocatalytic reduction of  $\text{CO}_2$  under visible light. The experiments were performed in a Praying Mantis diffuse reflectance accessory, which is equipped with high temperature reaction chamber (Fig. 1A) (Harrick Scientific, HVC-DRP). The dome of the DRIFTS cell had two KBr and one quartz windows which are transmissive to infrared and visible light, respectively (Fig. 1A). The authors found that the  $\text{Cu/TiO}_2$  catalyst pre-treated under hydrogen ( $\text{Cu/Ti(H}_2\text{)}$ ) exhibits higher concentration of  $\text{Cu}^+$  species compared to  $\text{Cu/Ti(air)}$ , as confirmed by *in-situ* CO adsorption experiments (more intense band at  $2109\text{ cm}^{-1}$ , Fig. 1B). This explains the superior photocatalytic activity of  $\text{Cu/Ti(H}_2\text{)}$ . The latter was deactivated during the reaction and was not restored even after re-treatment under  $\text{H}_2$  at  $200\text{ }^\circ\text{C}$ , which is related to the higher amount of  $\text{Cu}^{2+}$  in  $\text{Cu/Ti(H}_2\text{)}$  after reaction and the changes in chemical surrounding of  $\text{Cu}^+$  species after the regeneration process. This was evidenced by the shift of  $\text{Cu}^+(\text{CO})_2$  IR band from  $2109\text{ cm}^{-1}$  to  $2114\text{ cm}^{-1}$  (Fig. 1B). In another example, the *in-situ*  $\text{D}_2\text{O}$  exchange was used to verify possibility of incorporation of titanium(IV) oxide in Beta zeolite structure by formation Si-O-Ti bonds during preparation of new photocatalyst by cold  $\text{TiCl}_4$ -plasma process [23]. The IR results show the presence of an important feature at  $955\text{ cm}^{-1}$  in  $\text{TiO}_2$ -Beta sample. The assignment of this band was still in debate; it could be assigned to Si-O-Ti or  $\nu(\text{Si-OH})$  vibrations. In order to unravel the origin of this IR band, the authors performed isotopic exchange of silanol with 10 mbar of  $\text{D}_2\text{O}$ . After  $\text{D}_2\text{O}$  exchange, the band at  $930\text{ cm}^{-1}$  is shifted by  $20\text{ cm}^{-1}$  in the pure zeolite sample (Fig. 1C) which is attributed to the H-D exchange of silanol groups. In contrast, a negligible shift (from  $953\text{ cm}^{-1}$  to  $955\text{ cm}^{-1}$ ) is observed for the Ti-doped zeolite (Fig. 1C) which undoubtedly confirms the formation of Si-O-Ti bond. A similar study comparing silica-supported titania with titanium-silicalite and the effect of exposure to hydration also identify the Si-O-Ti bond vibration in the  $960\text{-}970\text{ cm}^{-1}$  window of titania-silicalite [24].

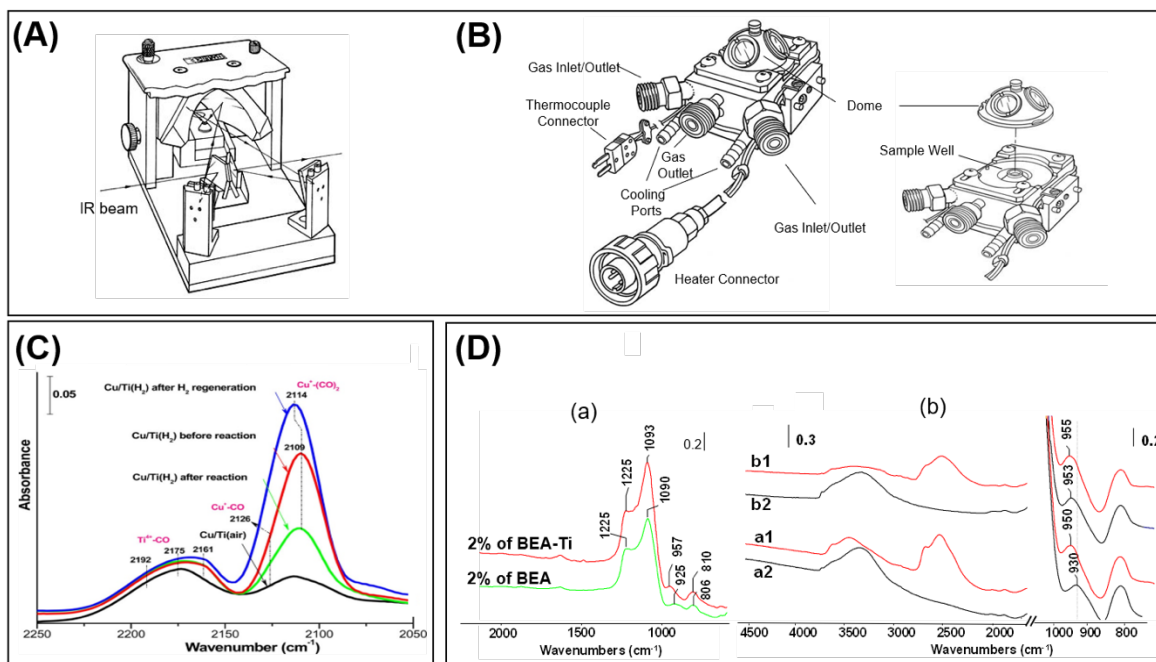


**Figure 1.** (A) Interior view of the Praying Mantis Diffuse Reflectance Accessory (DRP) with the model of the high temperature reaction chamber (HTC), (B) *In-situ* DRIFTS spectra of CO adsorption on Cu/Ti(air) and Cu/Ti(H<sub>2</sub>) before and after reaction and after thermal regeneration by H<sub>2</sub>, (C) (i) IR spectra of 2% of BEA-Ti (a) and 2% of BEA-ref (b) diluted in KBr and (ii) IR spectra of calcined Beta (a) and TiO<sub>2</sub>-Beta (b) samples diluted in KBr (5 wt%) before (1) and after (2) D<sub>2</sub>O exchange. (Copyright with the permission from Ref. [22,23]).

### 2.1.2. *In-situ* IR studies for investigating photocatalysis in gas phase

Modified *in-situ* IR cells were also used to study the reaction mechanism over TiO<sub>2</sub> during photocatalytic reaction involving a gas phase. However, this is an indirect method of investigation, since the reaction is performed under special conditions (partial vacuum) and the surface and gas phase analysis are performed separately. Some case studies describing various photocatalytic reactions are presented here. Fu *et al.* [25] used *in-situ* DRIFTS cell (Praying Mantis diffuse reflection accessory with high-temperature reaction chamber (Harrick Scientific)) to compare reactivity of adsorbed methanol species on {001} and {101} planes of titanium dioxide nanocrystals. The fresh catalyst was loaded into the reaction chamber, then evacuated at 40 °C until equilibrium and exposed to methanol or water through glass bulbs until saturation. The photocatalytic reaction was initiated by irradiation with 100 W high-pressure Hg arc lamp (Oriel 6281). On the basis of *in-situ* DRIFTS data, the authors established that both molecularly and dissociative adsorbed methanol species are photo-active on TiO<sub>2</sub>-{101} surface, while in the case of TiO<sub>2</sub> {001}, only methoxy species can be oxidized during the photocatalytic reaction with higher reactivity than those adsorbed on TiO<sub>2</sub>-{101} facets. The authors observed that the intensity of an IR band typical of methoxy species adsorbed on TiO<sub>2</sub>-{001} (band at ca. 2820 cm<sup>-1</sup>) was continuously decreasing upon exposition of the catalyst to light, while that of molecularly adsorbed methanol on TiO<sub>2</sub>-{001} (band at ca. 2950 cm<sup>-1</sup>) remained unchanged (Fig. 2A). In the case of TiO<sub>2</sub>-{101}, the intensity of IR bands typical of both molecularly (2950 cm<sup>-1</sup>) and dissociatively (2820 cm<sup>-1</sup>) adsorbed methanol molecules were decreasing over the reaction time (Fig. 2A).

Another example on the use of the *in-situ* DRIFTS is reported by Zhang *et al.* [26]. The authors investigate the impact of pretreatment conditions on the catalytic performance of TiO<sub>2</sub> in the photo-reduction of CO<sub>2</sub>. The photocatalysts (60 mg) were pressed into a thin wafer and loaded into the reaction cell. The photocatalytic reaction was then initiated by irradiation with UV light (5 W LED lamp;  $\lambda = 365$  nm). The authors found that pretreatment conditions (Ar vs. H<sub>2</sub> for 12 hours) have significant impact both on activity and selectivity of TiO<sub>2</sub> catalysts. The main product of photo-reduction of CO<sub>2</sub> over Ar-treated catalyst (Ar-12) was the carbon monoxide, while in the case of H<sub>2</sub>-treated sample (H-12) the main product was the formic acid. It was found that in the case of Ar-treated sample, CO<sub>2</sub> molecules were bound to the catalyst surface via bridging bidentate configuration (Fig. 2B; IR band at 1671 cm<sup>-1</sup>). In this adsorption mode, the carbon dioxide was interacting with two Ti<sup>3+</sup> sites formed near the oxygen vacancy. In the case of the surface IR spectra of H<sub>2</sub>-treated samples (i.e. H-2 and H-12), the authors observed an additional vibrational band at 1576 cm<sup>-1</sup>, assigned to CO<sub>2</sub> molecules bound to hydride-like -Ti-H-Ti- sites via a bridging bidentate configuration (Fig. 2B). This unique CO<sub>2</sub> adsorption mode, observed only for H<sub>2</sub>-treated samples, was found to be crucial for formation of C-H bonds and the selective production of formic acid during the photocatalytic reaction. The authors revealed also that

the adsorbate characterized by the IR band at 1588  $\text{cm}^{-1}$ , observed on both samples pretreated with Ar and  $\text{H}_2$ , is rather a spectator than an active intermediate species.

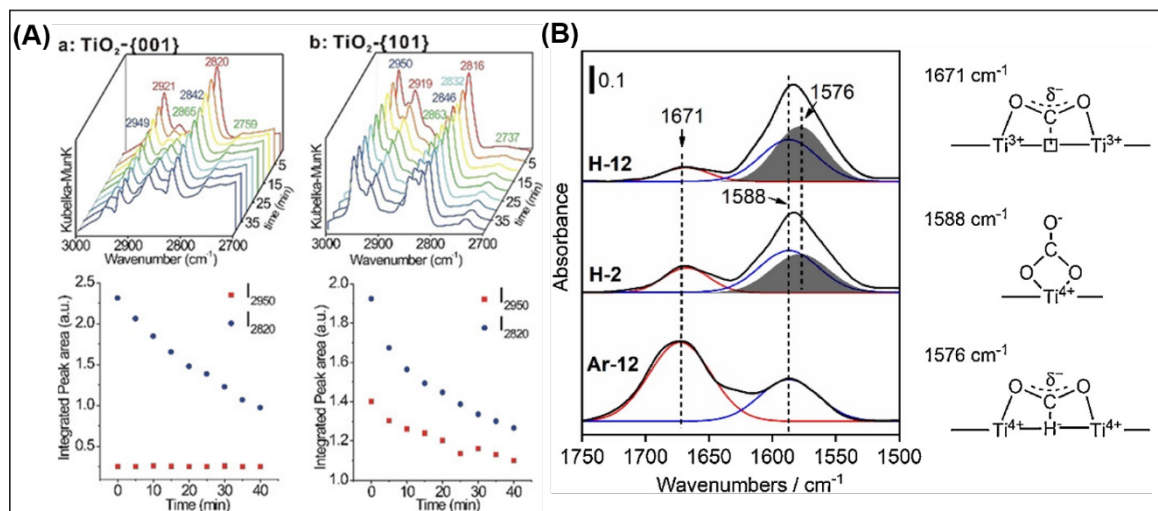


**Figure 2.** (A) In-situ DRIFTS spectra of  $\text{TiO}_2$  during the photocatalytic oxidation of adsorbed methoxy species ( $\text{CH}_3\text{O}_{(a)}$ ) and molecularly adsorbed methanol molecules ( $\text{CH}_3\text{OH}_{(a)}$ ) at 40  $^\circ\text{C}$  in a 10%  $\text{O}_2/\text{Ar}$  atmosphere with a flow rate of 30  $\text{cm}^3/\text{min}$  and (Bottom) coverages of  $\text{CH}_3\text{O}_{(a)}$  and  $\text{CH}_3\text{OH}_{(a)}$ , respectively represented by the integrated intensity of the vibrational features at 2820 and 2950  $\text{cm}^{-1}$ , as a function of photocatalytic oxidation time: (a)  $\text{TiO}_2$ -{001} and (b)  $\text{TiO}_2$ -{101} nanocrystals (NCs). DRIFTS spectra of corresponding bare  $\text{TiO}_2$  NCs were used as the background spectra; (B) FT-IR spectra of  $\text{CO}_2$  adsorption on the samples of Ar-12, H-2 and H-12 in the region of 1750–1500  $\text{cm}^{-1}$ . The background was collected just before the introduction of  $\text{CO}_2$ . (Copyright with permission from Ref. [25,26]).

The recent *in-situ* IR studies by Subbotina and Barsukov [27] allowed identification of surface peroxides as important reaction intermediates during photocatalytic oxidation of gaseous ethanol over  $\text{TiO}_2$ . In all the experiments the authors used a home-made *in-situ* cell in which the photocatalysts were deposited on thin (~0.4 mm) O-shaped Si slabs (8.5 cm of diameter). The irradiation was performed with a UV light emitting diode ( $\lambda = 365 \text{ nm}$ ; 10  $\text{mW cm}^{-2}$ ). The authors established that exposition of  $\text{TiO}_2$  to UV light in moist air led to the formation of surface peroxide species which were identified on the basis of the IR bands at ca. 852, 912 and 973  $\text{cm}^{-1}$ . These species are stable in the dark. However, upon UV irradiation the intensity of the typical IR bands of both ethanol and the surface peroxide species was continuously decreasing over the reaction time. In parallel, several new IR bands characteristic of partial oxidation products (bands at ca. 1130, 1020, 963  $\text{cm}^{-1}$ ) were observed. Interestingly, when ethanol and other organic intermediates were oxidized, the surface peroxide species were formed again and accumulated on the  $\text{TiO}_2$  surface.

Hirakawa *et al.* [28] reported that the selectivity of photocatalytic reduction of  $\text{NO}_3^-$  is strongly affected by the surface properties of commercial  $\text{TiO}_2$  (JRC-TIO-6). The experiments were carried out using a FT/IR-610 system (Jasco Corp.) equipped with an in-situ diffuse reflectance cell (Heat Chamber cold+HC-500, ST Japan, Inc.). Before the experiments, 50 mg of the catalyst were treated with 1.0 M  $\text{HNO}_3$  under continuous stirring for 6 h. The catalyst was then separated by centrifugation and dried at 333 K for 6 h. The catalyst containing  $\text{NO}_3^-$  species adsorbed on its surface was then placed inside the in-situ cell and evacuated at 303 K for 3 h. The photocatalytic reaction was initiated by irradiation with Xe lamp (300 W;  $\lambda > 350 \text{ nm}$ ) at 303 K. The results show that the formation of ammonia, as the most desirable product, was observed only in the presence of  $\text{TiO}_2$  catalysts with a high concentration of surface defects and a low number of Lewis acid sites, as revealed by *in-situ* DRIFTS analysis. As shown in Fig. 3Aa, exposure of the highly deficient JRC-TIO-6 (8) catalyst to visible light resulted in a significant decrease in the intensity of the IR bands typical of bidentate  $\text{NO}_3^-$  species adsorbed on  $\text{TiO}_2$  defects (IR band at 1610  $\text{cm}^{-1}$ ), parallel to an increase in the IR band intensity assigned to the  $\nu(\text{H-N-H})$  deformation in  $\text{NH}_4^+$  molecules (band at 1445  $\text{cm}^{-1}$ ). The latter indicated that  $\text{NH}_3$  was successfully formed by photocatalytic reduction of  $\text{NO}_3^-$ . In the case of the catalyst with a low concentration of defect sites and a high number of Lewis acid sites (JRC-TIO-1 (1)), a significant conversion of  $\text{NO}_3^-$  was also noticeable, but it was not associated with the increase in intensity of the IR band typical of  $\text{NH}_4^+$  (Fig.3Ac), suggesting that Lewis acid sites promoted the formation of other products of nitrate reduction. Different selectivity of the above-mentioned catalysts was explained by different strength of  $\text{NO}_3^-$  adsorption at the Lewis acid sites ( $\text{Ti}^{4+}$  ions) and the defect sites ( $\text{Ti}^{3+}$  atoms adjacent to oxygen vacancies). As depicted in Fig. 3A,  $\text{NO}_3^-$  species adsorbed on the surface defects were characterized by lower wavenumbers than those adsorbed at Lewis acid sites (1610 vs. 1635  $\text{cm}^{-1}$ , respectively). This shift is attributed to a strong electron donation from the surface defects to N=O antibonding orbital of  $\text{NO}_3^-$  species, which enabled much stronger adsorption of nitrates and



other intermediate products on the defect-rich sample, and this, in turn, promoted formation of  $\text{NH}_3$  instead of  $\text{N}_2$  (Fig. 3B).

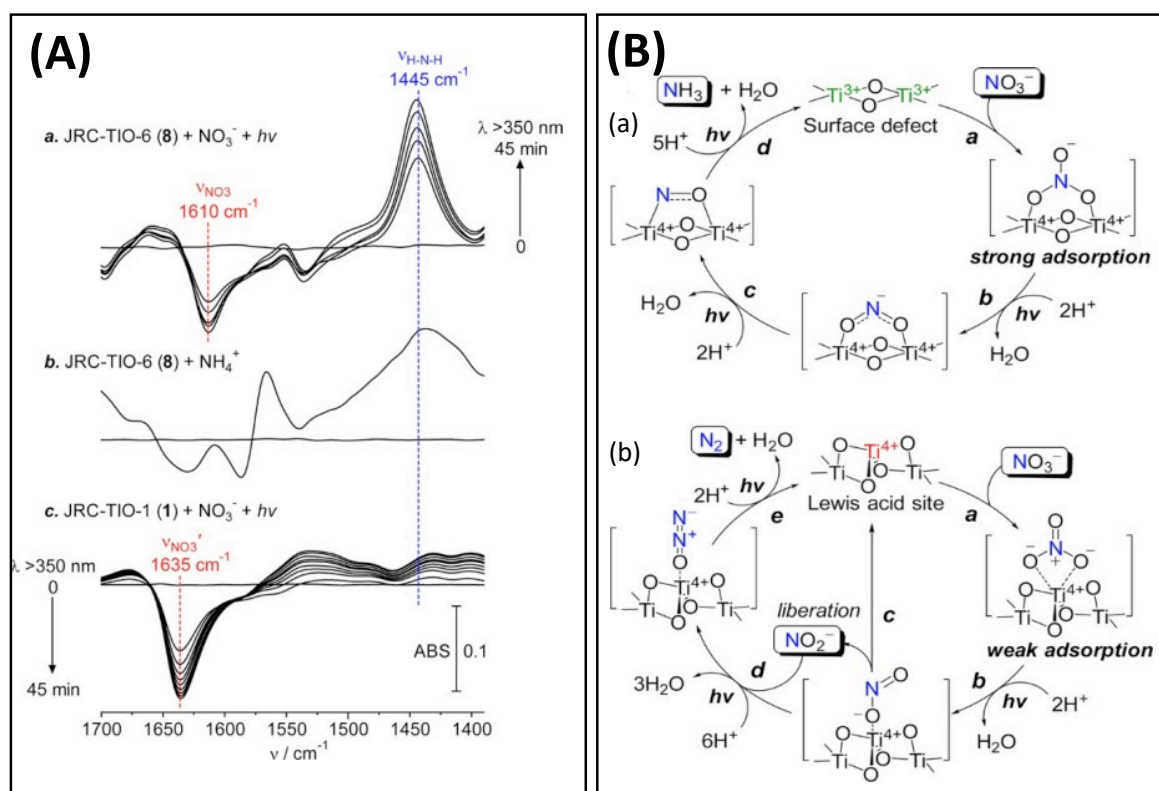


**Figure 3.** (A) Time-dependent change in the DRIFTS spectra of  $\text{NO}_3^-$  adsorbed on (a) JRC-TIO-6 (8) and (c) JRC-TIO-1  $\text{TiO}_2$  (1). The sample after adsorption of  $\text{NO}_3^-$  was measured at 303 K under photoirradiation ( $\lambda > 350 \text{ nm}$ ). (b) S spectrum of  $\text{NH}_4^+$  (21  $\mu\text{mol}$ ) adsorbed on JRC-TIO-6 (8). (B) Proposed Mechanisms for Photocatalytic Reduction of  $\text{NO}_3^-$  on (a) Surface Defect and (b) Lewis Acid Site of  $\text{TiO}_2$ . (Copyright with permission from Ref. [28]).

### 2.1.3. In-situ IR for investigating photocatalysis in liquid phase

To the best of our knowledge, the first *in-situ* FTIR photocatalytic study in liquid phase related to evaluation of photocatalytic activity of P25  $\text{TiO}_2$  in mineralization of malonic acid [29]. The authors used ATR-IR spectroscopy combined with modulation excitation spectroscopy and isotope labeling to enhance the sensitivity of the products detection. For this purpose, a dedicated flow-through cell was realized and mounted on an attachment for ATR measurements (Wilks Scientific) within the sample compartment of a Bruker Equinox-55 FTIR spectrometer equipped with a narrow-band MTC detector (Fig. 4A). Thanks to this tool and to the used approach, important mechanistic aspects were revealed. In particular, it appeared that at least two different pathways (concerning contribution of different oxygen sources, namely dissolved oxygen and oxygen from water) lead from the adsorbed malonates to the oxalate after the first photo-Kolbe reaction. Furthermore, dissolved oxygen would influence the rates of the different reaction steps, playing the role of an acceptor of photo-excited electrons, and accelerating the photocatalytic reactions by increasing efficiency of photo-excited charge carrier separation.

Another very interesting study reported cyclohexanone photooxidation over a  $\text{TiO}_2$  film using the *in-situ* ATR-FTIR spectroscopy [30]. All photocatalytic reactions were performed with the use of ATR cell which was made of quartz and had an inner volume of 4 mL (Fig. 4B). The photocatalytic reaction was initiated upon exposition to 75 W Xenon lamp. In order to eliminate radiation below 275 nm, the cell was covered by a Pyrex glass. For *in-situ* ATR studies, water solution of  $\text{TiO}_2$  nanoparticles was loaded on the ZnSe crystal of the ATR accessory and then evaporated under vacuum to form a  $\text{TiO}_2$  film (Fig. 4B). Before the measurements, the  $\text{TiO}_2$  powder was dried at 120  $^\circ\text{C}$  for 1 h and pre-illuminated under  $^{16}\text{O}_2/\text{He}$  or  $^{18}\text{O}_2/\text{He}$  atmosphere. In order to investigate the mechanism of photocatalytic oxidation of cyclohexane, the authors used oxygen isotopic exchange (OIE) to prepare variable amount of  $\text{Ti}^{18}\text{OH}$  species on the surface of  $\text{TiO}_2$ . They found that the dissolved oxygen is not directly involved in the photocatalytic oxidation of cyclohexane and the main source of the oxygen in the product of oxidation reaction are  $\text{TiO}_2$  associated active sites. Based on the IR results, the cyclohexanone

with a  $C=^{18}O$  carbonyl group (IR bands at 1657 and 1642  $cm^{-1}$ ) was formed only when oxygen isotopic exchange was performed before the photocatalytic process (Fig. 4C).

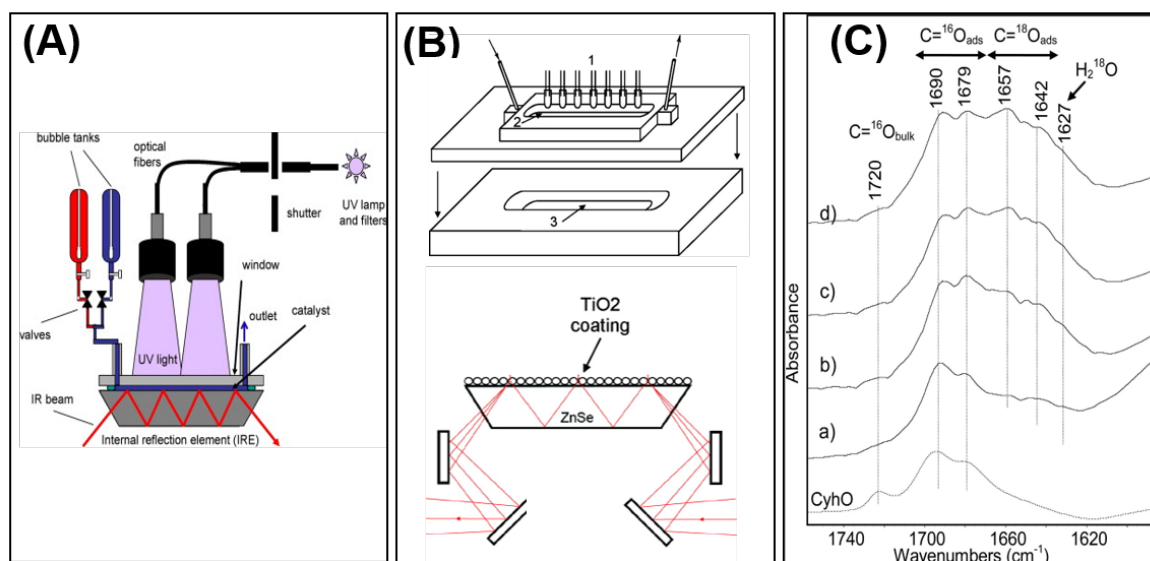


**Figure 4.** (A) Schematic setup for in situ ATR-IR spectroscopy of photocatalytic reactions in a small volume flow-through cell, (B) Scheme of the ATR-FTIR cell, including the light source (1), the quartz window on the top plate (2) and the internal reflection element (3) and representation of the IR path and penetration into the TiO<sub>2</sub> coating. In practice, 11 bounces were allowed by the crystal dimensions rather than the three bounces shown; (B) Infrared spectra after 10 min of cyclohexane photo-oxidation with 5% <sup>18</sup>O<sub>2</sub>/He on a TiO<sub>2</sub> catalyst which has been submitted to OIE for (a) 0 min, (b) 15 min, (c) 30 min, and (d) 60 min. The black dashed spectrum corresponds to the cyclohexanone (CyhO) adsorption. (Copyright with the authors permission [30,31]).

Belhadj *et al.* [32] used in-situ ATR-IR spectroscopy to investigate the influence of UV irradiation on H<sub>2</sub>O adsorption on the TiO<sub>2</sub> surface. The in-situ ATR experiments were performed with the use of a FTIR spectrometer (IFS 66 BRUKER) equipped with an internal reflection element 45° ZnSe crystal and a deuterated triglycine sulfate (DTGS) detector. The TiO<sub>2</sub> film was deposited on the surface of the ZnSe crystal by a simple evaporation method. Firstly, the aqueous suspension of TiO<sub>2</sub> (5.75 g/L) was sonicated for 15 min and placed on the surface of the crystal. Next, water was slowly evaporated at room temperature. The exposition of the TiO<sub>2</sub> film to UV light was obtained with the use of an LED lamp ( $\lambda = 365$  nm). Similarly to Subbotina and Barsukov [27], they found that surface hydroperoxy species (Ti-OOH), characterized by a vibrational band at 3483  $cm^{-1}$ , can be formed on TiO<sub>2</sub> only in the presence of molecular oxygen and UV light. The authors also found that exposure of TiO<sub>2</sub> to UV radiation in the presence of oxygen results in the formation of a greater number of surface hydroxyl groups, which in turn enhances the hydrophilicity of the metal oxide.

A new *in-situ* home-made glass reactor equipped with CaF<sub>2</sub> windows has been developed by El-roz *et al.* (Fig. 5A) for monitoring homogeneous and heterogeneous photocatalytic reactions in liquid phase [33]. The new *in-situ* FTIR reactor is dedicated for a real-time analysis of the gas products in transmission mode, but it cannot provide information on the evolution of catalyst surface during the reaction. However, it can offer an important information on the reaction selectivity and photocatalyst performance. Thanks to the different accessories, the system can operate as a batch or a continuous flow reactor. The total internal volume of the reactor is 160 mL and can be filled with 10 to 50 mL of solution. The UV-visible irradiation is provided by a Xe-Hg lamp connected to a UV-light guide mounted at the top of the IR cell with the possible control of temperature from 25-80 °C thanks to an unfix resistance and a thermocouple. This reactor solves the problems of i) irradiation homogeneity, ii) solvent condensation, iii) deformation of O-ring in presence of an organic solvent and iv) seal's ability of the reactor to control leaks, which is very important for air-sensitive reaction. The *in-situ* reactor was used to study different kinds of photocatalytic reactions in liquid phase such as formic acid decomposition [33], the photocatalytic CO<sub>2</sub> reduction [34,35] and the photodegradation of Methylene Blue (MB) [33]. This latter was performed on TiO<sub>2</sub> P25 under monochromatic irradiation at 365 nm. Using the new reactor, authors demonstrated that the total discoloration of MB observed after only 40 min of reaction, as shown by UV-Vis measurements (Fig. 5B)), is not linked with the total degradation/oxidation of the compound. The evolution of the IR spectra of the reaction head space demonstrates an increase in the CO<sub>2</sub> until reaching a plateau only after 125 min (Fig. 5C) which means 60 min after the total discoloration. Thus, the new reactor allows distinguishing between the discoloration and the total oxidation of the MB, which is widely used as a model to study the photocatalytic degradation performance of dyes.

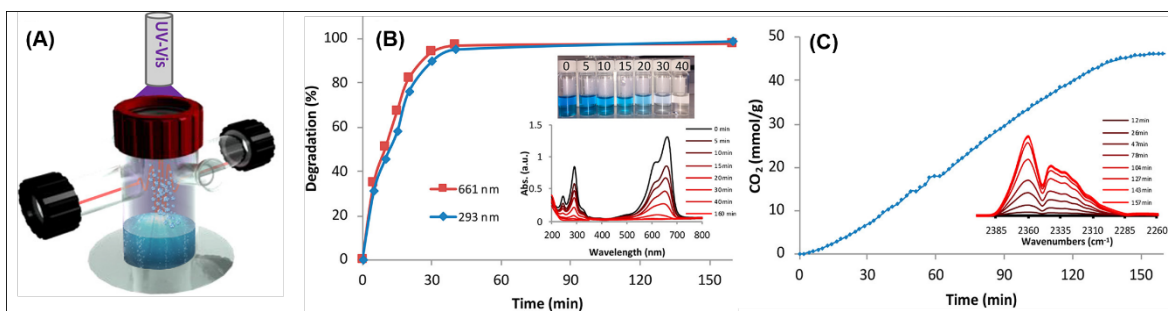


**Figure 5.** (A) The new *in-situ* FTIR reactor used for monitoring the gas headspace of a photocatalytic reaction in the liquid phase and (B) Evolution of the photocatalytic degradation of MB on TiO<sub>2</sub>-P25 versus the irradiation time as determined using UV-Visible absorbance of the MB. Inset: the corresponding samples and their UV-visible absorbance spectra. (C) Evolution of CO<sub>2</sub> in the gas headspace. Inset: the FTIR spectra of the headspace in the vibration region of CO<sub>2</sub> at different irradiation times. Reaction conditions:  $m_{\text{TiO}_2} = 50$  mg;  $V_{\text{water}} = 50$  mL;  $[\text{MB}] = 0.2$  mM; lamp, Xg-Xe (200W);  $\lambda = 365$  nm; irradiance, 15 mW/cm<sup>2</sup>. (Copyright with the authors permission [33]).

## 2.2. *In-situ* Raman spectroscopy

Raman spectroscopy is an experimental technique that allows identifying chemical compounds by utilizing the Raman effect, in which incident light is inelastically scattered from a sample and shifted in frequency by the energy of the excited molecular vibrations [36]. Depending on the energy of excitation laser and nature of the material, the incident light may penetrate the samples at a depth ranging from millimeters to nanometers [36]. Thus, this experimental technique may be used not only for the evolution of bulk and surface properties of the photocatalysts (e.g. precise analysis of structure and changes in composition of materials during reactions [37]), but also for tracking transformation of reagents on catalysts surface ([38]). In terms of application of Raman spectroscopy in heterogeneous catalysis, one of the most important limitations of this technique is its low signal intensity resulting from low frequency of the Raman scattering effect [39]. This drawback has been overcome by utilizing resonance effects in Raman spectroscopy and resulted in development of new experimental techniques (e.g. surface-enhanced Raman spectroscopy (SERS), shell-isolated nanoparticle enhanced Raman spectroscopy (SHINERS), or tip-enhanced Raman spectroscopy (TERS)); however, the applicability of those approaches imposes limitations on systems and reactions to characterize, particularly if *operando* conditions are sought. Recent advances in application of resonance Raman spectroscopy for characterization of nanomaterials and monitoring of catalytic reactions are described in reference[36,40]. As concerns photocatalytic processes, majority of literature reports in this field are related to application of *in-situ* SERS technique because of its high local sensitivity and spatial resolution that enable precise analysis of surface adsorbed species. To date, *in-situ* SERS studies have been used mainly for monitoring of numerous plasmon-driven surface reactions, e.g. demethylation of methylene blue [41], degradation of Rhodamine 6 G [42], dehalogenation of 4-iodothiophenol [43], transformation of benzylamine to N-benzylidenebenzylamine [38], hydrogenation of CO<sub>2</sub> [44], reduction of 4-nitrothiophenol [45], as well as dimerization of para-nitrothiophenol to p,p'-dimercaptoazobenzene [46]. The *in-situ* SERS studies included not only identification of reaction intermediates and products (e.g. [43,47]), but also detailed analysis of changes in surface properties of catalysts ([44]).

### 2.2.1. *In-situ* Raman spectroscopy in the photocatalysts characterization

Recently, *in-situ* SERS studies were applied to investigate efficiency of hot electrons transmission through various materials [48]. For this purpose, gold nanoparticles (Au NPs) were covered with a thin shell of SiO<sub>2</sub>, TiO<sub>2</sub> or Pd as a model insulator, semiconductor and metal, respectively. The as-prepared catalysts were then deposited on Au(111) single crystal covered with monolayer of para-aminothiophenol (pATP) (Fig. 6A-C). Efficiency of hot electrons transfer from Au NPs via shells composed of different materials was followed by measuring efficiency of photocatalytic transformation of pATP to p,p'-dimercaptoazobenzene (DMAB). The photocatalytic reactions were performed at 20 °C and initiated by irradiation with laser ( $\lambda = 633$  nm). On the basis of SERS spectra shown in Fig. 6D, the authors found that hot electrons formed on the surface of unmodified Au NPs can successfully initiate photo-conversion of pATP (Raman peaks at 1000, 1080, and 1178

$\text{cm}^{-1}$ ) to DMAB (Raman peaks at ca. 1140, 1392, and 1445  $\text{cm}^{-1}$ ). High efficiency of pATP photo-conversion was also observed for Au NPs covered with thin shell of  $\text{TiO}_2$ . As depicted in Fig. 5E, the relative intensity of the Raman signals typical of DMAB to that characteristic of pATP, calculated from *in-situ* SERS spectra recorded during the reaction with the use of the unmodified Au NPs and Au NPs covered with  $\text{TiO}_2$ , were comparable. Interestingly, significant decrease in efficiency of photocatalytic transformation of pATP to DMAB was observed for Au NPs covered with thin layer of  $\text{SiO}_2$  or Pd (Fig. 6E). In view of these observations, the authors established that the hot electrons can be transferred more efficiently within  $\text{TiO}_2$  shell than through the shells composed of Pd or  $\text{SiO}_2$ . Additional *in-situ* SERS studies with the use of Au NPs covered with various thicknesses of Pd or  $\text{TiO}_2$  shells allowed estimation of the distance at which the hot electrons can diffuse efficiently through the model semiconductor and the model metal. As depicted in Fig. 6F, the diffusion length of the hot electrons within the palladium shell was much shorter than that observed for the shell composed of titanium dioxide, such a sub-nm special resolution for hot electrons diffusion in  $\text{TiO}_2$  and Pd by changing the thickness of the  $\text{TiO}_2$  and Pd shells.

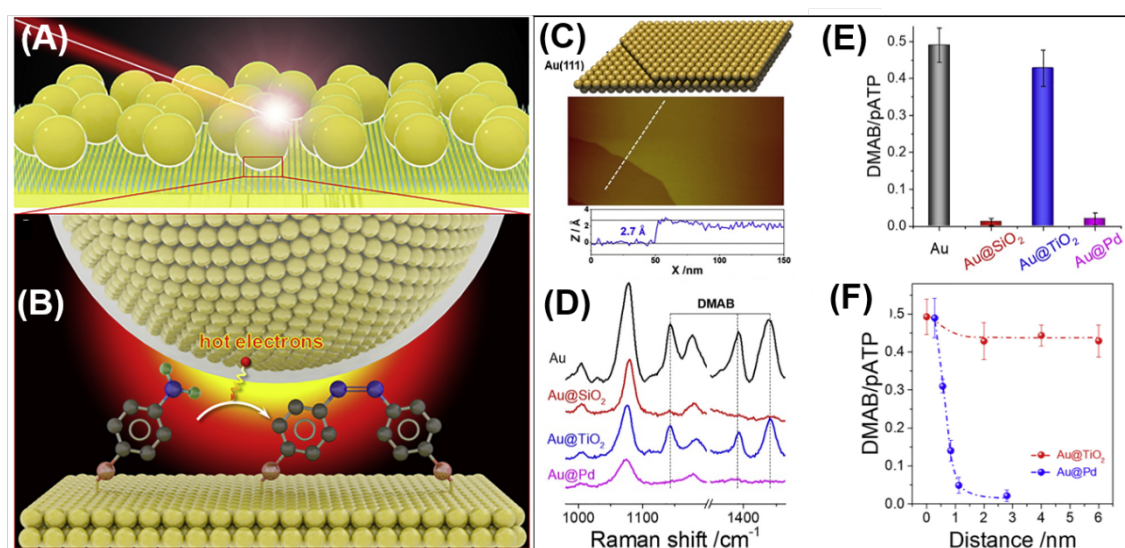


**Figure 6.** (A) and (B) Schematic illustration of *in-situ* SERS study on the interfacial transmission of hot electrons using the photocatalytic conversion of pATP to DMAB as a probe reaction; (C) Schematic and scanning tunneling microscopy (STM) image of the Au(111) single crystal surface. The STM image was obtained using a Pt-Ir tip with a dimension of 150 x 300  $\text{nm}^2$ . The bottom panel shows the height profiles corresponding to the white dashed line in the STM image; (D) SERS spectra of the conversion of pATP adsorbed on Au(111) catalyzed by different core-shell nanoparticles. Excitation laser, 633 nm; laser power, 0.1 mW; and exposure time, 10 s; (E) Relative Raman intensity of DMAB to pATP for different nanostructures shown in (D); (F) Relative Raman intensity of DMAB to pATP as a function of the shell thickness for Au@ $\text{TiO}_2$  and Au@Pd interfaces. (copyright with the authors permission [48]).

Another example is related to application of *in-situ* tip-enhanced Raman spectroscopy (TERS) for investigation of the role of reactive arrangement (i.e. orientation and surface coverage) of 4-nitrothiophenol (4-NTP) molecules on Au(111) single-crystal in photocatalytic coupling of 4-NTP to p,p'-dimercaptoazobenzene (DMAB) [49]. The different reactive arrangement of 4-NTP species was obtained by using two various experimental protocols: i) drop-cast method which allowed obtaining of self-assembled monolayer of 4-NTP characterized by low contribution of well-ordered 4-NTP domains (ca.  $7.8 \pm 1.0\%$ ) and ii) immersion protocol that enabled construction of self-assembled monolayer of 4-NTP characterized by high contribution of well-ordered 4-NTP domains (ca.  $74.3 \pm 5.5\%$ ). All TERS measurements were performed with a top-illumination TERS setup combining a scanning tunneling microscope (STM) with a Raman spectrometer (Fig. 7A). He-Ne laser ( $\lambda = 632.8$  nm; Spectra-Physics, Newport, Germany) was used as the excitation source. On the basis of high-resolution *in-situ* 2D TERS imaging of the reaction on the Au(111) crystal, the authors found that DMAB product was identified on almost whole surface of the drop-cast sample, but some negligible regions containing unreacted 4-NTP substrate were also noticeable (Fig. 7B(a)). This observation was further confirmed by results obtained from analysis of six TERS spectra from selected locations where DMAB (P1-P3) and unreacted substrate (P4-P6) were identified. As shown in Fig. 7B(b), Raman signals typical of DMAB (peaks at ca. 1146, 1390 and 1442  $\text{cm}^{-1}$ ) were found only in spectra from locations P1-P3. In contrast to the drop-cast sample, very

low efficiency of 4-NTP photo-conversion was found for the sample obtained by the immersion protocol. In this case, the DMAB product was formed only in several isolated locations (Fig. 7B(c,d)). In view of these observations, the authors established that the close-packed molecular arrangement of 4-NTP substrate on the surface of the sample prepared by the immersion method diminished significantly the efficiency of photocatalytic transformation of the substrate to the product. This conclusion was further supported by results obtained from analysis of zoomed-in TERS image of selected region from the drop-cast sample (Fig. 7B(e)). This TERS image, characterized by spatial resolution of ca. 3 nm, indicated that DMAB was formed at all marked positions except of 3, where steric hindrance inhibited photocatalytic conversion of 4-NTP to DMAB (Fig. 7B(f)).

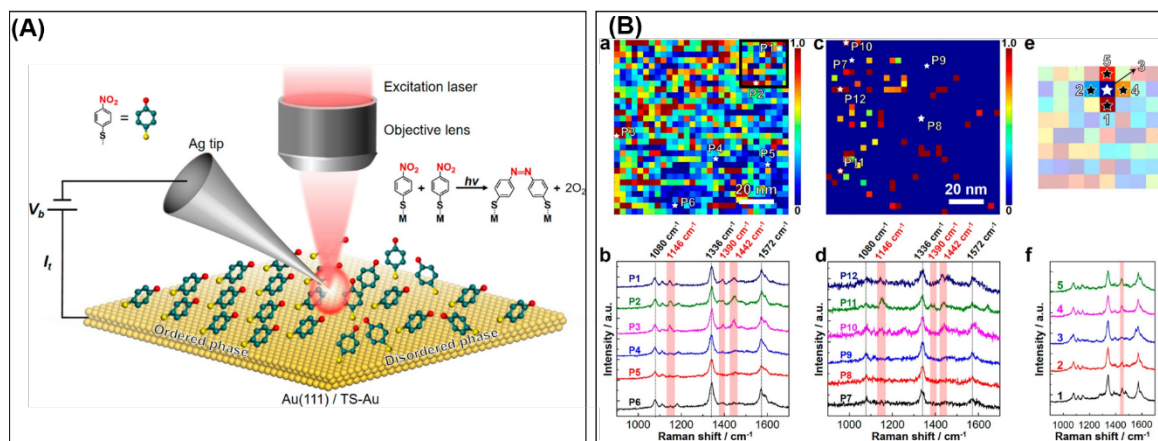


**Figure 7.** (A) Schematic diagram of the STM-TERS setup used in this study to investigate reactive arrangement in photocatalytic coupling of 4-NTP  $\rightarrow$  DMAB on polycrystalline and single-crystal Au surfaces; (B) High-resolution TERS images of  $I_{1442}/I_{1080}$  ratio measured on samples prepared via (a) drop-cast and (c) immersion protocols on single crystal Au(111) surfaces. Step size: 3.3 nm. Spectrum integration time: 1 s. (b, d) TERS spectra measured at the locations P1–P12 marked in (a) and (c). (e) Zoomed-in TERS image of the region marked in (a). Five pixels labeled as 1–5 are highlighted. (f) TERS spectra measured at the pixels labeled in (e). (copyright with the authors permission [49]).

### 2.2.2. *In-situ* Raman spectroscopy for investigating photocatalysis in liquid phase

As far as recent *in-situ* Raman studies are concerned, it is important to underline that Rößler et al. [50] developed new home-made glass reactor that allows *in-situ* monitoring of photocatalytic processes with the use of Raman spectroscopy (Fig. 8A). The reactor was made of glass and composed of a customized Schlenk-tube surrounded by 3D-printed illumination units (12 high-power LEDs, Nichia NCSG219B-V1, peak wavelength 520 nm, FWHM 30 nm). The reaction was monitored with the use of a short focus immersion probe with a sapphire tip mounted in the photo-reactor with GL-screw fittings (Bohlender, Grünsfeld, Germany). *In-situ* Raman spectra were collected with the use of RXN2 spectrometer (Kaiser Optical Systems, Lille, France) equipped with a laser source (785 nm). The new reactor enabled recording of Raman spectra with a temporal resolution of about one minute, i.e. much higher than that available for other offline sampling analyses. It shows great advantage of the new *in-situ* reactor for monitoring of fast photocatalytic processes which reach equilibrium state in several minutes. As an example, the authors described studies on photooxidation of 4-methoxythiophenol (4-MTP) to bis(4-methoxyphenyl)disulfide (4-MPD) catalyzed by eosin Y (EY). The authors found that the oxidation reaction may proceed under dark conditions but its efficiency is greatly accelerated upon exposition to green LED light. As depicted in Fig. 8B, concentration of 4-MTD (estimated from *in-situ* Raman spectra by a chemometric indirect hard model) increased immediately upon LED irradiation at the expense of 4-MTP). Detailed kinetic studies allowed estimating the reaction rate constants. It was established that the photocatalytic reaction was ca. 16 times faster than the reaction under dark conditions (reaction rate constants of  $0.013 \text{ min}^{-1}$  vs.  $0.21 \text{ min}^{-1}$ , respectively). This study was significantly affected by excitation-light induced fluorescence problems and care had to be taken to minimize such interference.

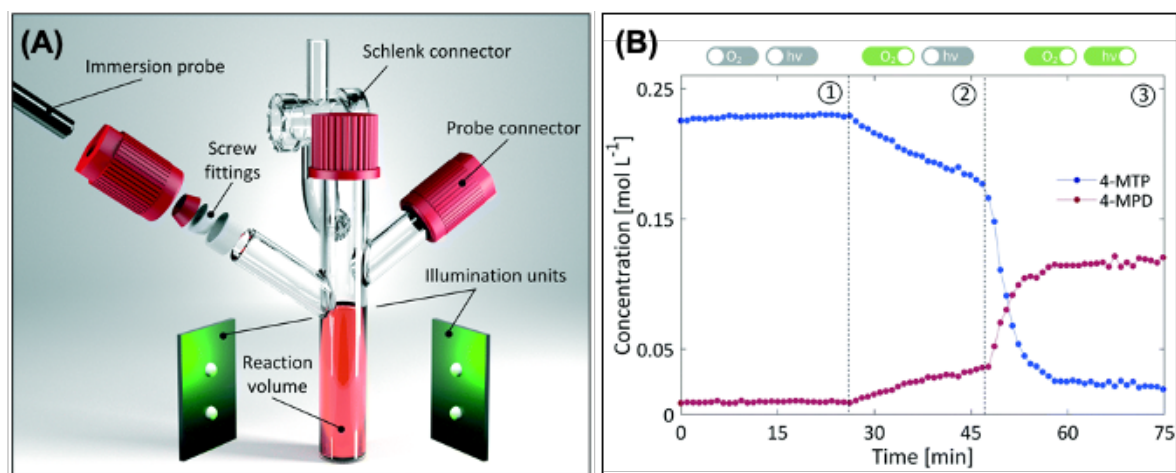


**Figure 8.** (A) Representation of the developed setup for studying photocatalytic reaction kinetics. The setup allows simultaneous LED irradiation and *in-situ* monitoring by various process analytical technologies (e.g. Raman spectroscopy); (B) Evaluation of the concentration–time course for 4-MTP (blue) and 4-MPD (red) by a chemometric indirect hard model (IHM) resolves the response to the applied reaction conditions. (Copyright with the authors permission [50]).

### 2.3. *In-situ* electron paramagnetic resonance (EPR) spectroscopy

EPR spectroscopy have been widely used in photocatalysis for monitoring the charge carrier trapping, recombination and transfer as well as for identification of radicals and Reactive Oxygen Species (ROS) [51]. The low frequency of the electromagnetic radiation used for the spin resonance of electrons assures no interference from the frequency of the light, which allow measuring the EPR spectra, in an *in-situ* manner, under irradiation and in dark conditions. Since the lifetime of radicals is usually very short, the detection of such species is often performed in presence of spin traps that selectively react with a given radical to form a more stable adduct [52]. For example, Zhang *et al.* [53] used *in-situ* EPR spectroscopy to confirm the formation of hydrogen atoms as an intermediate product during the photocatalytic H<sub>2</sub> production from water over the ternary Pt<sub>1</sub>@CNQDs/CNS catalyst (Pt<sub>1</sub> - single platinum atom, CNS - carbon nitride nanosheets, CNQDs-carbon nitride quantum dots) by using 5,5-dimethyl-1-pyrroline-N-oxide (DMPO) as spin trap. EPR spectra were recorded using the X band on a Bruker E500 spectrometer. The photocatalytic reaction was performed in a top-down illumination reactor using a Xe lamp with a UV-cut filter (400 nm <  $\lambda$  < 780 nm). Before the measurements, 15 mg of the photocatalyst was added to 150 mL aqueous solution of triethanolamine (10 %) as an electron donor and purged with nitrogen gas to remove the dissolved air. As depicted in Fig. 9A, the spin adduct was observed immediately after 20 s of visible light irradiation (nine signal peaks), indicating that H-atoms are formed as an intermediate during the reaction. By comparing the intensity of the EPR signal, the signal observed in presence of Pt-containing photocatalysts was much lower than that observed for Pt-free samples, suggesting that the reduction of protons takes place in carbon nitride quantum dots (CNQDs) in the Pt<sub>1</sub>@CNQDs/CNS system, while the recombination of H-atoms into H<sub>2</sub> takes place on single platinum atoms (Pt<sub>1</sub>). *In-situ* EPR technique with DMPO as spin trap were also used by Park *et al.* [54] to detect the methyl radical (CH<sub>3</sub>•) as one of the main intermediate products formed during the photocatalytic conversion of CO<sub>2</sub> and water into C<sub>1</sub> to C<sub>3</sub> hydrocarbons over CdS/(Cu-Titanate Nanotubes). More examples on the application of *in-situ* EPR with the use of spin trap in photocatalysis can be consulted elsewhere [55,56].

As far as application of *in-situ* EPR spectroscopy in photocatalysis is concerned, it is important to underline that this technique also allows for direct observation and monitoring of the paramagnetic active species during photocatalytic processes. For example, Zhang *et al.* [57] used *in-situ* EPR spectroscopy to confirm the formation of Cu<sup>+</sup> as active species in CuSA-TiO<sub>2</sub> (SA = Single Atom) during the photocatalytic hydrogen evolution reaction. EPR spectra were recorded at room temperature on a Bruker EMXnano spectrometer. The photocatalytic reaction was performed in a multichannel photothermal reactor (PCX-50C, Perfect Light Ltd.) using a Xe lamp as a simulated solar light source. Before the measurements, 20 mg of the photocatalyst was added to 120 mL of H<sub>2</sub>O/methanol mixture (vol. ratio = 1:2) and evacuated under vacuum to remove the dissolved air. The authors revealed that the EPR signal typical of Cu<sup>2+</sup> ions significantly decreased during the reaction and restored after exposition to air (Fig. 9B), suggesting the reduction of the Cu<sup>2+</sup> to EPR-silent Cu<sup>+</sup> species by photogenerated electrons formed in TiO<sub>2</sub>, resulting in very efficient production of hydrogen over CuSA-TiO<sub>2</sub> catalyst.

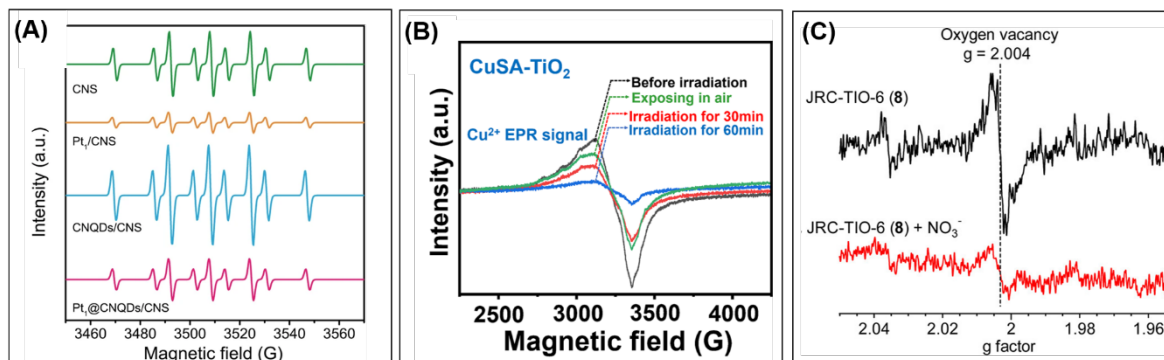


**Figure 9.** (A) Deconvolution of experimental EPR signals of DMPO spin adducts generated under irradiation of a 300 W Xe lamp ( $\lambda > 400$  nm) for the CNS, Pt<sub>1</sub>@CNS, CNQDs/CNS, and Pt<sub>1</sub>@CNQDs/CNS. (B) *In-situ* electron paramagnetic resonance spectra of CuSA-TiO<sub>2</sub> with various states. (C) ESR spectra measured at 77 K for JRC-TiO-6 (8) (black trace) and the sample after adsorption of NO<sub>3</sub><sup>-</sup> (red trace). (Copyright with the authors permission [28,53,57]).

EPR spectroscopy has also been recognized as a very powerful tool to investigate the role of defects in photocatalysis [58]. For example, Hirakawa *et al.* [28] used *in-situ* EPR spectroscopy to confirm the electron transfer from oxygen vacancies in TiO<sub>2</sub> (JRC-TiO-6 (8)) to the adsorbed NO<sub>3</sub><sup>-</sup> species during the selective NO<sub>3</sub><sup>-</sup>-to-NH<sub>3</sub> reduction under UV light ( $\lambda > 300$  nm) in presence of formic acid (HCOOH) as an electron donor. EPR spectra were recorded on a Bruker EMX-10/12 spectrometer. Before the measurement, 50 mg of the parent catalyst or the catalyst containing NO<sub>3</sub><sup>-</sup> species adsorbed on its surface was placed in a quartz tube and evacuated for 4 h. EPR measurements were performed at 77 K. After exposition of TiO<sub>2</sub> photocatalyst to nitrates, the EPR signal typical of unpaired electron of oxygen vacancies was significantly reduced (Fig. 9C), confirming that surface defects are associated with NO<sub>3</sub><sup>-</sup> through electron transfer from Ti<sup>3+</sup> to NO<sub>3</sub><sup>-</sup>, and behaves as a reduction site for NO<sub>3</sub><sup>-</sup>. The important role of defect sites during the photocatalytic NH<sub>3</sub> production via N<sub>2</sub> fixation using water was also reported by Shiraishi *et al.* [59]. The authors show that the signal assigned to the unpaired electrons of the Bi(II) sites in bismuth oxychloride (BiOCl) decreases upon N<sub>2</sub> injection, confirming the electron transfer from Bi(II) to N<sub>2</sub> and the formation of Bi(III) species. Although EPR is extremely sensitive, the measurements are often performed in presence of a spin trap and/or at low temperature (below 77 K) in order to improve detection of the highly reactive species with unpaired electrons. This is particularly important to monitor charge carriers in photocatalysts where room temperature measurements are commonly impossible due to fast recombination. Due to these specific drawbacks, the application of EPR in photocatalysis is still scarce under *operando* photocatalytic conditions.

#### 2.4. *In-situ* XAS spectroscopy

X-ray absorption spectroscopy represents a powerful technique to investigate structural and electronic configuration of metal sites in nanostructured and bulk catalysts [60,61]. XAS spectrum is traditionally divided into two parts: X-ray Absorption Near Edge Structure (XANES) and Extended X-ray Absorption Fine Structure (EXAFS). XANES region allows to probe variation in oxidation state, density of unoccupied states, chemical bond hybridization, while EXAFS part is more sensitive to bond lengths and coordination environment. Compared to the other techniques (IR, Raman), XAS presents the advantage in both surface and bulk sensitivities. XAS most frequently used in transmission mode where the absorption coefficient  $\mu(E)$  is registered as a difference in the X-ray flux before and after it pass through the sample in the certain energy range around absorbing threshold, however it is highly demanding to the homogeneity and thickness of the sample. Thus, for photocatalytic application XAS acquisition is more frequently performed via X-ray fluorescence which allows signal registration in high-resolution mode- HERFD-XAS (High Energy Resolution Fluorescence Detection-X-ray Absorption Spectroscopy) [62]. In photocatalytic applications, *operando* XAS spectroscopy (more details in the *operando's* section) is mostly employed to shed light on the active site's oxidation state upon reaction conditions, while in some cases it allows to retrieve valuable information about their structural evolution. XAS spectroscopy has been extensively used in the last years for *in-situ* studies in photocatalysis in order to unravel the possible modification of photocatalyst after reaction [63,64]. In this part we consider the recent work dedicated to CO<sub>2</sub> photoreduction over pretreated Cu/TiO<sub>2</sub> catalyst (under air or H<sub>2</sub>) [22]. Cu K-edge XANES and EXAFS detected in fluorescence mode were employed to unravel oxidation state and structural difference and elucidate the changes of Cu speciation in Cu/Ti(air) and Cu/Ti(H<sub>2</sub>) samples.

Quartz tube reactor cell firstly reported by Zhao *et al.* [65] for catalytic study was adopted for XAS and employed in this work. The sample was coated on a glass slide as a thin film, loaded on a stainless-steel holder and then placed inside quartz tube (Fig. 10A). The UV light and X-ray fluorescence propagation was ensured by making a circular hole was made and taped with Teflon film. At the two ends of the quartz tube, the valves were sealed with a Kapton film. IR and mercury vapor UV lamps were used as a sample heater and a light source, respectively. The experiment was carried out at beamline 10D at the Advanced Photon Source (APS) at Argonne National Laboratory. It was found that the post-treated sample at 200 °C under H<sub>2</sub> (Cu/Ti(H<sub>2</sub>)) exhibits more than 50% higher activity for CO<sub>2</sub> photoreduction than the air-calcined one (Cu/Ti(air)) (Fig. 10B). This is explained by the higher population of Cu<sup>+</sup> species, as the active sites, in Cu/Ti(H<sub>2</sub>). In dark (Fig. 10C), the Cu/Ti(air) surface is predominant by Cu<sup>2+</sup> with an insignificant number of Cu<sup>+</sup>, while the pre-reduced Cu/Ti(H<sub>2</sub>) sample is characterized by significantly more intensive Cu<sup>+</sup> feature with a Cu<sup>+</sup>/Cu<sup>2+</sup> ratio of about 60/40. Under UV irradiation at 150 °C (Fig. 10C), no significant difference was observed in the copper speciation of Cu/Ti(air) while further decrease of Cu<sup>+</sup> component was detected in Cu/Ti(H<sub>2</sub>) with an equimolar ratio of Cu<sup>+</sup>/Cu<sup>2+</sup> after 120 min of reaction. The authors demonstrated that the origin of Cu/Ti(H<sub>2</sub>) deactivation is related with substantial oxidation of Cu<sup>+</sup> to Cu<sup>2+</sup> that occurs during the reaction. In the same study, the *in-situ* DRIFTS was also used to investigate the CO<sub>2</sub> photoreduction over pretreated Cu/TiO<sub>2</sub> catalyst and similar results were obtained (see the *in-situ* FTIR part 2.1.1).

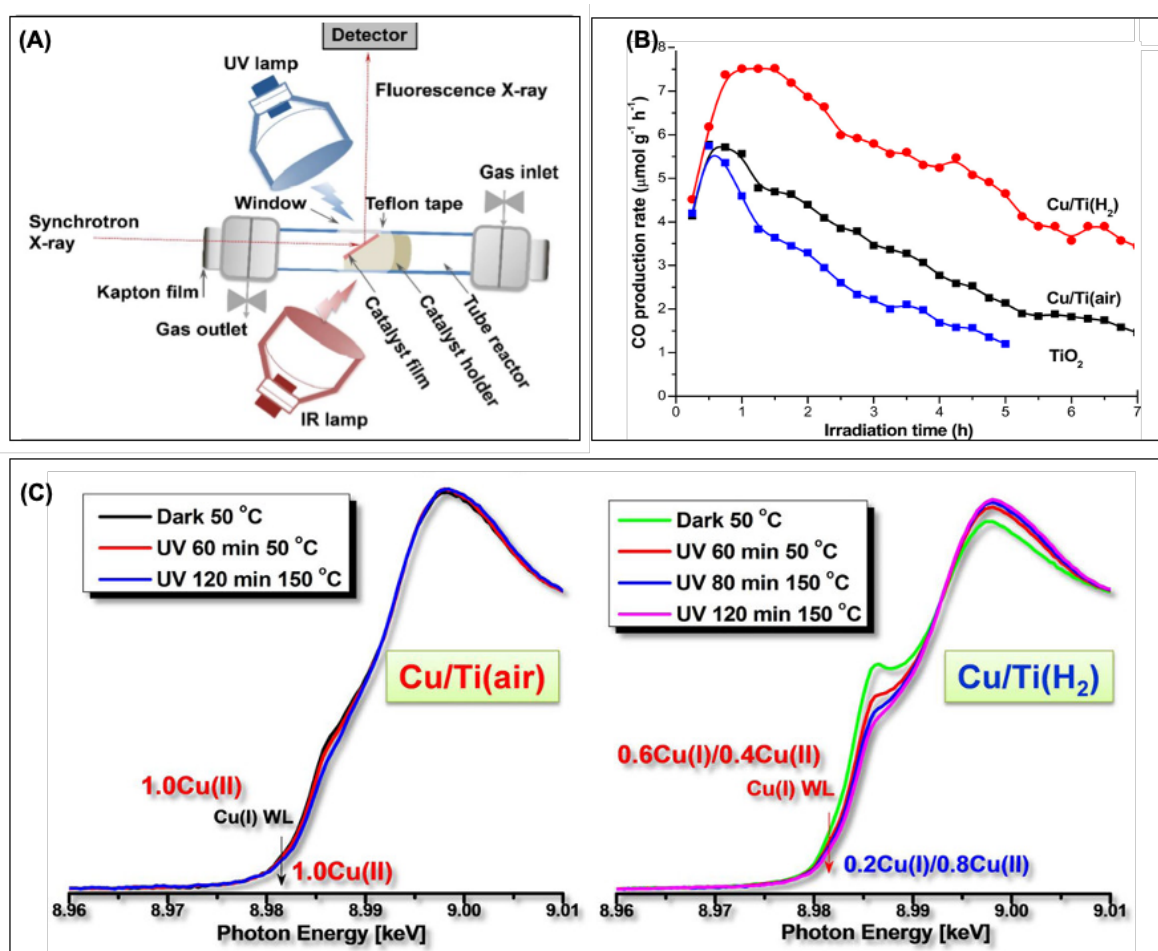


**Figure 10.** (A) Experimental setup based on quartz tube reactor allowing in situ XAS measurements, employed for similar catalyst in pellet form under CO<sub>2</sub> photoreduction conditions. (B) Rate of CO production from CO<sub>2</sub> photoreduction with H<sub>2</sub>O vapor over TiO<sub>2</sub>, Cu/Ti(air), and Cu/Ti(H<sub>2</sub>) under UV–vis irradiation. (C) *In-situ* XANES spectra for Cu/Ti(air) and Cu/Ti(H<sub>2</sub>) in dark at 50 °C and under different conditions of UV irradiations. (Copyright with the authors permission [22]).



### 3. Operando techniques in photocatalysis

To avoid a lengthy discussion, here we present the most used *operando* techniques in photocatalysis such as Infrared spectroscopy (DRIFTS, ATR-IR, SSITKA) [4,66-72], Raman [73] and X-ray absorption spectroscopy (EXAFS and XANES) [74,75,76] including some examples provided to better understand the reaction mechanisms.

#### 3.1. Operando FTIR spectroscopy in photocatalysis

*Operando* FTIR is a powerful technique to track the variations in the gas phase or on catalyst's surface at seconds time scale with high sensitivity and relatively rapid response. In photocatalysis, a homogeneous irradiation of the photocatalysts is very difficult. Consequently, the possible contribution of chemical reaction in the dark regions of the catalyst may complicate interpretation of the results. To overcome this problem, many reactors have been developed or modified for FTIR *operando* studies in photocatalysis [69,70,71,77]. The FTIR reactor must respond to a number of criteria such as: (i) homogeneous illumination of the photocatalyst; (ii) minimum leaching of photocatalysts in case of reaction in liquid phase; (iii) reduced dead volume (i.e. the residual space between the photoreactor windows and the sample (iv); (v) accurate control of the reaction parameters (e.g., contact time, temperature, irradiation intensity, reaction composition...). Here, the use of *operando* FTIR technique, essentially in transmission mode which allows to simultaneously and quantitatively analyze gas phase and the catalyst surface under the reaction conditions, will be illustrated by the most recent and conclusive case studies. Each case study, will present a brief description of the proper homemade/commercial reaction cells followed by the identification of the active sites and/or the reaction intermediates to unravel the reaction mechanism.

##### 3.1.1. Operando FTIR for investigating photocatalytic reactions in gas-phase

Despite the limitation of *operando* DRIFTS, this technique has been extensively used to study the photocatalytic reaction in gas phase [66,67,77,78,79]. For the sake of brevity, only the first we know of and a recent example are presented here. The Wu's work in 2006 [77] reported the *operando* study of the photocatalytic reaction of NO on TiO<sub>2</sub> and TiO<sub>2</sub>-supported Cu, V and Cr oxide catalysts in a Harrick HVC-DRP-1 cell. The DRIFT spectra show that NO adsorbs titrating surface hydroxyl, peroxy, or M=O species along with the formation of nitrosyls on oxide sites. DRIFTS show that bidentate nitrite oxidize to monodentate or bidentate nitrates upon photoexcitation, which appears associated with the generation of superoxy species. A recent *operando* DRIFTS addresses the photo-assisted hydrogenation of CO<sub>2</sub> over Au/TiO<sub>2</sub> under visible light at different temperatures from 150 to 500 °C [78]. In the experimental setup, 10 mg of the sieved catalyst (63-125 microns) was packed into the commercial Praying Mantis reactor. The reaction mixture of CO<sub>2</sub> (1 cc/min) and H<sub>2</sub> (4 cc/min) in argon (25 cc/min) as well as the gas products were monitored with mass spectrometer. The irradiation was provided by an external green (520 nm, 250.1 mW/cm<sup>2</sup>) and blue (445 nm, 320 mW/cm<sup>2</sup>) LED lights via an optical guide placed at the front quartz window of the reactor. Steady-State Isotopic Transient Kinetic Analysis (SSITKA) and kinetic isotope effect (KIE) were also performed to obtain transient condition by switching to labelled molecules (e.g. <sup>13</sup>CO<sub>2</sub> and D<sub>2</sub>) at the steady state of the reaction. The results show that the highest CO<sub>2</sub> conversion into CO over Au/TiO<sub>2</sub> is obtained at 500 °C under green light (Fig. 11A). The main reaction pathway is the direct dissociation of CO<sub>2</sub> at the oxygen vacancy (VO) of Au/TiO<sub>2</sub> via redox mechanism. When switching from <sup>12</sup>CO<sub>2</sub> to <sup>13</sup>CO<sub>2</sub> both in dark and under visible light, the IR peaks of surface bicarbonates (HCO<sub>3</sub><sup>\*</sup>, 1440 cm<sup>-1</sup>) and carbonates (CO<sub>3</sub><sup>\*</sup>, 1560 cm<sup>-1</sup>) gradually decrease, while that of formates (HCOO<sup>\*</sup>, 2955 cm<sup>-1</sup>) remains unchanged. A shift to lower wavenumber of CO<sub>3</sub><sup>\*</sup> and HCO<sub>3</sub><sup>\*</sup> IR peaks, without any changes in the HCOO<sup>\*</sup> band, was also observed after exchange with <sup>13</sup>CO<sub>2</sub> in absence of H<sub>2</sub>. Furthermore, no correlation was found between the surface residual time of CO<sub>3</sub><sup>\*</sup> and HCO<sub>3</sub><sup>\*</sup> surface species and that of produced CO. The former species were also not sensitive to the intensity of the incident light. This confirms that all of HCOO<sup>\*</sup>, CO<sub>3</sub><sup>\*</sup> and HCO<sub>3</sub><sup>\*</sup> surface species are spectators. The labelled CO<sub>2</sub> experiments conducted on a clean (without carbon species) and reduced Au/TiO<sub>2-x</sub> sample (with oxygen vacancies) in absence of H<sub>2</sub> at 200 °C, showed the shift to lower wavelength of two peaks at 2176 and 2077 cm<sup>-1</sup> assigned to <sup>12</sup>CO adsorbed on Ti<sup>4+</sup> and Au<sup>δ-</sup> sites of Au/TiO<sub>2-x</sub> (Fig. 11C). Furthermore, the H/D kinetic isotope effects (KIE) measured in dark and under visible irradiation in the range of 200-400 °C were smaller than 1 in all cases (Fig. 11B). This is an unambiguous evidence of dissociative adsorption of CO<sub>2</sub> on the Au/TiO<sub>2-x</sub> which rule out involving of the bond formation/cleavage with H/D as elementary steps.

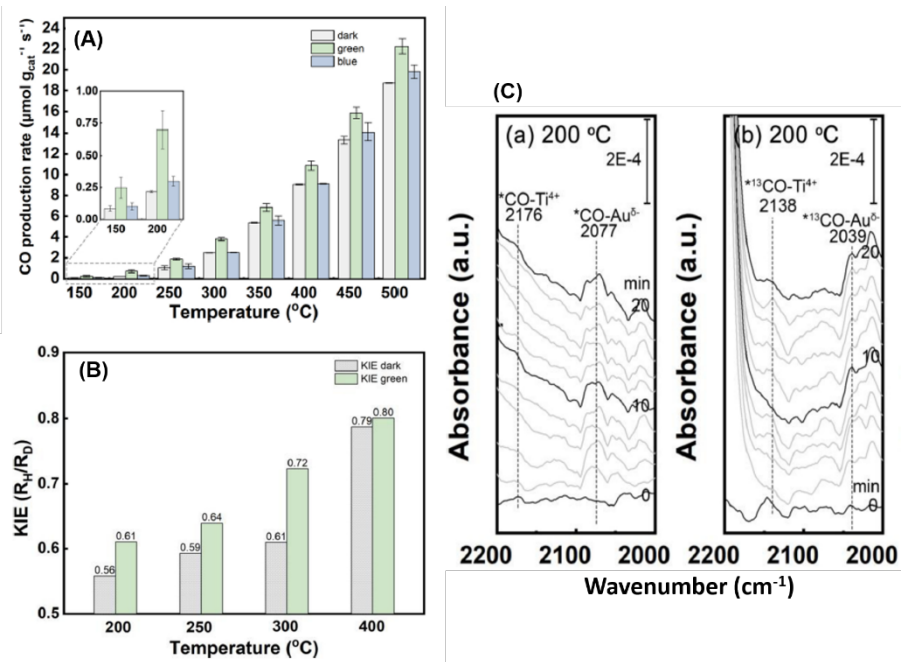


**Figure 11.** (A) The CO production rates over Au/TiO<sub>2</sub> photocatalyst during the photo-assisted CO<sub>2</sub> hydrogenation at temperature ranging from 150 to 500  $^{\circ}\text{C}$  under dark, green light and blue light irradiation. The inset is the magnification of columns at 150 and 200  $^{\circ}\text{C}$ . (B) H<sub>2</sub>/D<sub>2</sub> kinetic isotope effects of RWGS reaction under dark or green-light irradiation condition at different temperature. (C) time-resolved DRIFT spectra of CO<sub>2</sub> interaction with reduced Au/TiO<sub>2-x</sub> in flowing Ar with the absence of H<sub>2</sub>: (a)  $^{12}\text{CO}_2$  (b)  $^{13}\text{CO}_2$  at 200  $^{\circ}\text{C}$ . (copyright with the authors permission [78]).

Knowing that transmission IR is the technique of choice to simultaneously analyze the surface and gas phases during *operando* studies, some examples are discussed in details in this part. In 2009, the photooxidation of acetone over TiO<sub>2</sub>-ZrO<sub>2</sub> thin films has been studied by the *operando* FTIR technique [70] using a modified version of the IR transmission *in-situ* cell designed by M.A. Anderson group in 2004 [80]. In the new version, the contact time between the gas and the photocatalysts was maximized by flowing the gas on the two sides of catalyst (Fig. 12A). The cell is equipped with quartz and BaF<sub>2</sub> windows that are transparent to UV-Vis and IR irradiations, respectively. In the experimental set-up, the Si wafer coated with the photocatalytic thin films is placed in the reactor and then equilibrated with acetone vapor (0.5  $\mu\text{L}$  of liquid) for 40 min prior to the reaction with a total flow rate of 75  $\text{cm}^3/\text{min}$ . Then, the films are irradiated in air with four UV lamps externally placed in an aluminum frame. The total volume of the system was about 0.55 L. The FTIR spectrum are simultaneously recorded for the catalyst surface (200 scans, 4  $\text{cm}^{-1}$  of resolution) and the gas phase (64 scans, 1  $\text{cm}^{-1}$  of resolution), noting that interferences with the surface bands are not significant.

The obtained results indicate that the TiO<sub>2</sub>(90%)-ZrO<sub>2</sub>(10%) mixture exhibits the highest conversion rate for acetone photodegradation under UV-light, compared to Ti<sub>0.9</sub>Zr<sub>0.1</sub>O<sub>2</sub> mixed oxide and TiO<sub>2</sub>. The CO<sub>2</sub>, H<sub>2</sub>O and minor amount of CO are the only products detected in the gas phase over the three samples. It was concluded from surface analysis that the presence of Zr centers seems to promote the formation of formate beside formaldehyde as intermediates, while formaldehyde is the only surface species detected on the TiO<sub>2</sub> film. The reaction pathway over TiO<sub>2</sub>(90%)-ZrO<sub>2</sub>(10%) mixture contains three main steps (Fig. 12B): i) the rapid acetone adsorption equilibrium in dark, ii) the transformation of the adsorbed acetone to formaldehyde and formate as intermediate surface species upon UV-irradiation and the iii) oxidation of formaldehyde which is quicker than that of formate into CO<sub>2</sub>. This is confirmed by the evolution of the surface species and their integrated intensity during the photocatalytic reaction (Fig. 12B(a-b)), which shows the progressive decrease of IR acetone bands (1703, 1371, 1241  $\text{cm}^{-1}$ ) after tuning on the lamp. Then, formate and formaldehyde species appeared at 1569 (broad) and 1744  $\text{cm}^{-1}$ , respectively. However, after 120 min of irradiation, formate species were completely removed and a new band appeared at 1447  $\text{cm}^{-1}$  due to the formation of bicarbonates on catalyst surface. Two years later, the same IR transmission *in-situ* cell was used to understand the effect of the chemical structure of the pollutants (methylcyclohexane (MCH) and toluene) on the photocatalytic activity of TiO<sub>2</sub>-ZrO<sub>2</sub> thin films [66]. It was shown that the aromatic character of toluene plays a key role in the catalyst deactivation, while this process was inhibited during the photooxidation of cyclohexane. The deactivation process was correlated to the formation of benzoate complexes strongly adsorbed on the catalyst's surface, which block the access to the active sites and the regeneration of hydroxyl groups (deduced from the intensity of OH band at 3690  $\text{cm}^{-1}$ ) (Fig. 12C(a)). By contrast, no deactivation was observed during the photooxidation of MCH due to the weak interaction of the reaction intermediates (i.e. cyclohexanone) with the catalyst surface as well as the full regeneration of OH groups (Fig. 12C(b)). It should be noted that the configuration used in both studies, in

which the Si wafers were coated with the photocatalytic thin films, ensures full illumination of the sample with however a reduced signal intensity due to the low mass of the photocatalyst and low-efficient flow distribution due to the preferential paths.

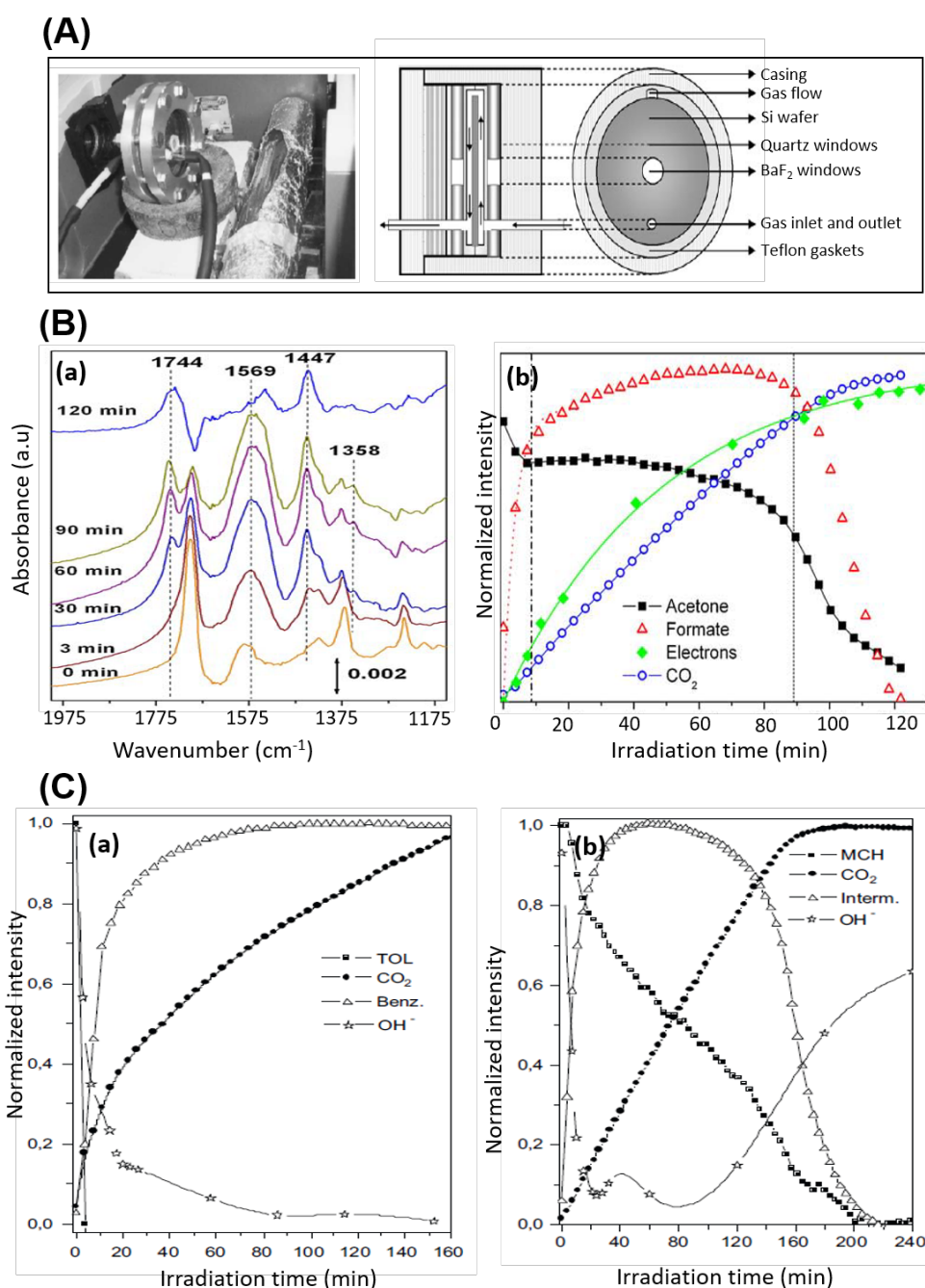
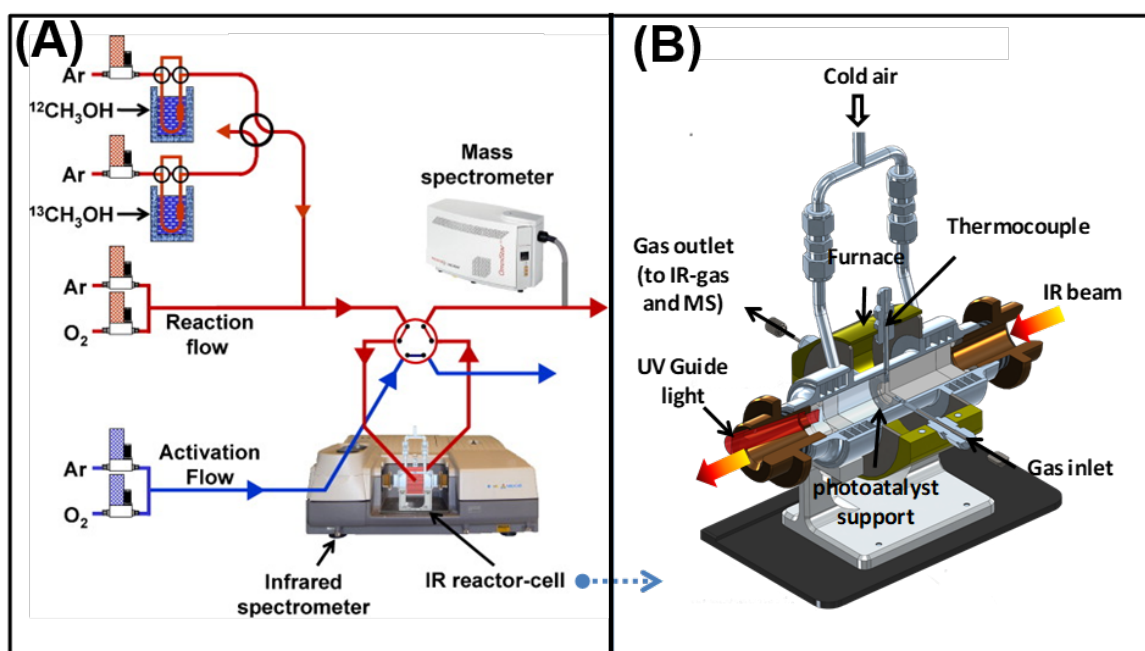


**Figure 12.** (A) picture and cross-section view of the transmission cell used to test the photocatalytic activity of the thin films showing the path followed by the gas stream inside this device and the materials used for manufacturing the different components. (B) (a) FTIR spectra in the 2000–1150  $\text{cm}^{-1}$  range of the  $\text{ZrO}_2(10\%)\text{-TiO}_2(90\%)$  sample contacted with acetone vapor ( $0.5 \mu\text{L}$  of liquid) and subsequently UV-irradiated for increasing periods of time as indicated in graphs. Spectra of the photocatalytic coating before acetone adsorption have been subtracted in order to highlight the bands corresponding to surface species and variation of the normalized intensities of adsorbed species; (b) Evolution of acetone (squares), formate (up-triangles), aldehydes (down-triangles),  $\text{CO}_2$  production (circles) and photogenerated electrons (diamonds) detected during UV-irradiation of the  $\text{ZrO}_2(10\%)\text{-TiO}_2(90\%)$  sample. The later are represented by plotting the increment in background intensity at ca.  $1020 \text{ cm}^{-1}$  as a function of irradiation time. Vertical lines mark the different stages of the photocatalytic processes. (C) Evolution of adsorbed (a) toluene and (b) MCH,  $\text{CO}_2$  and intermediates during UV irradiation over  $\text{TiO-ZrO}_2$  mechanical mixture. (Copyright with permission from Ref. [70,80]).

From 2012 and successively, a new *operando* IR reactor [81] has been reported by El-Roz *et al.* to study photocatalysis reaction for air purification (e.g. photooxidation of methanol, CO<sub>2</sub> photoreduction, photo-assisted Selective Catalytic Reduction of NO<sub>x</sub>) [4,82-86]. In the photocatalytic experiments (scheme 3), the light irradiation was delivered by UV-Vis lamp connected to an optical fiber light-guide placed at the entrance of the cell to ensure a homogeneous irradiation of the pellet (self-supported pellets of ~20 mg and 2 cm<sup>2</sup>). This reactor presents several advantages: (i) the thin pellet-shaped sample which limit the mass loss and ensures a homogeneous illumination of catalyst; (ii) the control of irradiation parameters (intensity, mono or polychromatic, UV or Vis light...) without replacement of the photoreactor; (iii) the reduced dead volume ~0.4 mL; (iv) the online analysis techniques (IR, GC, MS and etc..) providing high precision data and (v) the accurate control of the reaction temperature (25-600 °C), the gas composition/concentrations (from few ppm to a few percent) and the gas flow (1-50 cm<sup>3</sup>/min). In what follows, some examples on *operando* FTIR photocatalytic studies conducted by El-Roz group's using the FTIR reactor cell described above are presented.



**Scheme 3.** *Operando* setup (A) and Sandwich Reactor IR cell (B) modified by El Roz *et al* for studying UV-Vis Photocatalysis. (Copyright with the authors permission [82]).

The photocatalytic oxidation of methanol over TiO<sub>2</sub>-based catalysts has been extensively studied by El-Roz *et al.* as a model reaction. The FTIR *operando* spectroscopy coupled with SSITKA was used to clarify the role of formate species during methanol photooxidation over Hierarchical TiO<sub>2</sub> (TiO<sub>2</sub>-L) [4]. In the experimental set-up, the self-supported wafers (20 mg) were exposed to the reaction mixture of 400-1200 ppm MeOH and 20 % O<sub>2</sub> in argon with 25 cm<sup>3</sup>/min total flow. The UV irradiation was provided by a Xe-Hg lamp (200 W, I<sub>0</sub> = 2 mW/cm<sup>2</sup>). The photocatalytic reaction was simultaneously monitored by IR spectroscopy coupled with mass spectrometry (MS). It was concluded that only a minor part of formate species are involved in the reaction and most of them are spectators, while methoxy groups are the first intermediates during methanol photooxidation. This is confirmed by SSITKA experiments in which the isotopic exchange rate of surface methoxy groups (methoxy <sup>12</sup>C: 1150 cm<sup>-1</sup> and methoxy <sup>13</sup>C: 1090 cm<sup>-1</sup>) was similar to that of the final gas products, while formate species (formate <sup>12</sup>C: 1574 and 1366 cm<sup>-1</sup> and formate <sup>13</sup>C: 1515 and 1340 cm<sup>-1</sup>) reacted too slowly, compared to the CO<sub>2</sub> (2400-2200 cm<sup>-1</sup>) and methyl formate (1800-1600 cm<sup>-1</sup>) production rate (Fig. 13A-B). Interestingly, the *operando* experiments allow to highlight the possible sites for the formation of weakly or not active formate species. By plotting the IR band of surface formate species vs. that of the TiOH group at 3720 cm<sup>-1</sup>, a linear relationship was obtained which highlight the role of hydroxyls on the formation/stabilization of low-active formate species under UV irradiation (Fig. 13C).

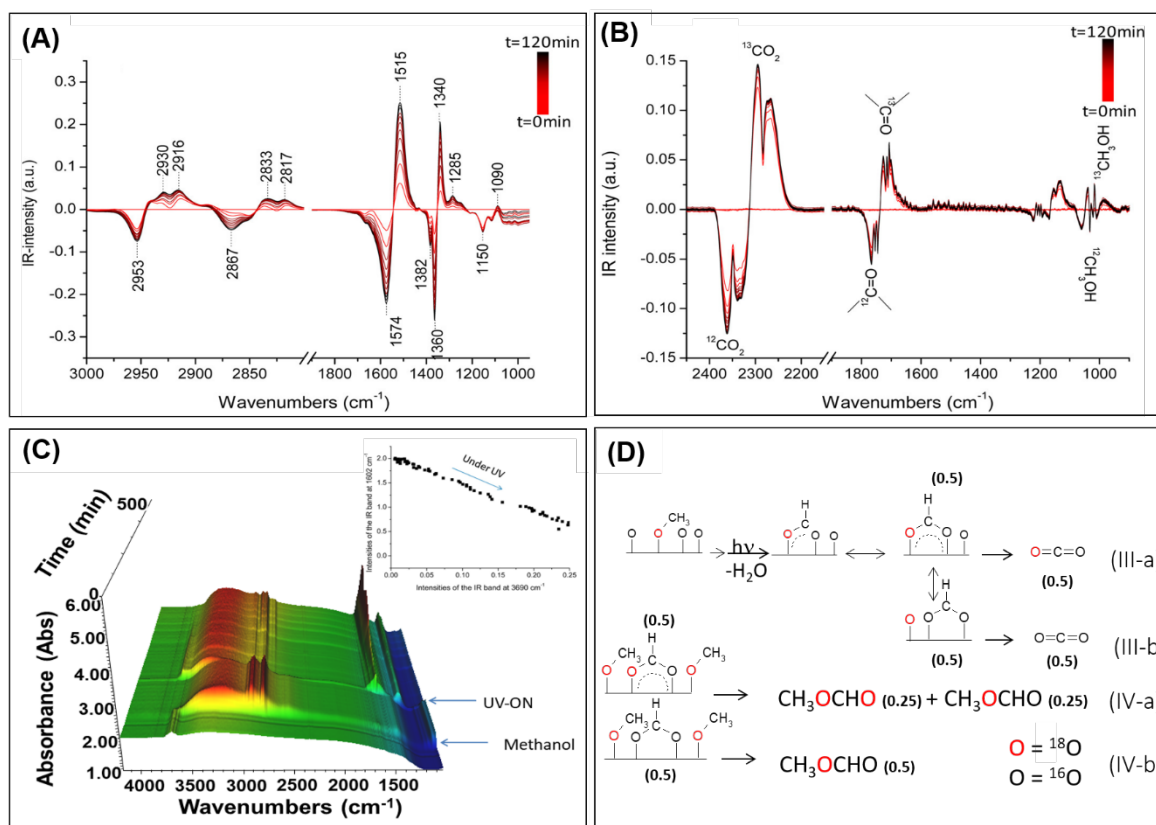


**Figure 13.** (A) IR spectra of TiO<sub>2</sub>-P25 and (B) the reaction gas phase during a SSITKA experiment for which an initial flow of 1200 ppm of <sup>12</sup>CH<sub>3</sub>OH, 20% of oxygen diluted in Ar (total flow = 25 cm<sup>3</sup> min<sup>-1</sup>) was switched to a similar but labeled (<sup>13</sup>CH<sub>3</sub>OH) flow (the spectrum recorded at  $t = 0$  was used as background). (C) Evolution of the IR spectra of TiO<sub>2</sub>-L during methanol photooxidation. Insert: correlation between the IR band areas at 1602 cm<sup>-1</sup> and 3690 cm<sup>-1</sup>. (D) Mechanism of the formation of carbon dioxide and methylformate during CH<sub>3</sub><sup>18</sup>OH photooxidation. <sup>16</sup>O (in black) correspond to the oxygen coming from TiO<sub>2</sub> surface (bridged oxygen) and/or molecular oxygen chemisorbed on TiO<sub>2</sub> (oxygen adatom), while <sup>18</sup>O (in red) is coming from CH<sub>3</sub><sup>18</sup>OH. (Copyright with permission from Ref. [4,84]).

The FTIR *operando* spectroscopy has been also used to study the methanol concentration effect on the activity/selectivity of hierarchical TiO<sub>2</sub> (TiO<sub>2</sub>-L) during methanol photooxidation [84]. It was concluded that the methanol concentration influences greatly the selectivity of TiO<sub>2</sub> during the MeOH photooxidation under UV light. At 500 ppm of MeOH, a total conversion and selectivity of MeOH into CO<sub>2</sub> and H<sub>2</sub>O were obtained, while they decreased (75 % MeOH conversion and 60 % CO<sub>2</sub> selectivity) by increasing the MeOH concentration at 1200 ppm due to the formation of a secondary product, i.e. methylformate (MF) in the gas phase. The formation of MF is favored by a high coverage of surface methoxy groups and their further cross-coupling reaction with the neighboring formyl/formate species. All of these results were discussed in details using CD<sub>3</sub>OH, CH<sub>3</sub><sup>18</sup>OH and CH<sub>3</sub>OH/<sup>13</sup>CH<sub>3</sub>OH SSITKA experiments. During the CH<sub>3</sub><sup>18</sup>OH experiments, the formation of 3% labelled CO<sub>2</sub> (C<sup>18</sup>O<sup>18</sup>O) via <sup>18</sup>O-formyl intermediates bridged over <sup>18</sup>O-surface sites was observed (Fig. 13D). It was suggested that the <sup>18</sup>O-surface sites originate from the scrambling of formate species on the TiO<sub>2</sub>. C<sup>16</sup>O<sub>2</sub> and CH<sub>3</sub><sup>18</sup>OCH<sup>16</sup>O were the unexpected major products. The difference between the expected statistical value of the intermediate and of the final products in respect to the experimental values confirms the formate scrambling hypothesis. In the same *operando* study [84], the authors shed light on the shading effect, i.e. inhomogeneous irradiation with the catalyst's depth, on the MeOH photooxidation under UV light over three different pellets: i) a self-supporting pellet of 20 mg (diameter 16 mm, thickness 50-70 μm), a supported pellet of 5 mg on a stainless still grid (diameter 6 mm, thickness 50-70 μm) and iii) supported TiO<sub>2</sub> (~ 3 mg) on a KBr window (diameter 16 mm, < 10 μm thickness). A significant activity difference was observed between the three cases confirming the shading effect, which was at minimum for TiO<sub>2</sub> powder supported on KBr. More recently, Wolski *et al.* [87] reported that the nature of the light source (UV *vs.* visible light) greatly influences the selectivity of MeOH photooxidation over the bimetallic Au-Cu-Nb<sub>2</sub>O<sub>5</sub> catalyst. Under visible light, both Cu and Au are activated, which promotes the total oxidation of MeOH into CO<sub>2</sub>. By contrast, the Cu, Au and Nb<sub>2</sub>O<sub>5</sub> are all excited under UV irradiation, leading to the formation of partial oxidation products such as formaldehyde, methyl formate and dimethoxymethane. These differences in the

reaction pathways were ascertained from the FTIR surface analysis during the reaction: the surface formate species (band at  $1583\text{ cm}^{-1}$ ) and all intermediates are immediately transformed into  $\text{CO}_2$  by changing the light source from UV to visible irradiation, without the formation of other intermediates.

### 3.1.2. Operando FTIR for investigating photocatalytic reactions in liquid-phase

Since that *operando* FTIR in DRIFTS or transmission mode are not suitable for photocatalytic reaction in liquid phase, the ATR-FTIR is the most used technique to monitor the catalyst surface in contact with a liquid phase. Very recently, an *operando* ATR-FTIR device was used to study the photocatalytic water splitting over  $\text{Ga}_2\text{O}_3$ -based photocatalysts ( $\text{Rh}_{0.5}\text{Cr}_{1.5}\text{O}_3/\text{Ga}_2\text{O}_3(\text{Zn})$ ) [88]. The ZnSe was coated with 1 mL of aqueous catalyst slurry (1.6 mg/mL) to form a catalyst film with 0.7 or 4.2  $\mu\text{m}$  of thickness. Then, 0.3 g of distilled water was introduced into the cell under He with 15 cc/min total flow. The UV-irradiation was provided by a laser ( $\lambda = 263\text{ nm}$ , power = 110 mW) fixed on the top of the catalyst film with an adjusted spot to match the shape of the catalyst by using a set of optics. During the reaction, the catalyst surface and the gas phase were monitored by ATR-IR and mass spectrometer, respectively. A direct hydroxyl radical formation from the oxygen atoms in  $\text{H}_2\text{O}$ , without evolving the lattice O atoms of the photocatalysts was proved. Under UV irradiation, the IR spectrum of the photocatalyst film in contact with water shows three bands at 872, 1382 and  $978\text{ cm}^{-1}$  (Fig. 13A(a)). The two first bands were assigned to the stretching and bending modes of the physically adsorbed  $\text{H}_2\text{O}_2$ , while the third one was attributed to the negatively charged hydroperoxide group, i.e.  $\text{Ga-OOH}^-$  surrounded by water molecules. These assignments were confirmed by the band shifts observed after isotopic exchange ( $\text{D}_2\text{O}$  and  $\text{H}_2^{18}\text{O}$ ) (Fig. 14A(a-b)). Noting that the frequencies of the stretching and bending mode of O-H in the physically adsorbed  $\text{H}_2\text{O}_2$  are respectively not sensitive to H-D and  $^{18}\text{O}$  isotopic exchange (Fig. 14A(c)). In addition, only  $^{18}\text{O}^{18}\text{O}$  was detected by mass spectroscopy in the  $\text{H}_2^{18}\text{O}$  isotopic-exchange. This confirms that the oxygen atoms in  $\text{H}_2\text{O}$  are the sole source of water splitting and that the lattice O atoms in the photocatalysts do not participate to the reaction.

*Operando* ATR-IR combined with modulation excitation spectroscopy (MES) was also reported and used to study the performance of Au-Fe/ $\text{TiO}_2$  nanocomposite during the photodegradation of azo dye (Orange II) under UV and at RT [89]. Catalyst layers were prepared by the deposition-evaporation method on Ge IRE. The OII solutions were connected to two ATR-IR reactor cells with and without catalyst layer in order to simultaneously monitor the catalyst's surface and the liquid phase during the reaction (Fig. 14B). Both surface and liquid spectra were recorded by altering the feeding of two different solutions (Orange II +  $\text{H}_2\text{O}$  +  $\text{O}_2$  + UV  $\leftrightarrow$   $\text{H}_2\text{O}$  +  $\text{O}_2$  + UV) over Au-Fe/ $\text{TiO}_2$  with different Au/Fe ratios (0, 1:2, 1:1 and 1:0.5). It was concluded that the increase of Fe loading in Au/ $\text{TiO}_2$  leads to slower the adsorption of Orange II and weakens the dye-catalyst interaction, resulting in a fast photodecomposition. By contrast, the stronger adsorption of Orange II on Au/ $\text{TiO}_2$  seems to suppress its photodecomposition.

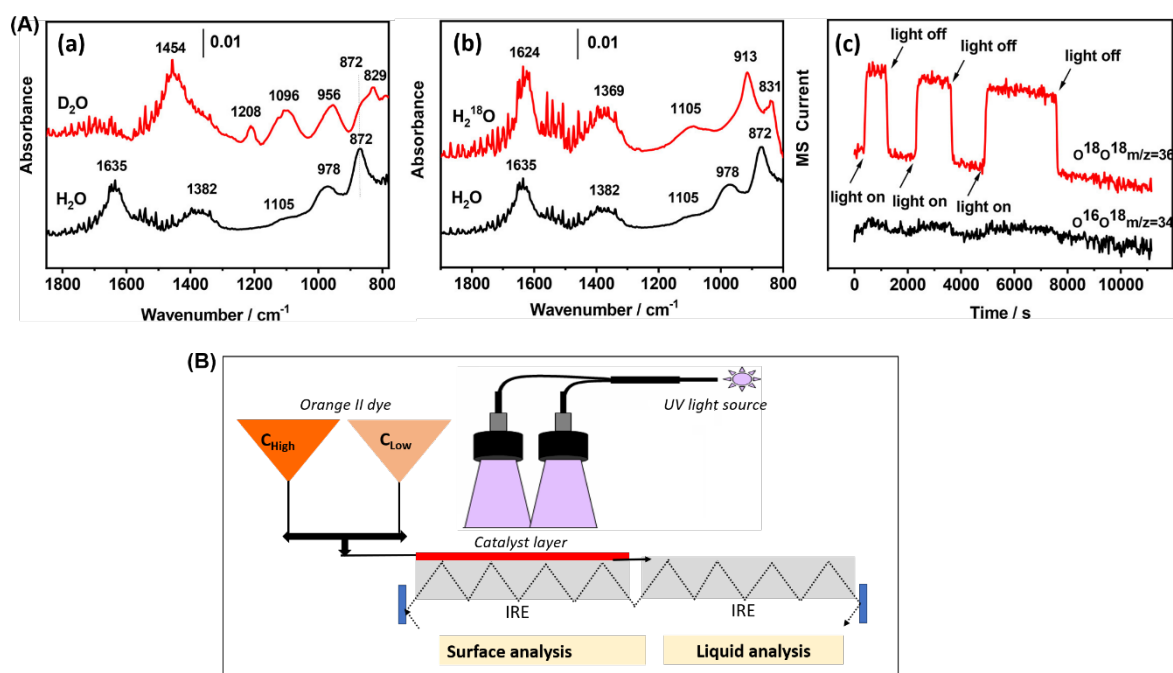


**Figure 14.** (A) ATR-FTIR absorption spectra of the 4.2  $\mu\text{m}$   $\text{Rh}_{0.5}\text{Cr}_{1.5}\text{O}_3/\text{Ga}_2\text{O}_3(\text{Zn})$  film in contact with (a)  $\text{D}_2\text{O}$  or  $\text{H}_2\text{O}$  and (b)  $\text{H}_2^{18}\text{O}$  or  $\text{H}_2\text{O}$  irradiated by 263 nm laser, with the spectrum taken before the laser irradiation as the background and (c) time courses of MS current for  $^{16}\text{O}^{18}\text{O}$  ( $m/z = 34$ ) and  $^{18}\text{O}^{18}\text{O}$  ( $m/z = 36$ )

evolved in the photocatalytic splitting of  $\text{H}_2^{18}\text{O}$  the photocatalyst. Three reaction cycles with the irradiation light being chopped on and off are shown. (B) Scheme of the MES-ATR-IR *operando* set-up during photodecomposition of Orange II over Au-Fe/TiO<sub>2</sub> (Copyright with the authors permission [88,89]).

### 3.2. *Operando* Raman spectroscopy

The *operando* Raman technique is a useful technique to monitor the structural transformation of photocatalysts as well as to identify the reaction intermediates under real reaction conditions. However, the application of *operando* Raman spectroscopy in photocatalytic reaction is still limited because photocatalysis excitation light may overwhelm Raman photons. For this reason, Raman is usually used in complementary to IR. To the best of our knowledge, the *operando* Raman spectroscopy is mainly used to monitor photocatalytic reactions in liquid phase. In this section, some case studies are presented where *operando* Raman spectroscopy is used to monitor process during photocatalytic reactions.

#### 3.2.1. *Operando* Raman for investigating photocatalysis in liquid-phase

For example, M. A. Bañares *et al.* [90] studied the photocatalytic epoxidation of cyclohexane in the presence of *tert*-butyl hydroperoxide (t-BuOOH) over V<sub>x</sub>Ti<sub>y</sub>/MCM-41 catalyst under UV-light using the real-time NIR-Raman spectroscopy. In the experimental set-up (Fig. 15A), the reaction in liquid phase was monitored with a Photonics immersion probe fitted to a Perkin-Elmer Raman Station 400F system. An NIR filter (cut off above 750 nm) was used to cancel any residual radiation that might interfere with Raman signals. The Raman spectra were acquired every 10 min with 6 accumulations of 10 s.

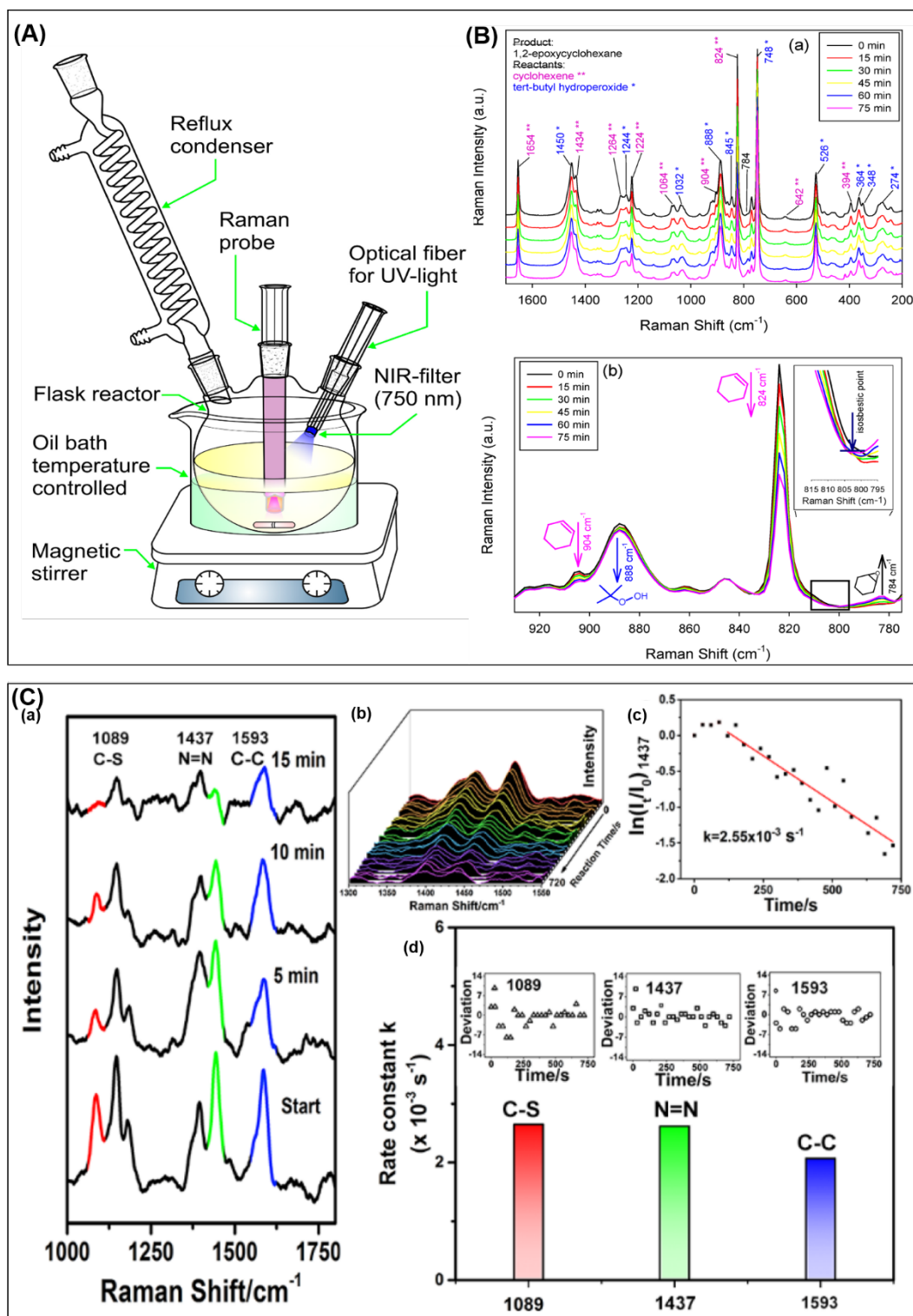


**Figure 15.** (A) Reaction system for the liquid-phase epoxidation and (B) Representative Raman spectra during the photocatalytic cyclohexene epoxidation with t-BuOOH over  $V_{0.25}Ti_2/MCM-41$  catalyst at 60 °C for 75 min: (a) full spectra; (b) partial spectra in range of 775–930  $cm^{-1}$ . (C) (a) SERS spectra of PATP on  $TiO_2$  IO under the irradiation of 532 nm laser for 15 min with a time interval of 5 min; (b) evolution of  $\nu N=N$  peak recorded with a time interval of 30 s; (c) the logarithm of  $(I/I_0)_{1437}$  processed using the normalized vibration peak intensity of  $TiO_2$  at 146  $cm^{-1}$  as an internal control; (d) reaction rate constants for the cleavage of C-S, N=N and C-C bonds under the long-time irradiation of 532 nm laser with a power of 5.0 mW and the corresponding wavenumber deviation collected at different time (inset). (Copyright with permission from ref [90,91]).

It was showed that the cyclohexene was directly photo-epoxidized over  $V_{0.25}Ti_2/MCM-41$  into 1,2-epoxycyclohexane (Raman peak at 784  $cm^{-1}$ ) with 100 % selectivity (Fig. 15B(a)). The presence of an isosbestic point at 800  $cm^{-1}$  between the decreased Raman band of cyclohexene (824  $cm^{-1}$ ) and the increased one of epoxide (784  $cm^{-1}$ ) indicates the absence of any stable intermediates during the reaction (Fig. 15B(b)). In



another example, the Surface Enhanced Raman Scattering (SERS) was used to monitor the photooxidation of p-aminothiophenol (PATP) on  $\text{TiO}_2$  under 532 nm laser irradiation [91]. In the experimental part, the  $\text{TiO}_2$  was used as the SERS substrate and the photocatalyst on which the PATP are chemisorbed. The SERS spectra were then collected with an accumulation time of 30 s. The  $\text{TiO}_2$  Raman band at  $146 \text{ cm}^{-1}$  was used as an internal intensity standard due to its stability during the long-time irradiation. The results show that the photodegradation of pATP is initiated by the formation of azo compounds (Fig. 15C(a)). Interestingly, the SERS allowed determining the decomposition rate of  $\text{N}=\text{N}$  ( $1437 \text{ cm}^{-1}$ ),  $\text{C}-\text{S}$  ( $1089 \text{ cm}^{-1}$ ) and  $\text{C}-\text{C}$  ( $1593 \text{ cm}^{-1}$ ), which follow a first-order kinetic process with a reaction rate in the range of  $2.1\text{-}2.7 \times 10^{-3} \text{ s}^{-1}$  (Fig. 15C(b-d)). The *operando* Raman has been recently used to study the photocatalytic Hydrogen Evolution Reaction (HER) over  $\text{MoS}_2\text{xSe}_{2(1-x)}$  nanosheets under realistic reaction conditions [92]. In the experimental set-up (Fig. 16A), the AM 1.5G illumination ( $100 \text{ mW cm}^{-2}$ ) was used as a light source. The laser wavelength was 532 nm with 5 mW of light intensity, and the exposure time was 5 s. It has been demonstrated that hydrogen atoms are initially adsorbed on the S and Se active sites to form S-H and Se-H intermediate species followed by its subsequent redox reaction (Fig. 16B). An exponential function relationship was established between the Raman intensity of these intermediate species and the number of reactive electrons, which can be used as a guideline to evaluate the hydrogen production performance of the photocatalyst. More recently, Wang *et al.* [93] have designed a simple method to measure the photocatalyst's surface temperature by *operando* Raman spectroscopy using 4-methoxyphenyl isocyanide (MI) as a probe molecule. The  $\nu\text{N}=\text{C}$  frequencies of MI adsorbed on the catalyst surface are linearly dependent on temperature (Fig. 16C(a-b)). This method was used to unravel the photocatalytic mechanism induced by hot carriers and photothermal effect during the HER over Ag-Au-Ag and Au-Ag/Ag<sub>2</sub>S heterojunction nanorods (HJNRs). Although the hot spots temperatures of the Ag-Au-Ag HJNRs are higher than those for the Au-Ag/Ag<sub>2</sub>S HJNRs, the latter exhibits higher photocatalytic activity due to the higher contribution of the hot carrier effect (Fig. 16C(c-d)).

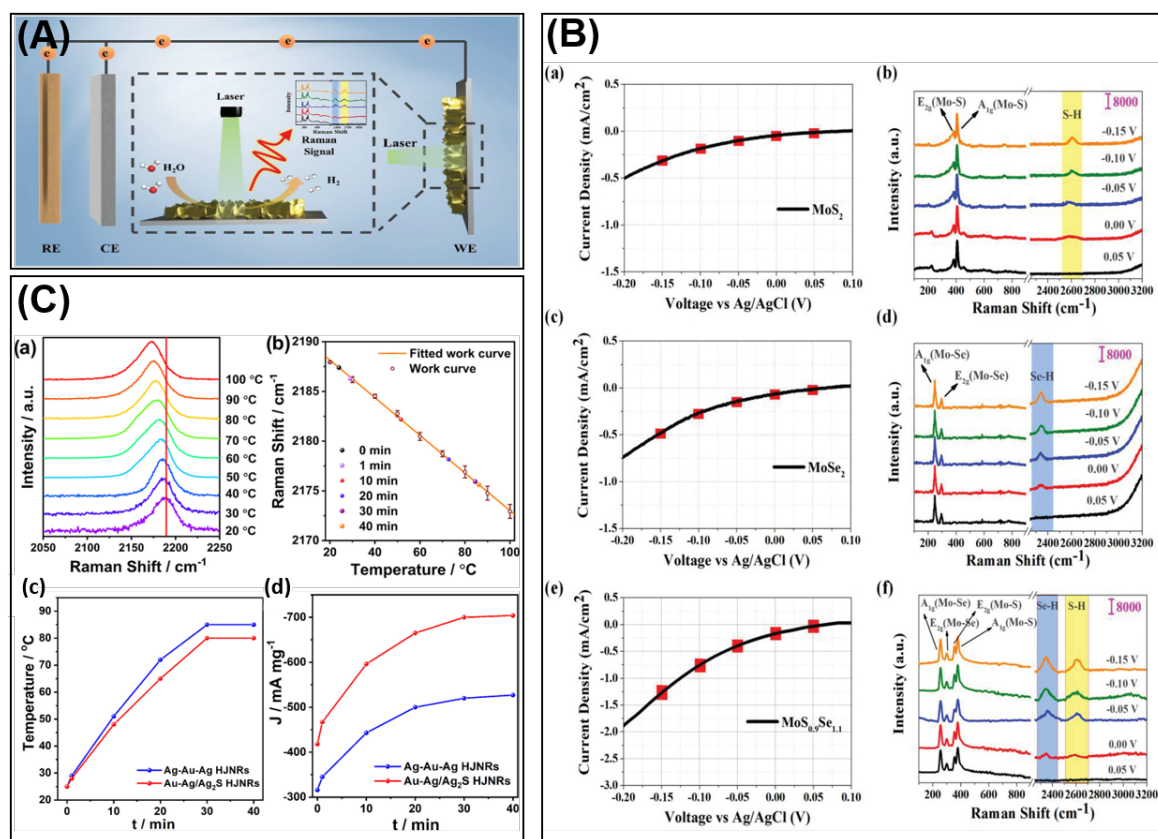


**Figure 16.** (A) The schematic of the photoelectrochemical system with LSV-Raman analysis. The measured material is  $\text{MoS}_{2x}\text{Se}_{2(1-x)}$ . The reference electrode, counter electrode, and working electrode are termed as RE, CE, and WE, respectively. Evolution of (B) LSV vs. the voltage (0.05, 0.00, -0.05, -0.10, and -0.15 V) and the Raman spectra of the samples (a,b)  $\text{MoS}_2$ , (c,d)  $\text{MoSe}_2$  and (e,f)  $\text{MoS}_{0.9}\text{Se}_{1.1}$ . (C) (a) SERS spectra of MI on the Au-Ag/Ag<sub>2</sub>S HJNRs at different temperatures. (b) Dependence of fitted temperature on the Raman shifts of MI for the Au-Ag/Ag<sub>2</sub>S HJNRs. (c) Hot spots temperatures of the Ag-Au-Ag and Au-Ag/Ag<sub>2</sub>S HJNRs illuminated for different times; (d) photocatalytic activity of the Ag-Au-Ag and Au-Ag/Ag<sub>2</sub>S HJNRs illuminated for different times. (Copyright with permission from Ref. [92,93]).

### 3.3. Operando XAS spectroscopy

In this section we will report some recent case studies where *operando* XAS has been applied on different photocatalytic reactions, such as methanol photo-reforming and photocatalytic HER. In the context of cell design, all the aforementioned criteria for FTIR cell are valid also for *operando* XAS reactors. Among listed criteria– matching between the light illuminated, reaction mixture exposed and the spectroscopic probed sample volumes – is of particular importance when XAS is used as a probe technique, being sensitive both to the bulk and surface species. The light propagation issue was thoroughly investigated for the most widespread Ti-based photocatalyst in the recent work by U. Caudillo-Flores and co-workers [73].

#### 3.3.1. Operando XAS for investigating photocatalysis in gas-phase

In the recent work by M.J. Munoz-Batista [74], spatially resolved XAS study of Cu-Ni TiO<sub>2</sub> catalytic bed upon methanol reforming using a micro-beam mode (BM23 beamline ESRF) was reported. The cell made of Inconel alloy with high resistance to reducing and oxidizing atmospheres for a wide range of temperatures 25-600 °C, is a modified version of that developed by Agostini *et al.* [94]. The cell can be separated into two parts: the main body and dome. The heater, thermocouple, sample holder and gas system are located in the body part, while the dome hosts IR and X-ray windows. The additional window implemented in the cell dome for X-ray fluorescence registration is the main difference in the new version. This upgrade makes the cell suitable for catalysts represented by dilute materials on top of heavy matrix or those with very low metal loading. The powder sample is fixed between two carbon-glass windows, transparent for X-rays with modified path in range from 1 to 5 mm. Metal grid below the powder (See Fig. 17A) can maximize the interaction between gas flow and catalyst. The lid of dome equipped with circular window of KBr and CaF<sub>2</sub> transparent to IR and UV irradiations. The latter was placed on top of the cell and the catalytic bed was monitored vertically at the different sample regions upon illumination. A water-methanol liquid mixture was injected into a He carrier gas and delivered to the cell. *In situ* micro-beam XAS detection was performed in a fluorescence mode.

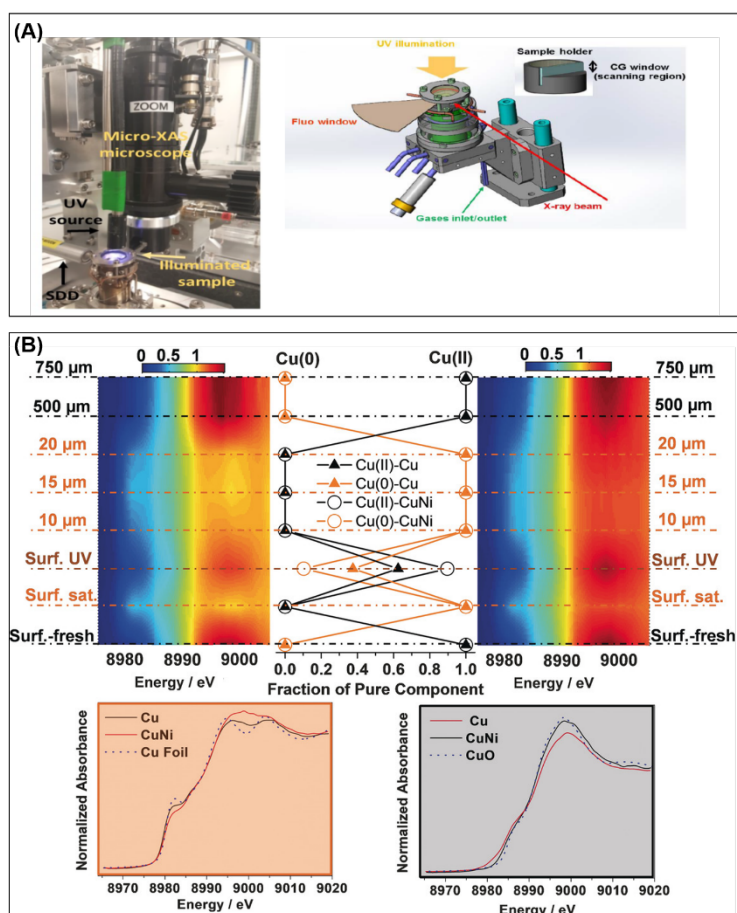


**Figure 17.** (A) Photographical view of the experimental set-up (left); Schematic view of the measurement cell (right). Inset: sample holder. (B) Contour plot of Cu K-edge XANES spectra obtained under illumination for the Cu (left) and CuNi (right) samples. For the surface position, the two previous states (fresh sample and after gas saturation) are included. Concentration profiles (central part) and XANES spectra (bottom) corresponding to pure chemical species obtained from PCA are included. Colors in the central panel are assigned to pure species: Cu<sup>II</sup> black, Cu<sup>0</sup> orange. (Copyright with the authors permission [74]).

It was found that in the outermost layer, the copper is present in fully reduced state in dark and in presence of methanol. The authors demonstrated that both monometallic Cu and bimetallic CuNi catalysts under illumination conditions undergo an oxidation process, fully reversible in the presence of reaction mixture. Contrary to the copper, XANES collected above Ni K-edge demonstrated that Ni maintains a dominant Ni<sup>2+</sup> both in surface and bulk positions and only negligible changes were observed under illumination. By comparing the XANES measurements in the different depth of the catalytic bed for mono-Cu (left) and bimetallic CuNi (right) catalysts (Fig. 17B), the difference in Cu oxidation state between the two catalysts can be observed only for surface layer upon UV irradiation. The amount of each component was quantified from Cu *K*-XANES through linear combination fit. Thus, the authors demonstrated that 38 and 11 mol. % of copper appears in oxidized Cu<sup>2+</sup> state in Cu and Cu-Ni samples, respectively, while the rest of copper remains as Cu<sup>0</sup>. The observed difference between Cu and CuNi catalysts would be significantly less obvious if XAS experiment would be performed using “standard” set-ups (lack of matching between X-ray and illumination photon volumes) which will render a zero valent metal XAS signal dominated by the exclusive effect of the reactants.

In the recent work reported by Piccolo *et al.* [75] a custom-made reactor cell was used for *operando* XAS experiment on photocatalytic hydrogen evolution over Pt/TiO<sub>2</sub> catalyst. The cell, made from engineering thermoplastic (polyoxomethylene), is equipped with three Kapton windows for X-rays thus allowing both transmission and fluorescence modes and quartz window for UV-vis illumination (Fig. 18A). XAS data were recorded in partial fluorescence mode using crystal analyzer spectrometer equipped with three spherically bent Ge (110) crystals in Rowland geometry and aligned at the maximum of the Pt-L<sub>α1</sub> line (9 442 eV). The sample in form of self-supported pellet located inside the cell maintaining the angle of 45° between the incident beam and pellet surface and 90° between the incident beam and fluorescence cone. Illumination is delivered from the top part of the cell via an optical fiber connected to a Xe lamp (300 W). Four-way valve allowed flowing helium (100 mL/min) either directly to the cell or first passing through the saturator containing a mixture of ethanol (10%) and distilled water. *Operando* XAS experiments were performed in order to shed light on the observed difference in photocatalytic hydrogen evolution reaction (PHER) efficiency of the samples containing ultra-dispersed Pt species on TiO<sub>2</sub>: P90-C, PC-500C and PC-500R (where -C and -R stands for pre-calcined and pre-reduced, respectively). Among the tested samples, the PC-500R exhibited the highest H<sub>2</sub> production rate (about 2 μmol/min) which is related to the presence of isolated Pt atoms coordinated solely by O and Ti from the support, known as strong metal-support interaction (Fig. 18B). By comparison with PtO<sub>2</sub> and Pt as references, it was shown that formal oxidation state of Pt in pre-calcined samples is close to +4, while it is near zero for the pre-reduced sample (Fig. 18C). Under the photocatalytic conditions the XANES of the pre-reduced remains almost unchanged, whereas the other two samples characterized by the white line (WL) peak decrease, and it's shift to the lower energy (Fig. 18C). These observations clearly reveal the reduction of Pt species. An additional examination was performed through quantitative EXAFS analysis. Thereby, for P90-C sample EXAFS analysis reveals a switch from Pt-O to predominant Pt-Pt coordination establishing Pt cluster formation under UV illumination. PC500-C sample which initially supposed to contain mostly single Pt sites demonstrate only slight clustering upon exposure to photocatalytic conditions. For the reduced Pt/PC500-R sample, in addition to Pt-O, the presence of Pt-Ti bonds has been identified which is not present for the other two samples.

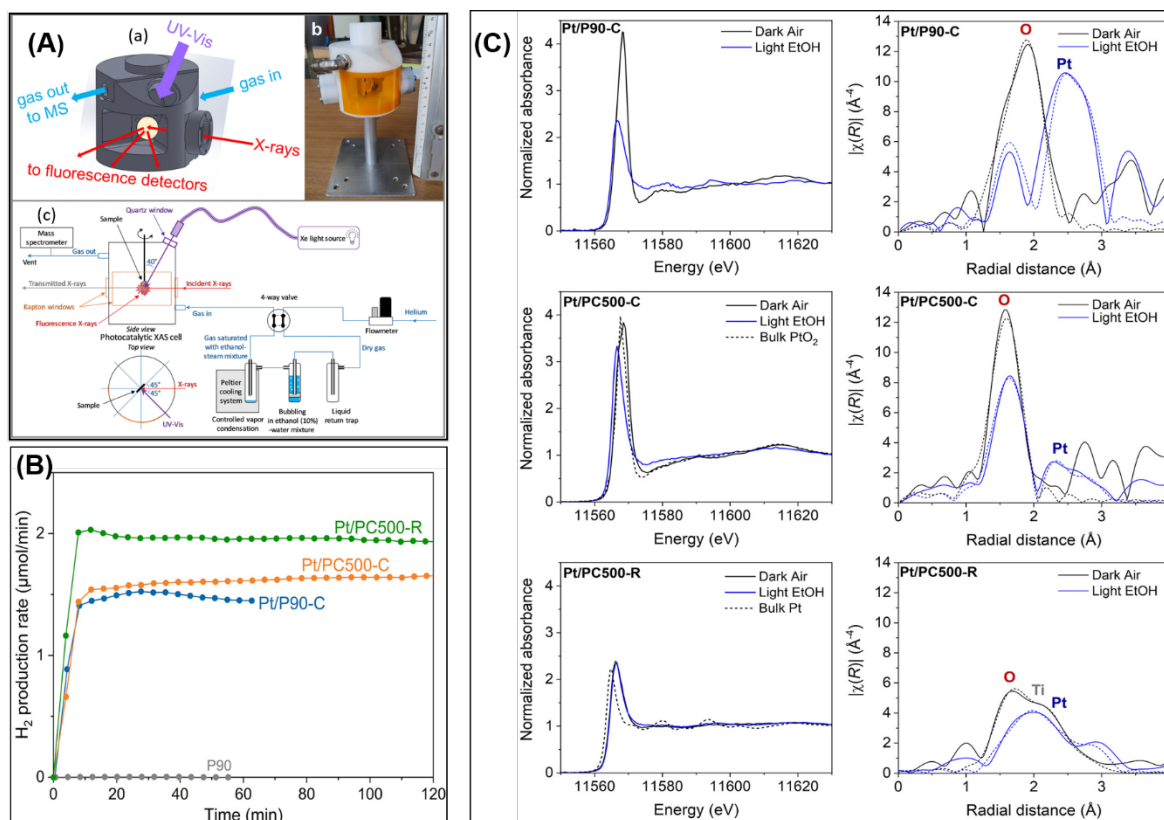


**Figure 18.** (A) *Operando* XAS reactor setup: (a) scheme of the photocatalytic cell, (b) photograph of the cell and (c) scheme illustrating the overall reaction setup. (B) Comparison of the various Pt (0.2 wt.%) /TiO<sub>2</sub>-based photocatalysts activities in the PHER from an ethanol/water/helium gas flow under UV irradiation at RT (laboratory reactor). (C) (left) Pt L<sub>3</sub>-edge HERFD-XANES spectra of 0.2 wt % Pt/TiO<sub>2</sub> photocatalysts in the dark under atmospheric air (dark air) versus under UV-Vis irradiation in ethanol/water/helium gas flow (light EtOH). Bulk PtO<sub>2</sub> and Pt reference spectra are represented with dotted lines. (right) Corresponding k<sup>3</sup>-weighted EXAFS FT moduli. Best fits are represented with dotted lines. The radial distance is not phase corrected. Rough positions of first-neighbor features are labeled with the proper elements. (Copyright with the authors permission [75]).

### 3.3.2. *Operando* XAS for investigating photocatalysis in liquid-phase

In the recent work by Spanu *et al.* [76] *operando* XAS were performed in fluorescence mode to study the PHER reaction over NiCu-TiO<sub>2</sub> catalyst under UV light irradiation in water-methanol solution. The cell adopted for XAS measurements was equipped with a Mylar window to ensure transparency both for X-rays and UV light (Fig. 19A). Both the UV LED source and the Passivated Implanted Planar Silicon (PIPS) fluorescence detector were located on the same side from the incident X-ray beam. The authors declared that the reported cell design maximizes X-ray fluorescence signal by adopting the possibility to work with minimized thickness of solution layer in front of the sample. The experiment was performed at P65 beamline (DESY-Petra III). From the dark conditions XANES analysis it was concluded that: (i) NiCu nanoparticles undergo surface oxidation when exposed to air; (ii) partial dissolution of surface Cu oxides in ethanol-water; and (iii) less dissolution of Ni oxides due to the less exposed Ni phase left behind TiO<sub>2</sub> NTs and protected by Cu. Under illumination, Cu and Ni, entirely in metallic form (~ 100%, Fig. 19B(c-d)), are active and can promote H<sub>2</sub> evolution via a Schottky junction-type mechanism. The authors emphasize that their findings differ significantly from those earlier reported by Muñoz-Batista and co-workers [74] on the similar catalytic system but in gas phase conditions, where dissolution and redeposition of Cu and Ni is not possible.

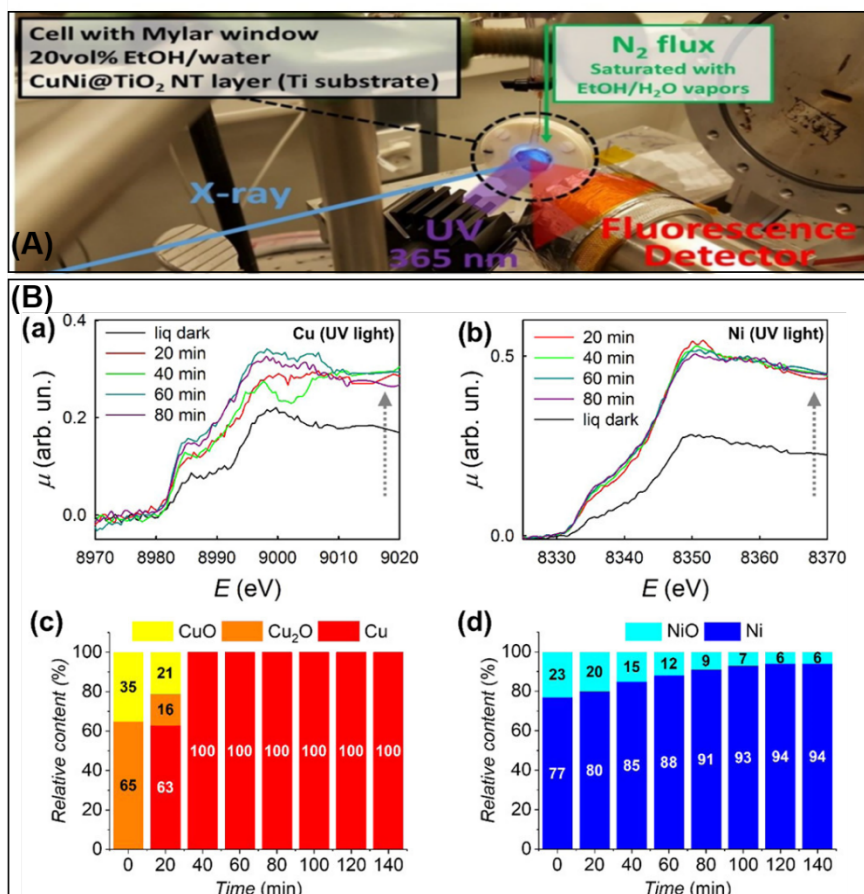


**Figure 19.** (A) Cell and sample environment from XAS *operando* liquid-phase experiment on photocatalytic H<sub>2</sub> evolution over NiCu-TiO<sub>2</sub> catalyst. (B) XAS spectra of (a) Cu K-edge and (b) Ni K-edge XAS spectra of 5Ni5Cu-TiO<sub>2</sub> immersed in the cell in a water-ethanol solution under UV light illumination for different exposure times; the last recorded XAS spectra for 5Ni5Cu immersed in the water-ethanol solution under dark conditions are reported as reference, which defines the sample condition prior to UV illumination; see black curves. (c) Cu and (d) Ni phase compositions determined by *operando* XAS measurements for 5Ni<sub>5</sub>Cu-TiO<sub>2</sub> immersed in a degassed ethanol-water solution under UV light irradiation. (Copyright with the authors permission [76]).

The photoelectric water oxidation using X-ray absorption spectroscopy has been recently reviewed by Deng and co-workers [95]. Here, we will give one example on the effect of illumination and potential on the oxidation state of FeNi overlayers on hematite photoanodes during water photooxidation [96]. Fe and Ni K-edges fluorescent XAS has been employed to track possible changes in FeNi overlayer under different conditions. The FeNi hydroxide layer (30 nm of thickness, (Fig. 20A) covered with 1 M of NaOH aqueous electrolyte was deposited in special electrochemical cell earlier employed for *operando* XAS on WO<sub>3</sub> photoanode [97]. High-power white light-emitting diode (ca. 100 mW/cm<sup>2</sup>) was used in the photocatalytic test. The experiment has been performed at the P64 beamline of PETRA III synchrotron. It was shown that the change of Fe K-edge XANES signal with potential was very small, but it became more pronounced under illumination. In contrast, Ni sites were more strongly affected by both potential and illumination (Fig. 20B). Combining the findings from both “dark” and “light” experiments it was revealed that both electrons and holes can be transferred between the hematite layers and FeNi overlayer. On the basis of linear combination fit of XANES dataset collected at both conditions (using NiO,  $\beta$ -NiOOH and for  $\gamma$ -NiOOH as a references for +2, +3 and +3.6 oxidation states, respectively), authors quantified the averaged Ni charge state under different voltages. In overall, the authors demonstrated that Ni sites need to be oxidized for more efficient OER. It was shown that the illuminated conditions allows Ni oxidation at the lower potentials due to the generated additional photovoltage. The quantitative analysis demonstrates that the Ni oxidation state saturated at ca.  $2.6 \pm 0.1$  under illumination conditions.

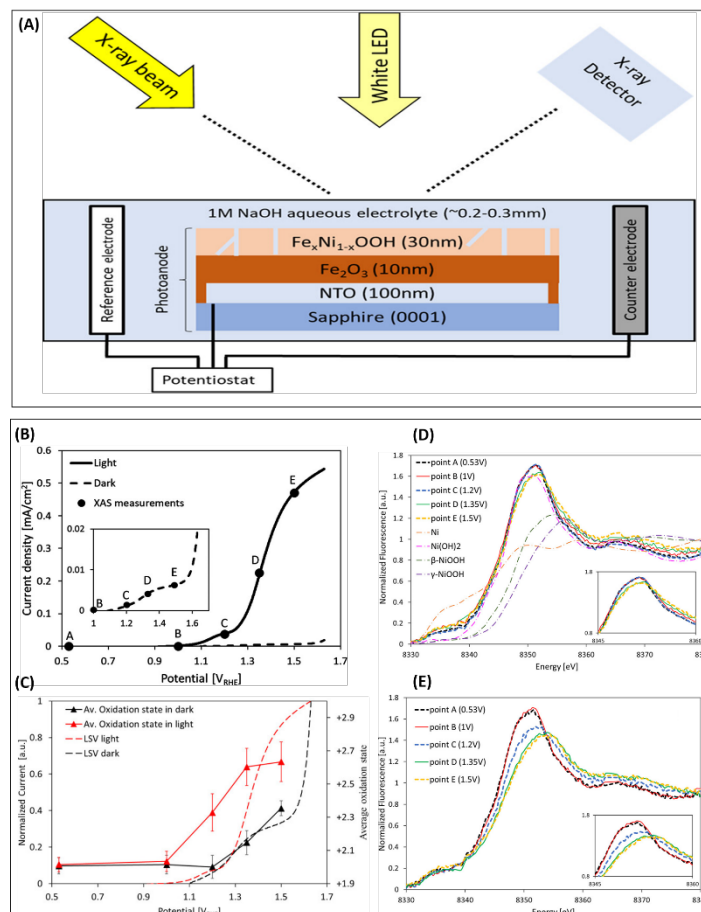


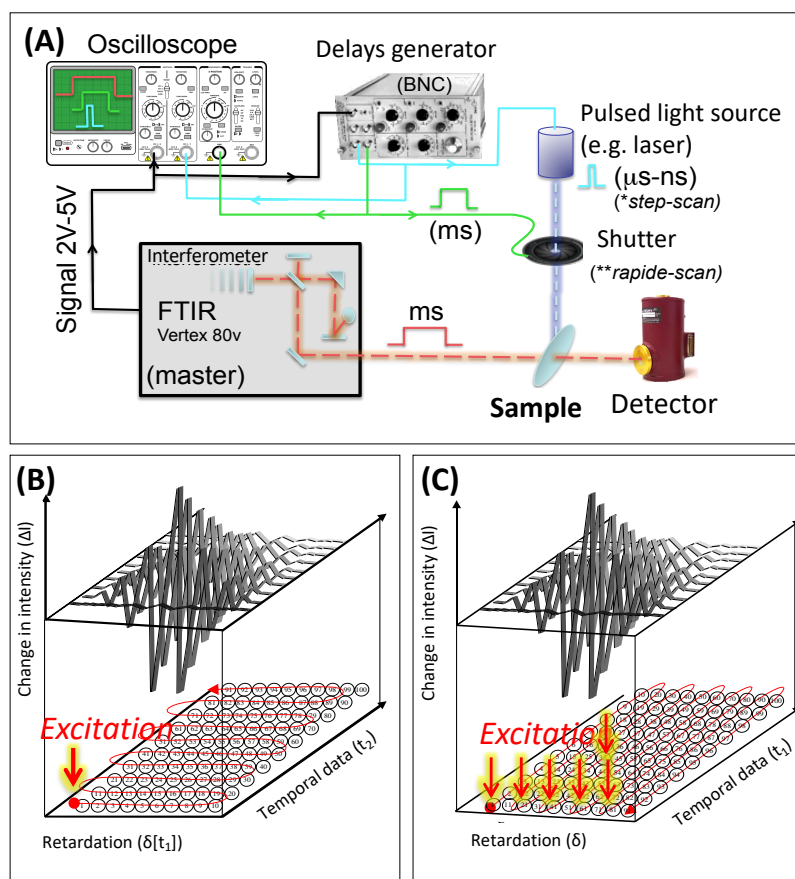
**Figure 20.** (A) Schematic top-view illustration of the *operando* XAS experiment (B) LSV voltammograms measured under dark (dashed line) and light (solid line) conditions within the beamline before the XAS measurements for hematite/FeNi (oxy)hydroxide. (C) Average oxidation state of Ni under dark (solid line with black triangles) and light (solid line with red triangles) conditions for hematite/FeNi, overlaid on the LSV voltammograms recorded during the XAS measurement under the same conditions. Dark and light currents were normalized by dividing by their respective currents at 1.63 V<sub>RHE</sub>. (D,E) Normalized Ni K-edge XANES spectra for hematite/FeNi (oxy)hydroxide under (D) dark and (E) light conditions. All of the potentials are versus RHE. Normalized Ni K-edge XANES spectra for NiO, β-NiOOH, and Ni standards used for the fitting are also presented in panel (e). (Copyright with the authors permission [96]).

#### 4. Time-resolved techniques in photocatalysis

Time-resolved techniques are frequently used to track the quick process in a given reaction at a high time resolution (sub-millisecond to nanoseconds). These measurements can provide valuable information in photocatalytic reaction to elucidate the microscopic mechanisms of photogenerated charge generation, transfer/recombination of charge carriers and surface reaction kinetics. Since numerous spatial and/or temporal resolution techniques have been emerged over the years and reviewed recently in details [98-101,102,103,104,105,106,107], in this part we will briefly discuss the time-resolved FTIR, the transient absorption and photoluminescence spectroscopies by giving one to two examples for each technique used in photocatalysis.

##### 4.1. Time-resolved FTIR

The charge transfer can be studied from ms (rapid scan) to ns (step scan) by time-resolved FTIR depending on duration of the event (scheme 3A). In the rapid scan (scheme 3B), the interferometer mirror moves very fast and each full forward-backward interferometer scan allows to extract up to 4 spectra. However, the number of spectra per second depends on spectral resolution since the duration of one scan is related to both mirror distance and velocity. For example, VERTEX 80/80v, from Bruker, can achieve around 110 spectra per second with 16 cm<sup>-1</sup> of resolution. Step Scan (scheme 3C) technique is often used to monitor the temporal progress of very fast events (transients). The interferometer mirrors are set at precise position where interferogram points are collected. Then, the moving the mirror are translated to a next position and the experiment is restarted again. Therefore, a highly reproducible experiment is required in the step-scan mode. The time resolution corresponds to the response of the detector and can reach a few nanoseconds.



**Scheme 3.** (A) Scheme of the Time-Resolved FTIR set-up in (B) rapid-scan and (C) step-scan modes.

In a recent study, an ultrafast time-resolved Quantum Cascade Laser (QCL)-assisted *operando* FTIR was used to monitor the photooxidation of MeOH over TiO<sub>2</sub> P25, Commercial Anatase (TiO<sub>2</sub> CA) and home-made Anatase (TiO<sub>2</sub> HA) at a resolution time of few  $\mu\text{s}$  [5]. The new set-up operates in rapid-scan mode with four quantum cascade lasers emitting at different wavenumbers. Each sample was subject to several photocatalytic tests with three successive UV on-off cycles under 0.1 vol.% of methanol and 20 vol.% of oxygen with 30 cc.min<sup>-1</sup> flow rate at 25 °C. At each wavenumber, the QCL (pulse rate = 10000 Hz, time-resolution = 100  $\mu\text{s}$ ) was tuned to monitor the formation (lamp on) and conversion (lamp off) of formate species at 1360, 1380, 1564 or 1580 cm<sup>-1</sup>. A direct relationship between the decomposition of surface formate species and the MeOH conversion rate (total yield of methyl formate + CO<sub>2</sub>) was established: the faster the reaction of surface formate species, the higher the photooxidation activity. This was confirmed by the evolution of the QCL beam absorbance at 1360 cm<sup>-1</sup> over TiO<sub>2</sub> P25, TiO<sub>2</sub> CA and TiO<sub>2</sub> HA during the first UV on/off cycle and the corresponding apparent rate of formate formation (lamp on, Fig. 21A(a,b,c)) and reaction (lamp off) (Fig. 21A(d,e,f)). Once the UV lamp is turned on, the accumulation of formate species on the catalyst surface was observed at different rate depending on the photocatalyst until reaching the steady-state, while these species decreased when the lamp is turned off due to their further conversion. The apparent rate of both formate formation and reaction are higher for TiO<sub>2</sub> P25 than the other two samples which is directly correlated to its superior photocatalytic activity. The conversion of formate was found to be the rate-limiting step. Other studies were conducted by Frei *et al.* to monitor the photocatalytic reactions using the rapid scan method can be consulted elsewhere [108,109,110].

In the nanoseconds regime, only few transient step-scan FTIR studies on photocatalytic systems have been published so far [111,112]. For example, Frei *et al.* studied the dynamic of CO in the channels of MCM-41 during the photodissociation of diphenyl cyclopropanone (DPCP) at RT by TR FTIR using both the step-scan and rapid-scan methods [112]. The TR measurements were conducted with a Bruker Model IFS88 spectrometer and initiated by 355 nm nanoseconds pulses of a Quanta Ray Model. In the step-scan experiments, the IR spectra were recorded from 0 to 530  $\mu\text{s}$  with a time-resolution of 1  $\mu\text{s}$ . In the rapid-scan experiments, the mirror velocity was 160 kHz with a spectral resolution of 8 cm<sup>-1</sup>. The study revealed the biphasic kinetics of CO diffusion in MCM-41 during the DPCP photolysis: the fast escape, in  $\mu\text{s}$ , of the physisorbed/or weakly adsorbed CO molecules and the slow residence, in ms, of CO molecules trapped between silanol groups, diphenyl-acetylene co-product and probably DPCP. From the TR FTIR data in the region of CO band (2220-2060 cm<sup>-1</sup>), the initial band centered at 2130 cm<sup>-1</sup> decays in the  $\mu\text{s}$  time-scale and emerged into two peaks at

2167 and 2105  $\text{cm}^{-1}$  (Fig. 21B(a)). The last two bands decay much more slowly after hundreds of ms (Fig. 21B(b)). The different decay times indicate the biphasic release of CO from the mesopores as confirmed by the time evolution of the integrated CO absorption spectrum (2220–2060  $\text{cm}^{-1}$ ) Figure 21B(c-d)).

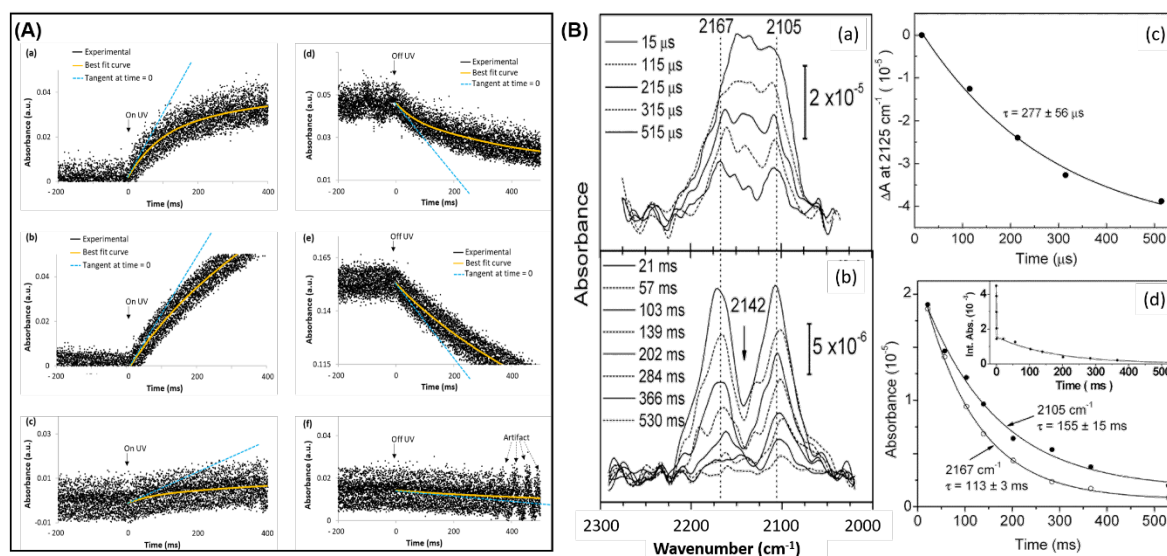


**Figure 21.** (A) QCL beam absorbance at 1360  $\text{cm}^{-1}$  vs. time over  $\text{TiO}_2$  P25 (a and d),  $\text{TiO}_2$  CA (B and e) and  $\text{TiO}_2$  HA (c and f) during the first UV on/off cycle (UV on a-b-c, UV off d-e-f) under reaction flow at 25 °C and atmospheric pressure, Conditions flow = 30 mL/min, 0.1 and 20 vol.% of methanol and oxygen in argon, respectively, Hg-Xe lamp (200 W), irradiance = 200  $\text{mW}/\text{cm}^2$ , In (a-b-c), time = 0 corresponds to the moment when the shutter in-between the lamp and the UV-light guide detected to the IR cell was opened to irradiate the sample, During the preceding 200 ms, the sample was already under reaction flow but still in the dark, In (d-e-f), time = 0 corresponds to the moment when the shutter was closed again still under reaction flow, The fall times to open and to close the shutter were around 6.5 ms and 3.2 ms, respectively, with a minimum pulse width of 13 ms. (B) Time-resolved FTIR absorption spectra of CO formed inside MCM-41 recorded upon laser-induced photolysis of DPCP: (a) step-scan FTIR spectra (average of 21 experiments) and (b) rapid-scan FTIR spectra (average of 12 experiments). The rapid-scan spectra were normalized so that (a) and (b) correspond to the same amount of DPCP depleted (and CO produced) per laser pulse. Note that the absorbance scale of the millisecond spectra is enlarged. (c) Single-exponential fit of the absorbance difference at 2125  $\text{cm}^{-1}$  yields a decay time of  $277 \pm 56 \mu\text{s}$ . Correcting for the 1420  $\mu\text{s}$  RC high-pass filter of the detector yields  $344 \pm 70 \mu\text{s}$ . (d) Single-exponential fit of the absorbance decay at 2105 and 2167  $\text{cm}^{-1}$  yields decay times of  $155 \pm 15 \text{ms}$  and  $113 \pm 3 \text{ms}$ , respectively. The insert shows the decay of the full CO profile (integrated from 2220 to 2060  $\text{cm}^{-1}$ ) in both the rapid-scan data and the step-scan data (corrected for the RC high-pass filter of the detector). Ordinate unit of insert:  $10^{-3} \text{cm}^{-1}$ . (Copyright with permission from Ref. [5,112]).

#### 4.2. Time Resolved Microwave Conductivity (TRMC)

TRMC is a useful technique for studying the primary processes in photocatalysis, i.e. the charge carrier dynamics with nanosecond time resolution [113]. During TRMC measurements, the semiconductor is illuminated by a nanosecond laser pulse which induces a change in the microwave power reflected from the sample. The microwave power can be then correlated to the photoinduced change in the sample conductance from which information on the charge-carrier generation, charge-carrier trapping, charge carrier recombination and electron/hole transfer can be obtained. Very recently, the TRMC technique was used to investigate the facet-dependent carrier dynamics of  $\text{Cu}_2\text{O}$  governing the photocatalytic  $\text{H}_2$  production from water under visible light [114]. The results show that the photoactivity of rhombic dodecahedral  $\text{Cu}_2\text{O}$  with dominant  $\{110\}$  facets (RD- $\text{Cu}_2\text{O}$ ) was 1.5-fold higher than that of cubic  $\text{Cu}_2\text{O}$  with  $\{100\}$  surfaces (CB- $\text{Cu}_2\text{O}$ ). This is explained by the higher carrier mobility of RD- $\text{Cu}_2\text{O}$  compared to CB- $\text{Cu}_2\text{O}$  at different laser pulse intensities, as revealed from TRMC measurements (Fig. 22A-B). Both carrier lifetimes ( $\tau_1$  and  $\tau_2$ ) and diffusion lengths (Fig. 21C), determined from the decay of the TRMC signals, are smaller for CB- $\text{Cu}_2\text{O}$  than that of RD- $\text{Cu}_2\text{O}$  suggesting that the charge carriers recombine/trap faster in CB- $\text{Cu}_2\text{O}$  due to the presence of more structural defects in this sample. The higher conductivity ( $\sigma$ ) and higher carrier density ( $N_a$ ) of CB- $\text{Cu}_2\text{O}$ , determined by dark microwave conductivity measurements (Fig. 22C), confirm the presence of more defects in CB- $\text{Cu}_2\text{O}$  than RD- $\text{Cu}_2\text{O}$ , which contribute to electron trapping and resulting in low photocatalytic activity.



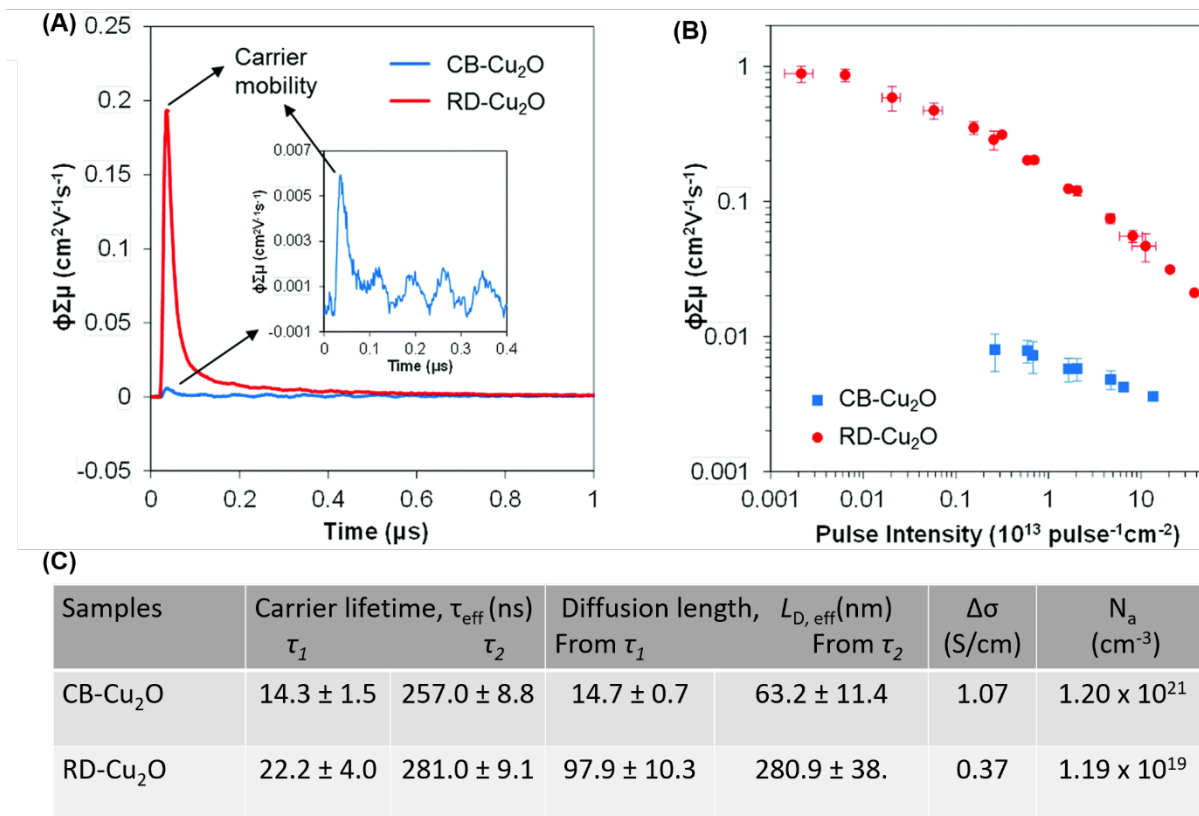


**Figure 22.** (A) TRMC signal of CB-Cu<sub>2</sub>O and RD-Cu<sub>2</sub>O over time at  $7.0 \times 10^{12}$  photons pulse<sup>-1</sup> cm<sup>-2</sup>, with the inset showing the magnification of the signal of CB-Cu<sub>2</sub>O, and (B) maximum TRMC signal as a function of incident pulse intensity of CB-Cu<sub>2</sub>O and RD-Cu<sub>2</sub>O. (C) Summary of average effective charge lifetime, diffusion length and parameters involved in dark microwave conductivity measurement of CB-Cu<sub>2</sub>O and RD-Cu<sub>2</sub>O (Copyright with permission from Ref [114]).

#### 4.3. Photoluminescence spectroscopy (PL)

PL is a light emission process from the electronic excited state of a molecule or materials to its ground state after excitation by an external light source. In photocatalysis, PL is widely used as one of the fundamental characterization tools to study the excited-state properties from ns to ms at a molecular level with high sensitivity and nondestructive nature. The time-resolved PL was used to explore the excited-state properties of the novel bimetallic supramolecular assembly of pyrene modified photosensitizer and RuPy...ReCOPy used for the CO<sub>2</sub> photoreduction under visible light [35]. It was shown that the novel assembly showed higher photocatalytic activity than the benchmark system (Ru(bpy)<sub>3</sub>Cl<sub>2</sub>(Ru) with Re(bpy)(CO)<sub>3</sub>Cl (ReCO)). This is due to an efficient electron transfer from Ru center to the pyrene moiety in RuPy and from the later to the rhenium center in ReCOPy. This is confirmed by the red-shifted photoluminescence (PL (620 vs. 670 nm) and the higher excited-state lifetime (0.13 vs. 0.9 μs) of <sup>3</sup>RuPy compared to <sup>3</sup>Py allowing a stronger Ru-Py interaction and a better electron transfer to Rhenium (Fig. 23A(a-b)). Furthermore, the <sup>3</sup>RuPy exhibits less sensitivity to the oxygen (insert in Fig. 23A(a-b)) and a faster electron transfer than <sup>3</sup>Py, concluded from the quenching of the <sup>3</sup>MLCT with triethanolamine (TEOA).

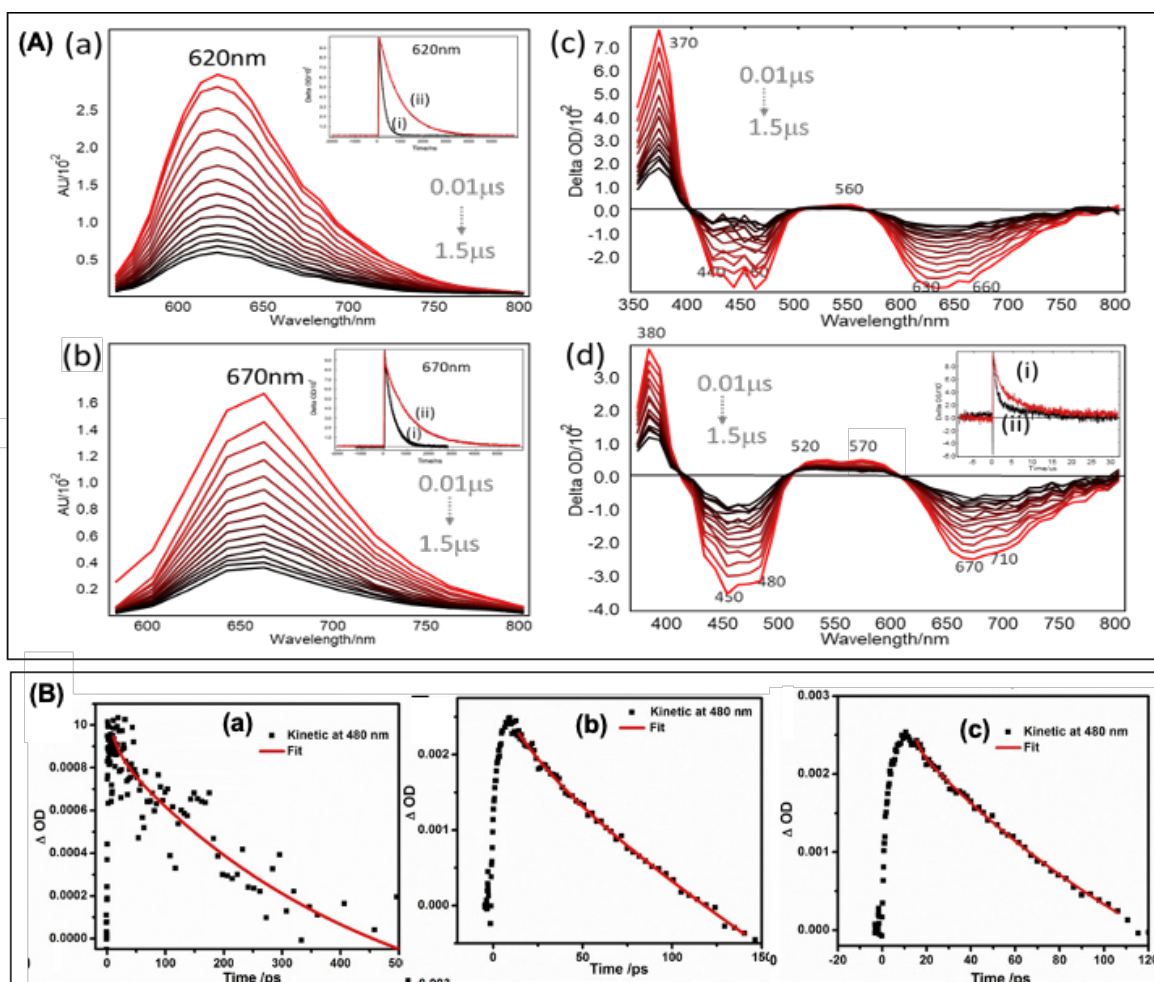


**Figure 23.** (A) (a and b) correspond to the nanosecond emission spectra (140 ns/spectrum) of the <sup>3</sup>MLCT of Ru and RuPy, respectively. In insert: normalized kinetic decay trace of <sup>3</sup>MLCT emission of Ru and RuPy monitored at 620 nm and 670 nm, respectively, under air (i) and argon (ii) atmospheres. (c and d) report the evolution vs the time (140 ns/ spectrum) of the absorption transition (AT) of Ru and RuPy. Insert of Fig. d: normalized kinetic decay traces of the AT at 520 nm (i) and 570 nm (ii).  $\lambda_{exc} = 532$  nm, [RuPy] = 1.7 mM; [Ru] = 3 mM; all spectra were recorded under Ar at 298 K. (B) The kinetics decay monitored at 480 nm of (A) WO<sub>3</sub>, (B) O<sub>v</sub>-WO<sub>3</sub>-600, and (C) O<sub>v</sub>-WO<sub>3</sub>-Pt. (Copyright with permission from Ref. [35,115]).

#### 4.4. Transient absorption spectroscopy (TA)

Transient absorption (TA) spectroscopy is used to evaluate the lifetimes of photogenerated charge carriers in range of ps to ns. If we come back to the previous example in part 4.2. [35], the red-shifted PL of <sup>3</sup>RuPy compared to <sup>3</sup>Py was also observed in the transient absorption of this complex, in addition to a new absorption transient at 520 nm with longer life-time 35 μs probably assigned to the (<sup>3</sup>(RuPy...RuPy) exciplex (Fig. 23A(c-d)). By using TA spectroscopy, it was shown that the presence of defect (O<sub>v</sub>) in WO<sub>3</sub> structure can generate more electron trapping states which inhibit the recombination of electron-hole pairs and increase the photocatalytic oxygen evolution [115]. This effect can be enhanced in presence of Pt as cocatalyst in O<sub>v</sub>-WO<sub>3</sub> structure. In WO<sub>3</sub> (Fig. 23B(a)), two decays were observed at 15.3 and 541.7 ps characteristics of the fast charge recombination and electron trapping, respectively. In contrast, significantly longer lifetimes of the excited states ( $\tau_1 = 27.1$  ps and  $\tau_2 = 749.1$  ps) were obtained for O<sub>v</sub>-WO<sub>3</sub> due to the electron trap states (Fig. 23B(b)). The heterojunction between the noble Pt and O<sub>v</sub>-WO<sub>3</sub> effectively reduces the recombination of charge carries with ultrafast electron injection from trap states to the metal (Fig. 23B(c)).

## 5. Summary, limitations and outlooks

In this review, we summarized the recent efforts of using *in-situ* and *operando* techniques, e.g. FTIR, Raman, EPR, XAS and Time-resolved spectroscopy, to perform real-time observations of one of the most complicated and multifunctional process such as photocatalysis.

*In-situ* IR spectroscopy can provide valuable and pertinent information on the adsorption sites of photocatalyst, both directly or via the adsorption of a probe molecules (the reactants themselves are always the best probe molecules). Physical chemical properties such as acidity, basicity and redox properties of the photocatalysts can be also described and quantified in strength and as site concentrations. The *in-situ* FTIR can be also dedicated for a real-time analysis of the gas products in photocatalysis, which allows determining the reaction selectivity and photocatalyst performance, but cannot provide information on the evolution of catalyst surface during the reaction. IR *operando* technique can complete such a view simultaneous monitoring of surface and gas/or liquid species as the best way to establish the reaction pathways. It is possible to observe at what time different intermediates or by-products are formed and to deduce which site (active site or spectator) is responsible for a given photocatalytic step. In such a way, it is possible, step by step as a jigsaw puzzle, to reconstruct all the reaction mechanism. However, studying very short-lived intermediates cannot be achieved with standard FTIR spectroscopy. Thus, very high time resolution ( $\mu$  to ns) is mandatory and can be achieved by using special recording techniques such as step scan and rapid scan interferometry. In this case, the photocatalytic experiment needs to be well controlled in time but also highly reproducible.

Raman is used to monitor the structural transformation of photocatalysts as well as to identify the reaction intermediates under real reaction conditions. However, the application of *operando* Raman spectroscopy in photocatalytic reaction is still limited because of the overwhelming of photocatalysis excitation light with Raman photons and the low signal intensity resulting from low frequency of the Raman scattering effect. The latter drawback has been overcome by development of new experimental techniques (e.g. surface-enhanced Raman spectroscopy (SERS), shell-isolated nanoparticle enhanced Raman spectroscopy (SHINERS), or tip-enhanced Raman spectroscopy (TERS)); however, the applicability of those approaches imposes limitations on systems and reactions to characterize, particularly if *operando* conditions in photocatalysis are sought.

EPR spectroscopy has been widely used in photocatalysis for i) monitoring the charge carrier trapping, recombination and transfer, ii) identification of reactive radicals/oxygen species and direct observation of the paramagnetic active species in photocatalysis. However, the EPR measurements are often performed in presence of a spin trap and/or at low temperature (below 77 K) in order to improve detection of the highly reactive species with unpaired electrons. Due to these specific drawbacks, the application of EPR in photocatalysis is still scarce under *operando* conditions.

X-ray absorption spectroscopy represents a powerful technique to investigate structural and electronic configuration of metal sites in nanostructured and bulk catalysts. XANES region allows to probe variation in oxidation state, density of unoccupied states, chemical bond hybridization, while EXAFS part is more sensitive to bond lengths and coordination environment. Compared to the other techniques (IR, Raman), XAS presents the advantage in both surface and bulk sensitivities. However, *operando* XAS experiments in photocatalysis are mainly conducted at synchrotron facilities, which limits the available experimental set-up and the possibility of performing long-term experiments. Therefore, the development of additional suitable laboratory based XAS setups with the implementation of adequate *operando* cells is primordial for performing long-term experiments in house and extending the characterization time scales.

Time-resolved techniques, such as Time-Resolved FTIR, Time-Resolved Microwave Conductivity (TRMC), Transient Absorption and photoluminescence, are frequently used to track the quick process in photocatalysis on sub-millisecond to picoseconds time scales. These measurements can be used to study the photogenerated charge generation, transfer/recombination of charge carriers and their lifetimes. Some works have already given important insights in this field, but many of these methods need to be adapted to investigate the photocatalysts under reaction conditions.

However, a more comprehensive picture of a working photocatalyst is still necessary for the quest of the entire mechanistic process in order to extract design principles for more active and/or stable photocatalysts. Therefore, improved experimental studies with combined techniques such as IR, Raman, XAS and EPR can provide a detailed picture of photocatalytic systems. Furthermore, other techniques not mentioned above such as NMR, UV-Vis, XPS, neutron spectroscopy and microscopies, operated *in-situ* or using *operando* methodology, can provide complementary information about photocatalytic systems. Thus, a range of powerful methods must be used together in order to probe the photocatalytic processes in a spatiotemporal manner with the time domain from femtoseconds to milliseconds and the space domain from 0.1 nm to 10 mm.

**Table 2.** List of the advanced techniques reviewed in this article for photocatalysis and their limitations.

Techniques	Time resolution	Provided information's in photocatalysis	Limitations
FTIR	ms	Identification and quantification of adsorption sites Acidity/basicity and redox properties of photocatalysts: strength and concentration Determination of reaction selectivity and photocatalyst performance/stability or deactivation Discrimination between spectator and active sites Identification of the reaction intermediates under real reaction condition Simultaneous monitoring of photocatalyst's surface and gas or liquid phase to elucidate the reaction mechanism	Very short-lived intermediates cannot be detected Surface-sensitive techniques
Raman	ms	Monitoring changes in surface properties of photocatalysts Identification of the reaction intermediates under real reaction condition	Complementary technique to IR Surface-sensitive techniques Overwhelming of photocatalysis excitation light with Raman photons Low signal intensity resulting from low frequency of the Raman scattering effect Easily affected by fluorescence phenomenon
EPR	ms	Tracking electron trapping, recombination and transfer Identification of radical and Reactive Oxygen Species Direct observation and monitoring of the paramagnetic active species	Performed in presence of a spin trap and/or at low temperature (below 77 K) in order to improve detection of the highly reactive species with unpaired electrons
XAS (EXAFS and XANES)	ms	Surface and bulk sensitive technique Prob of variation in oxidation state, density of unoccupied states, chemical bond hybridization, bond lengths and coordination environment	Mainly conducted at synchrotron facilities limitations in the available experimental set-up and the possibility of performing long-term experiments
Time-resolved FTIR (rapid and step scan)	ms to ns	Tracking of charge transfer in photocatalysis Identification of short-lived intermediates	Not well-developed for <i>operando</i> studies in photocatalysis
Time-resolved Microwave spectroscopy	ns	Tracking charge-carrier generation, charge-carrier trapping, charge carrier recombination and electron/hole transfer	
Photoluminescence	ms to ns	Study the excited-state properties of photocatalysts	
Transient Absorption	ns to ps	Lifetimes of photogenerated charge carriers	

## 6. Concluding remarks

Understanding the structure-activity/selectivity relationship is of a significant importance to design new materials with high performance in photocatalysis. *In-situ* spectroscopic techniques have been widely used to provide fundamental information about the photocatalyst structure and surface species under controlled conditions, i.e. under vacuum, in presence of a probe molecule or a under reactive atmosphere (O<sub>2</sub>, H<sub>2</sub>, etc.). For example, the *in-situ* FTIR technique can be used as a characterization tool for the i) determination of oxidation/coordination state of the active sites, ii) identification/quantification of Lewis and Brønsted acidity and iii) calculation of the entropy and enthalpy of adsorption. However, this technique is essentially limited to the characterization of surface species, thus it is important to be used in complementary with other techniques such as the *in-situ* Raman and XAS spectroscopies. On one hand, the *in-situ* Raman spectroscopy is used to investigate the surface properties of the photocatalysts, i.e. to analyze the structure of photocatalysts and its changes under controlled conditions. On the other hand, the *in-situ* EPR provides information on the radical and unpaired electron species formation, while XAS spectroscopy is related to the structural/electronic configuration of metal sites of the photocatalysts. The *in-situ* measurements can also be conducted under reaction conditions to identify the reaction intermediates and reveal the reaction mechanism in photocatalysis. However, it is an indirect method, since the reaction is performed under special conditions (partial vacuum) and the surface and gas/liquid phase analysis are performed separately. Thus, true understanding of the structure-activity/selectivity relationship requires the monitoring of photocatalysts under realistic catalytic conditions which points to the importance of *operando* spectroscopy (e.g. *operando* FTIR, *operando* Raman, *operando* XAS and etc.). This methodology allows to simultaneously monitor the catalyst surface and the gas/liquid phase on the same sample under real reaction conditions. Noting that the design of the associated reaction cell as well as the reaction conditions are critical here and can affect the overall performance of the photocatalytic process. However, some intermediates remain elusive under steady-state conditions of *operando* spectroscopy. Thus, the use of transient conditions (for example via isotopic substitution, i.e. using the SSITKA approach) is sometimes of particular significance. Time resolution and discrimination of reaction intermediates can also be done by modulation excitation spectroscopy, allowing to discriminate transient states. Time-Resolved (TR) techniques are also required to detect and determine the reactivity and kinetic significance of reaction intermediates that would otherwise escape detection at steady-state. For example, TR FTIR techniques allow monitoring the photocatalyst surface at the time scale of 10 milliseconds and slower by using the rapid-scan method. For FT-IR monitoring in the time range from 10 nanoseconds to  $\mu$ s, the step-scan is the method of choice. Time-resolved microwave conductivity (TRMC) is a useful technique to study the charge-carrier generation, trapping and recombination, as ultrafast processes that occur at very short times (femto-nano seconds) after irradiation of photocatalysts. Moreover, Photoluminescence (PL) and Transient absorption (TA) spectroscopy can be used to study the excited-state properties from ns to ms at a molecular level and to follow the short lifetimes of photogenerated charge carriers in range of ps to ns, respectively. However, catalysis occurs in time and space [116], thus *operando* imaging during reaction is the next big step to understand catalysis in shaped catalysts, this will be particularly challenging when it comes to photocatalytic processes. Since the overall efficiency of photocatalysis is the multiplication of all the elemental efficiencies, the latter should be measured together for a reaction. However, in the presented case study, only one or two techniques were used to monitor the photocatalytic reaction under reaction conditions which cannot allow to identify all the elemental steps and increase the incoherent reproducibility caused by separated measurements. Thus, the use of multi-techniques and/or a multidisciplinary approach in one photocatalytic reaction to conduct measurements and modeling of all these steps are required to fully understand and improve the efficiency of photocatalysis. For example, the combination of *operando* XAS and FTIR can provide deep insight into the understanding of dynamic structural of photocatalysts and the formation of surface intermediates under the reaction conditions. On the other hand, the development of *in-situ/operando* to monitor the photocatalytic reactions in a pilot-scale or even industrial scale under real industrial conditions is also envisaged, so that future researches will be more efficient and less time and money wasting.

## Author Contributions

The manuscript was prepared written through the contributions of all authors. All authors have approved the final version of the manuscript.

## ACKNOWLEDGMENT

Mohamad El-Roz and Houeida Issa Hamoud acknowledge the Normandy region (H<sub>2</sub>CO<sub>2</sub> project) for the financial support.

Lukasz Wolski gratefully acknowledges the Foundation for Polish Science (FNP) (decision no. START 95.2021) and the Polish Minister of Education and Science (decision no. SMN/16/0997/2020) for the financial support.

Iliia Pankin acknowledges the Ministry of Science and Higher Education of the Russian Federation for financial support (State assignment in the field of scientific activity, № 0852-2020-0019).

On behalf of all authors, the corresponding author states that there is no conflict of interest.

## References

- [1] Turro, N. J., Ramamurthy, V., & Scaiano, J. C. (2017). *Modern molecular photochemistry of organic molecules*. University Science Books, Sausalito: Viva Books. <https://doi.org/10.1002/anie.201003826>.
- [2] Takanabe, K. (2017). Photocatalytic water splitting: quantitative approaches toward photocatalyst by design. *ACS Catalysis*, 7(11), 8006-8022. <https://doi.org/10.1021/acscatal.7b02662>.
- [3] Coy, E., Siuzdak, K., Grądzka-Kurzaj, I., Sayegh, S., Weber, M., Ziółek, M., ... & Iatsunskiy, I. (2021). Exploring the effect of BN and BN bridges on the photocatalytic performance of semiconductor heterojunctions: Enhancing carrier transfer mechanism. *Appl. Mater. Today*, 24, 101095. <https://doi.org/10.1016/j.apmt.2021.101095>.
- [4] El-Roz, M., Bazin, P., Daturi, M., & Thibault-Starzyk, F. (2013). Operando infrared (IR) coupled to steady-state isotopic transient kinetic analysis (SSITKA) for photocatalysis: Reactivity and mechanistic studies. *ACS Catalysis*, 3(12), 2790-2798. <https://doi.org/10.1021/cs4006088>.
- [5] Schnee, J., Daturi, M., & El-Roz, M. (2020). Ultrafast time-resolved quantum cascade laser diagnostic for revealing the role of surface formate species in the photocatalytic oxidation of methanol. *Catal. Sci. Technol.*, 10(16), 5618-5627. <https://doi.org/10.1039/D0CY00865F>.
- [6] Kim, D. W., Leem, Y. A., Yoo, S. D., Woo, D. H., Lee, D. H., & Woo, J. C. (1993). Measurement of the exciton binding energy in a narrow GaAs-Al<sub>x</sub>Ga<sub>1-x</sub>As quantum well by photoluminescence excitation spectroscopy. *Phys. Rev. B*, 47(4), 2042. <https://doi.org/10.1103/PhysRevB.47.2042>.
- [7] Inoue, Y. (2009). Photocatalytic water splitting by RuO<sub>2</sub>-loaded metal oxides and nitrides with d 0- and d 10-related electronic configurations. *Energy Environ. Sci.*, 2(4), 364-386. <https://doi.org/10.1039/B816677N>.
- [8] Weckhuysen, B. M. (2002). Snapshots of a working catalyst: possibilities and limitations of in situ spectroscopy in the field of heterogeneous catalysis. *Chem. Com.*, (2), 97-110. <https://doi.org/10.1039/B107686H>.
- [9] Weckhuysen, B. M. (2015). Studying birth, life and death of catalytic solids with operando spectroscopy. *Natl. Sci. Rev.*, 2(2), 147-149. <https://doi.org/10.1093/nsr/nwv020>.
- [10] Weckhuysen, B. M. (2002). Snapshots of a working catalyst: possibilities and limitations of in situ spectroscopy in the field of heterogeneous catalysis. *Chem. Com.*, (2), 97-110. <https://doi.org/10.1039/B107686H>.
- [11] Jones, C. W., Tao, F., & Garland, M. V. (2012). Introduction to special issue on operando and in situ studies of catalysis. <https://doi.org/10.1021/cs3006692>.
- [12] Bañares, M. A. (2005). Operando methodology: combination of in situ spectroscopy and simultaneous activity measurements under catalytic reaction conditions. *Catal. today*, 100(1-2), 71-77. <https://doi.org/10.1016/j.cattod.2004.12.017>.
- [13] Ferri, D. (2021). Toward Operando Infrared Spectroscopy of Heterogeneous Catalysts. *Heterogeneous Catalysts: Advanced Design, Characterization and Applications*, 1, 311-338. <https://doi.org/10.1002/9783527813599.ch18>.
- [14] Rasmussen, S. B., Perez-Ferreras, S., Bañares, M. A., Bazin, P., & Daturi, M. (2013). Does pelletizing catalysts influence the efficiency number of activity measurements? Spectrochemical engineering considerations for an accurate operando study. *ACS Catalysis*, 3(1), 86-94. <https://doi.org/10.1021/cs300687v>.
- [15] Harrick, N.J. (1979). *Internal Reflection Spectroscopy*. Harrick Scientific Corporation.
- [16] Vimont, A., Thibault-Starzyk, F., & Daturi, M. (2010). Analyzing and understanding the active site by IR spectroscopy. *Chem. Soc. Rev.*, 39(12), 4928-4950. <https://doi.org/10.1039/B919543M>.
- [17] Lercher, J. A., Grundling, C., & Eder-Mirth, G. (1996). Infrared studies of the surface acidity of oxides and zeolites using adsorbed probe molecules. *Catal. Today*, 27(3), 353-376. [https://doi.org/10.1016/0920-5861\(95\)00248-0](https://doi.org/10.1016/0920-5861(95)00248-0).
- [18] Hadjiivanov, K. I., & Vayssilov, G. N. (2002). Characterization of oxide surfaces and zeolites by carbon monoxide as an IR probe molecule. [https://doi.org/10.1016/S0360-0564\(02\)47008-3](https://doi.org/10.1016/S0360-0564(02)47008-3).
- [19] Ivanova, E., Mihaylov, M., Aleksandrov, H. A., Daturi, M., Thibault-Starzyk, F., Vayssilov, G. N., ... & Hadjiivanov, K. I. (2007). Unusual Carbonyl–Nitrosyl Complexes of Rh<sup>2+</sup> in Rh–ZSM-5: A Combined FTIR Spectroscopy and Computational Study. *J. Phys. Chem. C*, 111(28), 10412-10418. <https://doi.org/10.1021/jp067531f>.
- [20] Kunkeler, P. J., Zuurdeeg, B. J., Van Der Waal, J. C., van Bokhoven, J. A., Koningsberger, D. C., & Van Bekkum, H. (1998). Zeolite beta: the relationship between calcination procedure, aluminum configuration, and Lewis acidity. *J. Catal.*, 180(2), 234-244. <https://doi.org/10.1006/jcat.1998.2273>.
- [21] Drenchev, N. L., Chakarova, K. K., Lagunov, O. V., Mihaylov, M. Y., Ivanova, E. Z., Strauss, I., & Hadjiivanov, K. I. (2016). In situ FTIR Spectroscopy as a Tool for Investigation of Gas/Solid Interaction: Water-Enhanced CO<sub>2</sub> Adsorption in UiO-66 Metal-Organic Framework. MyJoVE Corporation. <https://doi.org/10.3791/60285>.

- [22] Liu, L., Zhao, C., Miller, J. T., & Li, Y. (2017). Mechanistic study of CO<sub>2</sub> photoreduction with H<sub>2</sub>O on Cu/TiO<sub>2</sub> nanocomposites by in situ X-ray absorption and infrared spectroscopies. *J. Phys. Chem. C*, 121(1), 490-499. <https://doi.org/10.1021/acs.jpcc.6b10835>.
- [23] El-Roz, M., Lakiss, L., El Fallah, J., Lebedev, O. I., Thibault-Starzyk, F., & Valtchev, V. (2013). Incorporation of clusters of titanium oxide in Beta zeolite structure by a new cold TiCl<sub>4</sub>-plasma process: physicochemical properties and photocatalytic activity. *Phys. Chem. Chem. Phys.*, 15(38), 16198-16207. <https://doi.org/10.1039/C3CP52478G>.
- [24] Deo, G., Turek, A. M., Wachs, I. E., Huybrechts, D. R., & Jacobs, P. A. (1993). Characterization of titania silicalites. *Zeolites*, 13(5), 365-373. [https://doi.org/10.1016/0144-2449\(93\)90151-r](https://doi.org/10.1016/0144-2449(93)90151-r).
- [25] Fu, C., Li, F., Zhang, J., Li, D., Qian, K., Liu, Y., ... & Huang, W. (2021). Site Sensitivity of Interfacial Charge Transfer and Photocatalytic Efficiency in Photocatalysis: Methanol Oxidation on Anatase TiO<sub>2</sub> Nanocrystals. *Angew. Chem. Int. Ed.*, 133(11), 6225-6234. <https://doi.org/10.1002/ange.202014037>.
- [26] Zhang, H., Li, Y., Wang, J., Wu, N., Sheng, H., Chen, C., & Zhao, J. (2021). An unprecedented hydride transfer pathway for selective photocatalytic reduction of CO<sub>2</sub> to formic acid on TiO<sub>2</sub>. *Appl. Catal. B: Environ.*, 284, 119692. <https://doi.org/10.1016/j.apcatb.2020.119692>.
- [27] Subbotina, I. R. F., & Barsukov, D. V. E. (2020). Direct evidence of the key role of UV-formed peroxide species in photocatalytic gas–solid oxidation in air on anatase TiO<sub>2</sub> particles. *Phys. Chem. Chem. Phys.*, 22(4), 2200-2211. <https://doi.org/10.1039/C9CP04728J>.
- [28] Hirakawa, H., Hashimoto, M., Shiraishi, Y., & Hirai, T. (2017). Selective Nitrate-to-Ammonia Transformation on Surface Defects of Titanium Dioxide Photocatalysts. *ACS Catal.* 7, 3713–3720. <https://doi.org/10.1021/acscatal.7b00611>.
- [29] Dolamic, I., Bürgi, T. (2007). Photocatalysis of dicarboxylic acids over TiO<sub>2</sub>: An *in-situ* ATR-IR study. *J. Catal.*, 248(2), (268-276). <https://doi.org/10.1016/j.jcat.2007.03.020>.
- [30] Almeida, A. R., Moulijn, J. A., & Mul, G. (2011). Photocatalytic Oxidation of Cyclohexane over TiO<sub>2</sub>: Evidence for a Mars– Van Krevelen Mechanism. *J. Phys. Chem. C*, 115(4), 1330-1338. <https://doi.org/10.1021/jp107290r>.
- [31] Almeida, A. R., Moulijn, J. A., & Mul, G. (2008). In situ ATR-FTIR study on the selective photo-oxidation of cyclohexane over anatase TiO<sub>2</sub>. *J. Phys. Chem. C*, 112(5), 1552-1561. <https://doi.org/10.1021/jp077143t>.
- [32] Belhadj, H., Hakki, A., Robertson, P.K.J., & Bahnemann, D.W. (2015). In situ ATR-FTIR study of H<sub>2</sub>O and D<sub>2</sub>O adsorption on TiO<sub>2</sub> under UV irradiation. *Phys. Chem. Chem. Phys.*, 17, 22940-22946. <https://doi.org/10.1039/C5CP03947A>.
- [33] Telegeiev, I., Thili, O., Lanel, A., Bazin, P., Levaque, Y., Fernandez, C., & El-Roz, M. (2018). In Situ FTIR Reactor for Monitoring Gas-Phase Products during a (Photo) catalytic Reaction in the Liquid Phase. *Anal. Chem.*, 90(24), 14586-14592. <https://doi.org/10.1021/acs.analchem.8b04754>.
- [34] Li, S. Y., Meng, S., Zou, X., El-Roz, M., Telegeiev, I., Thili, O., ... & Zhu, G. (2019). Rhenium-functionalized covalent organic framework photocatalyst for efficient CO<sub>2</sub> reduction under visible light. *Micropor. Mesopor. Mat.*, 285, 195-201. <https://doi.org/10.1016/j.micromeso.2019.05.026>.
- [35] Nasrallah, H., Lyu, P., Maurin, G., & El-Roz, M. (2021). Highly efficient CO<sub>2</sub> reduction under visible-light on non-covalent Ru··· Re assembled photocatalyst: Evidence on the electron transfer mechanism. *J. Catal.*, 404, 46-55. <https://doi.org/10.1016/j.jcat.2021.09.007>.
- [36] Hess, C. (2021). New advances in using Raman spectroscopy for the characterization of catalysts and catalytic reactions. *Chem. Soc. Rev.*, 50(5), 3519–3564. <https://doi.org/10.1039/D0CS01059F>.
- [37] Ricci, P.C., Carbonaro, C.M., Stagi, L., Salis, M., Casu, A., Enzo, S., Delogu, F. (2013). Anatase-to-Rutile Phase Transition in TiO<sub>2</sub> Nanoparticles Irradiated by Visible Light. *J. Phys. Chem. C*, 117(15), 7850–7857. <https://doi.org/10.1021/jp312325h>.
- [38] Swaminathan, S., Rao, V.G., Bera, J.K., Chandra, M. (2021). The Pivotal Role of Hot Carriers in Plasmonic Catalysis of C–N Bond Forming Reaction of Amines. *Angew. Chem. Int. Ed.*, 60(22), 12532–12538. <https://doi.org/10.1002/anie.202101639>.
- [39] Feng, K., Wang, Y., Guo, M., Zhang, J., Li, Z., Deng, T., Zhang, Z., Yan, B. (2021). In-situ/operando techniques to identify active sites for thermochemical conversion of CO<sub>2</sub> over heterogeneous catalysts. *J. Energy Chem.*, 62 153–171. <https://doi.org/10.1016/j.jechem.2021.03.054>.
- [40] Chakrabarti, A., Ford, M. E., Gregory, D., Hu, R., Keturakis, C. J., Lwin, S., ... & Wachs, I. E. (2017). A decade + of operando spectroscopy studies. *Catal. Today*, 283, 27-53. <https://doi.org/10.1016/j.cattod.2016.12.012>.
- [41] Kookhaee, H., Tesema, T.E., Habteyes, T.G. (2020). Switching a Plasmon-Driven Reaction Mechanism from Charge Transfer to Adsorbate Electronic Excitation Using Surface Ligands. *J. Phys. Chem. C*, 124(41), 22711–22720. <https://doi.org/10.1021/acs.jpcc.0c07479>.
- [42] Cheng, Y., Wang, W., Yao, L., Wang, J., Han, H., Zhu, T., Liang, Y., Fu, J., Wang, Y. (2020). 3D Ag/ZnO microsphere SERS substrate with ultra-sensitive, recyclable and self-cleaning performances: application for rapid in site monitoring catalytic dye degradation and insight into the mechanism. *Colloids Surf., A Physicochem. Eng. Asp.*, 607, 125507. <https://doi.org/10.1016/j.colsurfa.2020.125507>.



- [43] Jiang, P., Dong, Y., Yang, L., Zhao, Y., Xie, W. (2019). Hot Electron-Induced Carbon–Halogen Bond Cleavage Monitored by in Situ Surface-Enhanced Raman Spectroscopy. *J. Phys. Chem. C*, 123(27), 16741–16746. <https://doi.org/10.1021/acs.jpcc.9b03238>.
- [44] Kumari, G., Kamarudheen, R., Zoethout, E., Baldi, A. (2021). Photocatalytic Surface Restructuring in Individual Silver Nanoparticles. *ACS Catalysis*, 11(6), 3478–3486. <https://doi.org/10.1021/acscatal.1c00478>.
- [45] Qiu, L., Pang, G.A., Zheng, G., Bauer, D., Wieland, K., Haisch, C. (2020). Kinetic and Mechanistic Investigation of the Photocatalyzed Surface Reduction of 4-Nitrothiophenol Observed on a Silver Plasmonic Film via Surface-Enhanced Raman Scattering. *ACS Appl. Mater. Interfaces*, 12(18), 21133–21142. <https://doi.org/10.1021/acsami.0c05977>.
- [46] Huang, J., Niu, W., Li, C., Tan, C., Yin, P., Cheng, H., Hu, Z., Yang, N., He, Q., Nam, G.-H., Zhang, H. (2020). In-Situ Probing of Crystal-Phase-Dependent Photocatalytic Activities of Au Nanostructures by Surface-Enhanced Raman Spectroscopy. *ACS Mater. Lett.*, 2(4), 409–414. <https://doi.org/10.1021/acsmaterialslett.0c00060>.
- [47] Zhang, G., Chen, L., Fu, X., Wang, H. (2018). Cellulose Microfiber-Supported TiO<sub>2</sub>@Ag Nanocomposites: A Dual-Functional Platform for Photocatalysis and in Situ Reaction Monitoring. *Ind. Eng. Chem. Res.*, 57(12), 4277–4286. <https://doi.org/10.1021/acs.iecr.8b00006>.
- [48] Zhang, H., Wei, J., Zhang, X.-G., Zhang, Y.-J., Radjenovica, P.M., Wu, D.-Y., Pan, F., Tian, Z.-Q., Li, J.-F. (2020). Plasmon-Induced Interfacial Hot-Electron Transfer Directly Probed by Raman Spectroscopy. *Chem*, 6(3), 689–702. <https://doi.org/10.1016/j.chempr.2019.12.015>.
- [49] Cai, Z.-F., Merino, J.P., Fang, W., Kumar, N., Richardson, J.O., De Feyter, S., Zenobi, R. (2021). Molecular-Level Insights on Reactive Arrangement in On-Surface Photocatalytic Coupling Reactions Using Tip-Enhanced Raman Spectroscopy. *JACS*. <https://doi.org/10.1021/jacs.1c11263>.
- [50] Rößler, M., Huth, P.U., Liauw, M.A. (2020). Process analytical technology (PAT) as a versatile tool for real-time monitoring and kinetic evaluation of photocatalytic reactions. *React. Chem. Eng.* 5(10), 1992–2002. <https://doi.org/10.1039/D0RE00256A>.
- [51] Qian, R., Zong, H., Schneider, J., Zhou, G., Zhao, T., Li, Y., ... & Pan, J.H. (2019). Charge carrier trapping, recombination and transfer during TiO<sub>2</sub> photocatalysis: An overview. *Catal. Today* 335, 78-90. <https://doi.org/10.1016/j.cattod.2018.10.053>.
- [52] Chiesa, M., Giamello, E., Livraghi, S., Paganini, M. C., Polliotto, V., & Salvadori, E. (2019). Electron magnetic resonance in heterogeneous photocatalysis research. *J. Phys.: Condens. Matter*. 31, 444001. <https://doi.org/10.1088/1361-648X/ab32c6>.
- [53] Zhang, Y., Dai, Y., Li, H., Yin, L., & Hoffmann, M.R. (2020). Proton-assisted electron transfer and hydrogenatom diffusion in a model system for photocatalytic hydrogen production. *Commun. Mater.* 1, 66. <https://doi.org/10.1038/s43246-020-00068-0>.
- [54] Park, H., Ou, H.-H., Colussi, A.J., & Hoffmann, M.R. (2015). Artificial Photosynthesis of C<sub>1</sub>–C<sub>3</sub> Hydrocarbons from Water and CO<sub>2</sub> on Titanate Nanotubes Decorated with Nanoparticle Elemental Copper and CdS Quantum Dots. *J. Phys. Chem. A* 119, 4658–4666. <https://doi.org/10.1021/jp511329d>.
- [55] Bonke, S. A., Risse, T., Schnegg, A. & Brückner, A. (2021). In situ electron paramagnetic resonance spectroscopy for catalysis. *Nat Rev Methods Primers* 1, 33. <https://doi.org/10.1038/s43586-021-00031-4>.
- [56] Al-Madanat, O., Nunes, B. N., AlSalka, Y., Hakki, A., Curti, M., Patrocinio, A. O. T., & Bahnemann, D. W. (2021). Application of EPR Spectroscopy in TiO<sub>2</sub> and Nb<sub>2</sub>O<sub>5</sub> Photocatalysis. *Catalysts*, 11(12), 1514. <https://doi.org/10.3390/catal11121514>.
- [57] Zhang, Y., Zhao, J., Wang, H., Xiao, B., Zhang, W., Zhao, X., ... & Liu, Q. (2022). Single-atom Cu anchored catalysts for photocatalytic renewable H<sub>2</sub> production with a quantum efficiency of 56%. *Nat. Commun.* 13, 58. <https://doi.org/10.1038/s41467-021-27698-3>.
- [58] Mario Chiesa, Elio Giamello, Stefano Livraghi, Maria Cristina Paganini, Valeria Polliotto and Enrico Salvadori. (2019). Electron magnetic resonance in heterogeneous photocatalysis research. *J. Phys.: Condens. Matter* 31, 444001. <https://doi.org/10.1088/1361-648X/ab32c6>.
- [59] Shiraiishi, Y., Hashimoto, M., Chishiro, K., Moriyama, K., Tanaka, S., & Hirai, T. (2020). Photocatalytic Dinitrogen Fixation with Water on Bismuth Oxychloride in Chloride Solutions for Solar-to-Chemical Energy Conversion. *J. Am. Chem. Soc.* 142, 7574–7583. <https://dx.doi.org/10.1021/jacs.0c01683>.
- [60] Koningsberger, D. C. (1988). Principles, applications, techniques of EXAFS, SEXAFS and XANES. *X-ray Absorption*.
- [61] Van Bokhoven, J. A., & Lamberti, C. (2016). X-ray absorption and X-ray emission spectroscopy: theory and applications (Vol. 1). John Wiley & Sons.
- [62] Singh, J., & van Bokhoven, J. A. (2010). Structure of alumina supported platinum catalysts of different particle size during CO oxidation using in situ IR and HERFD XAS. *Catal. Today*, 155(3-4), 199-205. <https://doi.org/10.1016/j.cattod.2009.12.006>.

- [63] Deng, J., Zhang, Q., Lv, X., Zhang, D., Xu, H., Ma, D., & Zhong, J. (2020). Understanding photoelectrochemical water oxidation with X-ray absorption spectroscopy. *ACS Energy Letters*, 5(3), 975-993. <https://doi.org/10.1021/acseenergylett.9b02757>.
- [64] Coronado, J. M., Fresno, F., & Iglesias-Juez, A. (2021). Approaching photocatalysts characterization under real conditions: In situ and operando studies. In *Materials Science in Photocatalysis* (pp. 139-156). Elsevier. <https://doi.org/10.1016/B978-0-12-821859-4.00030-1>.
- [65] Zhao, C., Liu, L., Rao, G., Zhao, H., Wang, L., Xu, J., & Li, Y. (2015). Synthesis of novel MgAl layered double oxide grafted TiO<sub>2</sub> cuboids and their photocatalytic activity on CO<sub>2</sub> reduction with water vapor. *Catal. Sci. Technol.*, 5(6), 3288-3295. <https://doi.org/10.1039/C5CY00216H>.
- [66] Hernández-Alonso, M. D., García-Rodríguez, S., Suárez, S., Portela, R., Sánchez, B., & Coronado, J. M. (2013). Operando DRIFTS study of the role of hydroxyls groups in trichloroethylene photo-oxidation over titanate and TiO<sub>2</sub> nanostructures. *Catal. today*, 206, 32-39. <https://doi.org/10.1016/j.cattod.2012.01.029>.
- [67] Saqlain, S., Cha, B. J., Kim, S. Y., Sung, J. Y., Choi, M. C., Seo, H. O., & Kim, Y. D. (2021). Impact of humidity on the removal of volatile organic compounds over Fe loaded TiO<sub>2</sub> under visible light irradiation: Insight into photocatalysis mechanism by operando DRIFTS. *Mater. Today Commun.*, 26, 102119. <https://doi.org/10.1016/j.mtcomm.2021.102119>.
- [68] Hernández-Alonso, M. D., Tejedor-Tejedor, I., Coronado, J. M., & Anderson, M. A. (2011). Operando FTIR study of the photocatalytic oxidation of methylcyclohexane and toluene in air over TiO<sub>2</sub>-ZrO<sub>2</sub> thin films: Influence of the aromaticity of the target molecule on deactivation. *Appl. Catal. B: Environ.*, 101(3-4), 283-293. <https://doi.org/10.1016/j.apcatb.2010.09.029>.
- [69] Bravo-Suárez, J. J., & Srinivasan, P. D. (2017). Design characteristics of in situ and operando ultraviolet-visible and vibrational spectroscopic reaction cells for heterogeneous catalysis. *Catal. Rev.*, 59(4), 295-445. <https://doi.org/10.1080/01614940.2017.1360071>.
- [70] Hernández-Alonso, M. D., Tejedor-Tejedor, I., Coronado, J. M., Anderson, M. A., & Soria, J. (2009). Operando FTIR study of the photocatalytic oxidation of acetone in air over TiO<sub>2</sub>-ZrO<sub>2</sub> thin films. *Catal. Today*, 143(3-4), 364-373. <https://doi.org/10.1016/j.cattod.2009.02.033>.
- [71] El-Roz, M., Kus, M., Cool, P., & Thibault-Starzyk, F. (2012). New operando IR technique to study the photocatalytic activity and selectivity of TiO<sub>2</sub> nanotubes in air purification: influence of temperature, UV intensity, and VOC concentration. *J. Phys. Chem. C.*, 116(24), 13252-13263. <https://doi.org/10.1021/jp3034819>.
- [72] Haselmann, G. M., Baumgartner, B., Wang, J., Wieland, K., Gupta, T., Herzig, C., ... & Eder, D. (2020). In Situ Pt Photodeposition and Methanol Photooxidation on Pt/TiO<sub>2</sub>: Pt-Loading-Dependent Photocatalytic Reaction Pathways Studied by Liquid-Phase Infrared Spectroscopy. *ACS Catal.*, 10(5), 2964-2977. <https://doi.org/10.1021/acscatal.9b05588>.
- [73] Caudillo-Flores, U., Muñoz-Batista, M. J., Kubacka, A., & Fernández-García, M. (2018). Operando Spectroscopy in Photocatalysis. *ChemPhotoChem*, 2(9), 777-785. <https://doi.org/10.1002/cptc.201800117>.
- [74] Muñoz-Batista, M. J., Motta Meira, D., Colón, G., Kubacka, A., & Fernández-García, M. (2018). Phase-Contact Engineering in Mono-and Bimetallic Cu-Ni Co-catalysts for Hydrogen Photocatalytic Materials. *Angew. Chem. Int. Ed.*, 57(5), 1199-1203. <https://doi.org/10.1002/anie.201709552>.
- [75] Piccolo, L., Afanasiev, P., Morfin, F., Len, T., Dessal, C., Rousset, J. L., ... & Llorca, J. (2020). Operando X-ray Absorption Spectroscopy Investigation of Photocatalytic Hydrogen Evolution over Ultradispersed Pt/TiO<sub>2</sub> Catalysts. *ACS catal.*, 10(21), 12696-12705. <https://doi.org/10.1021/acscatal.0c03464>.
- [76] Spanu, D., Minguzzi, A., Recchia, S., Shahvardanfard, F., Tomanec, O., Zboril, R., ... & Altomare, M. (2020). An Operando X-ray Absorption Spectroscopy Study of a NiCu-TiO<sub>2</sub> Photocatalyst for H<sub>2</sub> Evolution. *ACS catal.*, 10(15), 8293-8302. <https://doi.org/10.1021/acscatal.0c01373>.
- [77] Wu, J. C., & Cheng, Y. T. (2006). In situ FTIR study of photocatalytic NO reaction on photocatalysts under UV irradiation. *J. Catal.*, 237(2), 393-404. <https://doi.org/10.1016/j.jcat.2005.11.023>.
- [78] Wang, K., Cao, M., Lu, J., Lu, Y., Lau, C. H., Zheng, Y., & Fan, X. (2021). Operando DRIFTS-MS investigation on plasmon-thermal coupling mechanism of CO<sub>2</sub> hydrogenation on Au/TiO<sub>2</sub>: The enhanced generation of oxygen vacancies. *Appl. Catal. B: Environ.*, 296, 120341. <https://doi.org/10.1016/j.apcatb.2021.120341>.
- [79] Yan, T., Wang, L., Liang, Y., Makaremi, M., Wood, T. E., Dai, Y., ... & Ozin, G. A. (2019). Polymorph selection towards photocatalytic gaseous CO<sub>2</sub> hydrogenation. *Nat. Com.*, 10(1), 1-10. <https://doi.org/10.1038/s41467-019-10524-2>.
- [80] Kataoka, S., Tejedor-Tejedor, M. I., Coronado, J. M., & Anderson, M. A. (2004). Thin-film transmission IR spectroscopy as an in-situ probe of the gas-solid interface in photocatalytic processes. *J. Photochem. Photobiol.*, 163(3), 323-329. <https://doi.org/10.1016/j.jphotochem.2004.01.004>.
- [81] Lesage, T., Verrier, C., Bazin, P., Saussey, J., & Daturi, M. (2003). Studying the NO<sub>x</sub>-trap mechanism over a Pt-Rh/Ba/Al<sub>2</sub>O<sub>3</sub> catalyst by operando FT-IR spectroscopy. *Phys. Chem. Chem. Phys.*, 5(20), 4435-4440. <https://doi.org/10.1039/B305874N>.

- [82] El-Roz, M., Bazin, P., & Thibault-Starzyk, F. (2013). An operando-IR study of photocatalytic reaction of methanol on new\* BEA supported TiO<sub>2</sub> catalyst. *Catal. today*, 205, 111-119. <https://doi.org/10.1016/j.cattod.2012.08.023>.
- [83] Hamoud, H. I., Lafjah, M., Douma, F., Lebedev, O. I., Djafri, F., Valchev, V., ... & El-Roz, M. (2019). Photo-assisted SCR over highly dispersed silver sub-nanoparticles in zeolite under visible light: An Operando FTIR study. *Sol. Energy*, 189, 244-253. <https://doi.org/10.1016/j.solener.2019.07.020>.
- [84] El-Roz, M., Bazin, P., Daturi, M., & Thibault-Starzyk, F. (2015). On the mechanism of methanol photooxidation to methylformate and carbon dioxide on TiO<sub>2</sub>: an operando-FTIR study. *Phys. Chem. Chem. Phys.*, 17(17), 11277-11283. <https://doi.org/10.1039/C5CP00726G>.
- [85] El-Roz, M., Lakiss, L., Telegeiev, I., Lebedev, O. I., Bazin, P., Vicente, A., ... & Valtchev, V. (2017). High-visible-light photoactivity of plasma-promoted vanadium clusters on nanozeolites for partial photooxidation of methanol. *ACS Appl. Mater. Interfaces*, 9(21), 17846-17855. <https://doi.org/10.1021/acsami.7b02161>.
- [86] Li, S. Y., Meng, S., Zou, X., El-Roz, M., Telegeiev, I., Thili, O., ... & Zhu, G. (2019). Rhenium-functionalized covalent organic framework photocatalyst for efficient CO<sub>2</sub> reduction under visible light. *Micropor. Mesopor. Mat.*, 285, 195-201. <https://doi.org/10.1016/j.micromeso.2019.05.026>.
- [87] Wolski, L., El-Roz, M., Daturi, M., Nowaczyk, G., & Ziolk, M. (2019). Insight into methanol photooxidation over mono-(Au, Cu) and bimetallic (AuCu) catalysts supported on niobium pentoxide—An operando-IR study. *Appl. Catal. B: Environ.*, 258, 117978. <https://doi.org/10.1016/j.apcatb.2019.117978>.
- [88] Chen, T., Ding, Q., Wang, X., Feng, Z., & Li, C. (2021). Mechanistic Studies on Photocatalytic Overall Water Splitting over Ga<sub>2</sub>O<sub>3</sub>-Based Photocatalysts by Operando MS-FTIR Spectroscopy. *J. Phys. Chem. Lett.*, 12(26), 6029-6033. <https://doi.org/10.1021/acs.jpcclett.1c01621>.
- [89] Waheed, A., Shi, Q., Maeda, N., Meier, D. M., Qin, Z., Li, G., & Baiker, A. (2020). Strong activity enhancement of the photocatalytic degradation of an azo dye on Au/TiO<sub>2</sub> doped with FeO<sub>x</sub>. *Catalysts*, 10(8), 933. <https://doi.org/10.3390/catal10080933>.
- [90] Chan, H. Y., Nguyen, V. H., Wu, J., Calvino-Casilda, V., Bañares, M. A., & Bai, H. (2015). Real-time Raman monitoring during photocatalytic epoxidation of cyclohexene over V-Ti/MCM-41 catalysts. *Catalysts*, 5(2), 518-533. <https://doi.org/10.3390/catal5020518>.
- [91] Yan, X., Xu, Y., Tian, B., Lei, J., Zhang, J., & Wang, L. (2018). Operando SERS self-monitoring photocatalytic oxidation of aminophenol on TiO<sub>2</sub> semiconductor. *Appl. Catal. B: Environ.*, 224, 305-309. <https://doi.org/10.1016/j.apcatb.2017.10.009>.
- [92] Guo, S., Li, Y., Tang, S., Zhang, Y., Li, X., Sobrido, A. J., ... & Wei, B. (2020). Monitoring hydrogen evolution reaction intermediates of transition metal dichalcogenides via operando raman spectroscopy. *Adv. Funct. Mater.*, 30(35), 2003035. <https://doi.org/10.1002/adfm.202003035>.
- [93] Wang, Q. Y., Chen, Y. Y., Ye, R. K., Liu, Q., Chen, H. Y., Yang, H., ... & Fang, P. P. (2021). Instantly Detecting Catalysts' Hot Spots Temperature In Situ during Photocatalysis by Operando Raman Spectroscopy. *Anal. Chem.*, 93(46), 15517-15524. <https://doi.org/10.1021/acs.analchem.1c03666>.
- [94] Agostini, G., Meira, D., Monte, M., Vitoux, H., Iglesias-Juez, A., Fernandez-Garcia, M., ... & Gorges, B. (2018). XAS/DRIFTS/MS spectroscopy for time-resolved operando investigations at high temperature. *J. Synchrotron Radiat.*, 25(6), 1745-1752. <https://doi.org/10.1107/S160057751801305X>.
- [95] Deng, J., Zhang, Q., Lv, X., Zhang, D., Xu, H., Ma, D., & Zhong, J. (2020). Understanding photoelectrochemical water oxidation with X-ray absorption spectroscopy. *ACS Energy Lett.*, 5(3), 975-993. <https://doi.org/10.1021/acsenergylett.9b02757>.
- [96] Tsyganok, A., Ghigna, P., Minguzzi, A., Naldoni, A., Murzin, V., Caliebe, W., ... & Ellis, D. S. (2020). Operando X-ray absorption spectroscopy (XAS) observation of photoinduced oxidation in FeNi (oxy) hydroxide overlayers on hematite ( $\alpha$ -Fe<sub>2</sub>O<sub>3</sub>) photoanodes for solar water splitting. *Langmuir*, 36(39), 11564-11572. <https://doi.org/10.1021/acs.langmuir.0c02065>.
- [97] Fracchia, M., Cristino, V., Vertova, A., Rondinini, S., Caramori, S., Ghigna, P., & Minguzzi, A. (2019). Operando X-ray absorption spectroscopy of WO<sub>3</sub> photoanodes. *Electrochim. Acta*, 320, 134561. <https://doi.org/10.1016/j.electacta.2019.134561>.
- [98] Gao, Y., Nie, W., Wang, X., Fan, F., & Li, C. (2020). Advanced space-and time-resolved techniques for photocatalyst studies. *Chem. Com.*, 56(7), 1007-1021. <https://doi.org/10.1039/C9CC07128H>.
- [99] Paz, Y. (2019). Transient IR spectroscopy as a tool for studying photocatalytic materials. *Journal of Physics: Condensed Matter.*, 31(50), 503004. <https://doi.org/10.1088/1361-648X/ab3eda>.
- [100] Li, Q., Anpo, M., & Wang, X. (2020). Application of photoluminescence spectroscopy to elucidate photocatalytic reactions at the molecular level. *Res. Chem. Intermed.*, 46(10), 4325-4344. <https://doi.org/10.1007/s11164-020-04209-5>.
- [101] Miao, T. J., & Tang, J. (2020). Characterization of charge carrier behavior in photocatalysis using transient absorption spectroscopy. *J. Chem. Phys.* 152(19), 194201. <https://doi.org/10.1063/5.0008537>.

- [102] Van Schroyen Lantman, E. M., Deckert-Gaudig, T., Mank, A. J., Deckert, V., & Weckhuysen, B. M. (2012). Catalytic processes monitored at the nanoscale with tip-enhanced Raman spectroscopy. *Nat. Nanotechnol.*, 7(9), 583-586. <https://doi.org/10.1038/nnano.2012.131>.
- [103] Dürr, R. N., Maltoni, P., Tian, H., Joussetme, B., Hammarstrom, L., & Edvinsson, T. (2021). From NiMoO<sub>4</sub> to  $\gamma$ -NiOOH: Detecting the Active Catalyst Phase by Time Resolved in Situ and Operando Raman Spectroscopy. *ACS nano*, 15(8), 13504-13515. <https://doi.org/10.1021/acsnano.1c04126>.
- [104] Piercy, V. L., Saeed, K. H., Prentice, A. W., Neri, G., Li, C., Gardner, A. M., ... & Cowan, A. J. (2021). Time-resolved Raman spectroscopy of polaron formation in a polymer photocatalyst. *J. Phys. Chem. Lett.*, 12(44), 10899-10905. <https://doi.org/10.1021/acs.jpcclett.1c03073>.
- [105] Ismail, A. S., Uemura, Y., Park, S. H., Kwon, S., Kim, M., Elnaggar, H., ... & De Groot, F. M. (2020). Direct observation of the electronic states of photoexcited hematite with ultrafast 2p3d X-ray absorption spectroscopy and resonant inelastic X-ray scattering. *Phys. Chem. Chem. Phys.*, 22(5), 2685-2692. <https://doi.org/10.1039/C9CP03374B>.
- [106] Baran, T., Fracchia, M., Vertova, A., Achilli, E., Naldoni, A., Malara, F., ... & D'Acapito, F. (2016). Operando and time-resolved X-ray absorption spectroscopy for the study of photoelectrode architectures. *Electrochim. Acta*, 207, 16-21. <https://doi.org/10.1016/j.electacta.2016.04.153>.
- [107] Lai, T. H., Katsumata, K. I., & Hsu, Y. J. (2021). In situ charge carrier dynamics of semiconductor nanostructures for advanced photoelectrochemical and photocatalytic applications. *Nanophotonics*, 10(2), 777-795. <https://doi.org/10.1515/nanoph-2020-0472>.
- [108] Zhang, M., De Respinis, M., & Frei, H. (2014). Time-resolved observations of water oxidation intermediates on a cobalt oxide nanoparticle catalyst. *Nat. Chem.*, 6(4), 362-367. <https://doi.org/10.1038/nchem.1874>.
- [109] Sheng, H., Oh, M. H., Osowiecki, W. T., Kim, W., Alivisatos, A. P., & Frei, H. (2018). Carbon dioxide dimer radical anion as surface intermediate of photoinduced CO<sub>2</sub> reduction at aqueous Cu and CdSe nanoparticle catalysts by rapid-scan FT-IR spectroscopy. *JACS*, 140(12), 4363-4371. <https://doi.org/10.1021/jacs.8b00271>.
- [110] Sheng, H., & Frei, H. (2016). Direct observation by rapid-scan FT-IR spectroscopy of two-electron-reduced intermediate of tetraaza catalyst [CoII(N4H (MeCN))<sup>2+</sup> converting CO<sub>2</sub> to CO. *JACS*, 138(31), 9959-9967. <https://doi.org/10.1021/jacs.6b05248>.
- [111] Paz, Y. (2019). Transient IR spectroscopy as a tool for studying photocatalytic materials. *J. Phys. Condens. Matter.*, 31(50), 503004. <https://doi.org/10.1088/1361-648X/ab3eda>.
- [112] Andersen, L. K., & Frei, H. (2006). Dynamics of CO in mesoporous silica monitored by time-resolved step-scan and rapid-scan FT-IR spectroscopy. *J. Phys. Chem. B*, 110(45), 22601-22607. <https://doi.org/10.1021/jp0640326>.
- [113] Colbeau-Justin, C., & Valenzuela, M. A. (2013). Time-resolved microwave conductivity (TRMC) a useful characterization tool for charge carrier transfer in photocatalysis: a short review. *Revista mexicana de física*, 59(3), 191-200.
- [114] Toe, C. Y., Lamers, M., Dittrich, T., Tahini, H. A., Smith, S. C., Scott, J., ... & Ng, Y. H. (2022). Facet-dependent carrier dynamics of cuprous oxide regulating the photocatalytic hydrogen generation. *Materials Advances*, 3(4), 2200-2212. <https://doi.org/10.1039/D1MA00934F>.
- [115] Wei, Z., Wang, W., Li, W., Bai, X., Zhao, J., Tse, E. C & Zhu, Y. (2021). Steering Electron-Hole Migration Pathways Using Oxygen Vacancies in Tungsten Oxides to Enhance Their Photocatalytic Oxygen Evolution Performance. *Angew. Chem. Int. Ed.*, 60(15), 8236-8242. <https://doi.org/10.1002/anie.202016170>.
- [116] Portela, R., Perez-Ferreras, S., Serrano-Lotina, A., & Bañares, M. A. (2018). Engineering operando methodology: Understanding catalysis in time and space. *Front. Chem. Sci. Eng.* 12(3), 509-536. <https://doi.org/10.1007/s11705-018-1740-9>.